THE EFFECT OF STABLE STRATIFICATION ON THE NATURAL CONVECTION IN A SQUARE CAVITY

THE EFFECT OF STABLE STRATIFICATION ON THE NATURAL CONVECTION IN A SQUARE CAVITY CAUSED BY A HORIZONTAL TEMPERATURE DIFFERENCE

By

WENJIANG WU, B.ENG.

A Thesis

Submitted to the School of Graduate Studies

in Partial Fulfillment of the Requirements

for the Degree

Master of Applied Science

McMaster University

MASTER OF APPLIED SCIENCE (2004)
(Mechanical Engineering)

McMaster University
Hamilton, Ontario

TITLE: The Effect of Stable Stratification on the Natural Convection in a Square Cavity Caused by a Horizontal Temperature Difference

AUTHOR: Wenjiang WU,
B.ENG. (Dalian University of Technology, P.R.China)

SUPERVISOR: Dr. Chan Ching
Department of Mechanical Engineering

Dr. Dan Ewing
Department of Mechanical Engineering

NUMBER OF PAGES: xxi, 126

Abstract

The effect of stable stratification on the natural convection heat transfer characteristics in an air-filled square cavity with a horizontal temperature difference was investigated experimentally. The temperature distribution at different positions along the hot vertical wall was measured using a thermocouple, and these temperature profiles were used to compute the heat transfer. It was found that varying the thermal boundary conditions of the top and bottom walls of the cavity changed the stratification, and in turn the natural convection heat transfer characteristics in the square cavity. The measurements indicated that when the top wall temperature increased, it caused a local recirculation region near the top wall, and this secondary circulation approached the hot vertical wall. The non-uniformity in the temperature profiles near the top wall is relatively independent of the temperature of the bottom wall indicating the recirculatory region is independent of the bottom wall temperature. In all cases, it was found that the local heat transfer along the hot vertical wall could be expressed by the correlation $Nu = CRa^{0.315}$. The constant C increased when the top wall temperature was increased, and decreased slightly when the bottom wall temperature was decreased. The constant C was found to correlate with the stratification rate, defined as the non-dimensionalized temperature gradient of the ambient air in the vertical direction in the core region of the cavity, and the non-dimensionalized mean temperature in the vertical direction of the cavity. The average Nusselt number for the hot vertical wall $\overline{Nu_H}$ increased with an increase in the vertical Grashof number Gr_V.

Acknowledgements

The author would like to express his gratitude to Drs. Chan Ching and Dan Ewing for their valuable guidance and support. The author would also like to express his appreciation to the people and organizations that helped him with his current work:

- Dr. Tony Robinson for his advice and suggestions during the designing of the test facility.
- The technicians, Mr. Andrew Buyers, Mr. Ron Lodewyks, Mr. Dave Schick, and Mr. Joe Verhaeghe for their help and patience in designing and building the test facility.
- Mr. Mike Shertzer for his assistance on assembling the rig and in performing the measurements.
- NSERC and Pratt & Whitney Canada (P&WC) for funding the present work.
- My friend Mr. Li Pan for his encouragement and selfless help.

Finally, I would like to express my sincere appreciation to my parents and older brother, who always encouraged and supported me.

Table of Contents

List of Figures

List of Tables

Nomenclature

C	constant for the Nusselt Rayleigh number correlation. $Nu = C \cdot Ra^{0.315}$.
H	height of the cavity, m.
L	width of the cavity, m.
Q	heat transfer rate, W.
T_H	temperature of the hot vertical wall in the cavity, $^{\circ}C$.
T_C	temperature of the movable vertical wall in the cavity, $^{\circ}C$.
T_{Top}	temperature of the top wall in the cavity, $^{\circ}C$.
T_{Bottom}	temperature of the bottom wall in the cavity, $^{\circ}C$.
T_{∞}	ambient temperature outside of the flow near the hot vertical wall, $^{\circ}C$.
$T_{w,i}$	temperature of water measured at the inlet of the cooling channel, $^{\circ}C$.
$T_{w,o}$	temperature of water measured at the outlet of the cooling channel, $^{\circ}C$.
Bi	Biot number, $\frac{hs}{k}$.
Gr	local Grashof number, $Gr = \frac{g\beta(T_H - T_{\infty})y^3}{\nu^2}$.
Gr_H	horizontal Grashof number, $Gr_H = \frac{g\beta(T_H - T_C)L^3}{\nu^2}$.

Gr_V	vertical Grashof number, $Gr_V = \frac{g\beta(T_{Top} - T_{Bottom})H^3}{\nu^2}$.
Nu	local Nusselt number, $Nu = \frac{hy}{k}$.
$\overline{Nu}_H$	average Nusselt number for the hot vertical wall, $\overline{Nu}_H = \frac{\overline{h}H}{k}$.
Pr	Prandtl number, $Pr = \frac{\nu}{\alpha}$.
Ra	local Rayleigh number, $Ra = \left(\frac{\beta}{\alpha\nu}\right) \cdot g \cdot (T_H - T_\infty) \cdot y^3$
S	Stratification rate, the non-dimensionalized temperature gradient of the ambient air in the vertical direction in the core region of the cavity.
S_V	non-dimensionalized temperature difference between the top and bottom walls, $S_V = \frac{T_{Top} - T_{Bottom}}{T_H - T_C}$.
$\overline{T}_V$	non-dimensionalized mean temperature in the vertical direction of the cavity, $\overline{T}_V = \frac{(T_{Top} + T_{Bottom})/2}{(T_H - T_C)}$.
g	gravity acceleration, m/s^2.
h	heat transfer coefficient, $W/m^2 \cdot {}^\circ C$.
$\overline{h}$	average heat transfer coefficient for the hot vertical wall, $W/m^2 \cdot {}^\circ C$.
s	thickness of the plate, m.
n	exponent for the Nusselt Rayleigh number correlation, $Nu = C \cdot Ra^{0.315}$.

ΔT	temperature difference between the temperature of the hot vertical wall and the local ambient temperature, $T_H - T_\infty$, $^\circ C$.
α	thermal diffusivity, m^2/s.
β	volume expansion coefficient at constant pressure, K^{-1}.
c_P	specific heat, $J/kg \cdot ^\circ C$.
k	thermal conductivity, $W/m \cdot ^\circ C$.
ν	kinematic viscosity, m^2/s.
δ	thickness of the hydrodynamic boundary layer, m.
δ_T	thickness of the thermal boundary layer, m.
υ	flow velocity parallel to the vertical walls, m/s.
ρ	density, kg/m^3.
$\dot{m}$	mass flow rate of the water, kg/s.
q''	heat flux, W/m^2.

Chapter 1 Introduction

There have been a number of investigations of the natural convection in an air-filled rectangular enclosure with two parallel vertical walls held at different temperatures and adiabatic top and bottom walls, as shown in Figure 1.1. For a small temperature difference across the cavity, the heat is conducted through the air. As the temperature difference increases, a natural convection flow develops within the cavity, and the heat transfer due to the convection of the fluid from the hot to the cold wall is larger than conduction, so the natural convection determines the heat transfer across the cavity. In this case, the flow inside the cavity is primarily in the thermal boundary layer near the walls where the flow is driven by the buoyancy force caused by the gravitational acceleration and the density difference between the fluid in the ambient and in the boundary layer. In the thermal boundary layer along the hot vertical wall, the buoyancy force overcomes the viscous forces between the flow and the wall, and the fluid outside of the thermal boundary layer, accelerating the flow up the wall. As the flow moves along the top wall, the viscous forces on the wall reduce the momentum of the flow. Along the cold vertical wall, the dynamics are similar to the hot vertical wall and the flow accelerates in the thermal boundary layer.

Although the flow in the cavity is driven by the temperature difference across the cavity, the flow along each vertical wall is driven by the temperature difference between

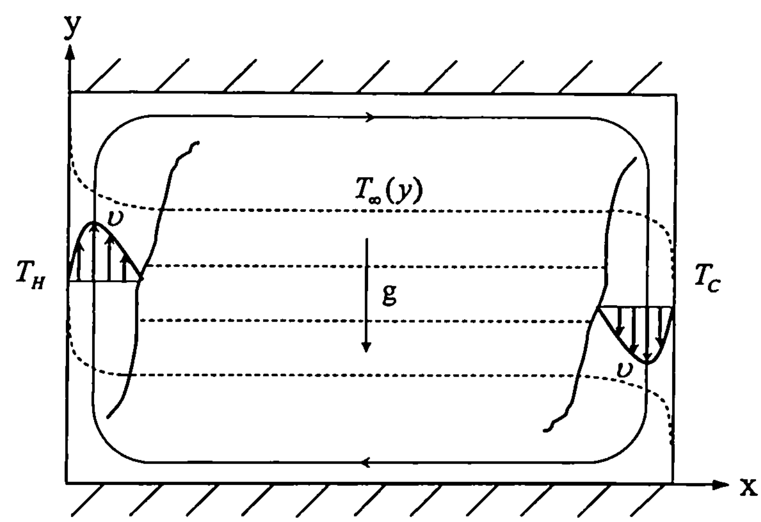

Figure 1.1 Schematic of the natural convection in a rectangular enclosure with temperature difference in the horizontal direction.

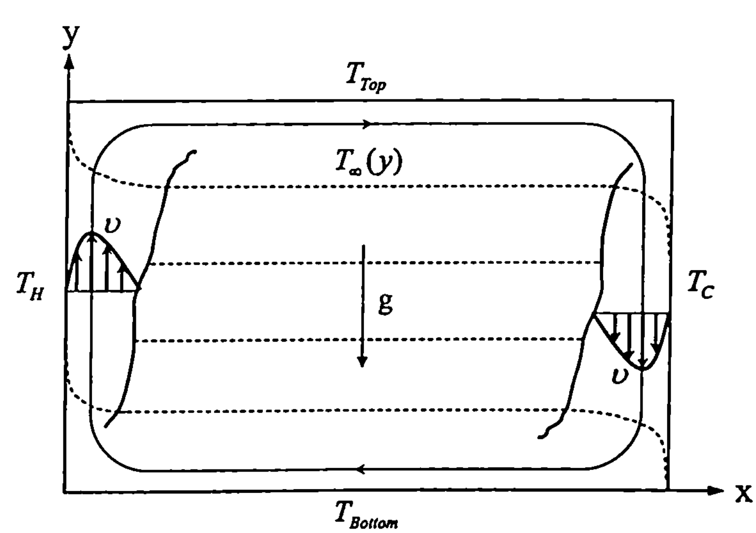

Figure 1.2 Schematic of the natural convection in a rectangular enclosure with temperature differences in the horizontal and vertical directions.

the wall and the core region. There have been a number of investigations that have found that the fluid is stably stratified inside the enclosure so the driving force in the natural convection flow along the vertical walls varies along these walls. In addition, if the distance between the vertical walls is large enough or the viscous forces are large enough, the flow velocity along the horizontal walls could decrease significantly before reaching the vertical walls, thereby significantly changing the flow pattern inside the rectangular enclosure. Thus, the aspect ratio of the enclosure influences the natural convection inside the enclosure (Emery and Chu, 1965).

In many practical applications, the upper and lower walls in the cavity may be heated or cooled as shown in Figure 1.2. This difference of the temperature in the vertical direction would change the stratification in the vertical direction and affect the heat transfer in the enclosure. However, there have been only few investigations that have focused on the effect of stable stratification on the natural convection heat transfer in rectangular enclosures caused by horizontal temperature differences. For example, Ostrach and Raghavan (1979) investigated the effect of stabilizing thermal gradients on the natural convection in a rectangular enclosure filled with silicone oil that had a large Prandtl number. Their study focused on the velocity field and they found that the stabilizing thermal gradient retarded the flow inside the enclosure. But the temperature field was not measured.

The objective of the present work is to investigate the effect of stable stratification on the natural convection in a square cavity caused by a horizontal temperature difference. The effect of the top and bottom wall temperatures on the natural convection heat transfer in the square cavity was investigated. An experimental facility was designed and constructed that allowed control of both horizontal and vertical temperature differences in an air-filled rectangular enclosure. In this thesis, attention is focused on the effect of the stable stratification for enclosures with an aspect ratio of one.

This thesis contains five chapters. The previous investigations on natural convection in enclosures are summarized in Chapter two. The experimental facilities, procedure and the data reduction are documented in Chapter three. The results are discussed in Chapter four. Finally, in Chapter five, the conclusions are presented.

Chapter 2 Literature Review

There have been a number of investigations of the natural convection that occurs in enclosures that are heated and cooled on the side walls. Many of these investigations have focused on two generic configurations, the rectangular cavity and the horizontal cylinder. The current work focuses on the natural convection in a rectangular cavity so the results for this geometry are discussed in detail first. The investigations of natural convection in a horizontal cylinder are then presented. Finally, an overview of the investigations in other geometries is presented.

2.1 Natural convection in a rectangular enclosure

Most of the investigations of natural convection in rectangular enclosures have focused on the case where the two vertical side walls are at different temperatures, while the top and bottom walls are insulated. Emery and Chu (1965) found that the ratio of the height to the width of the rectangular enclosure had a significant effect on the natural convective heat transfer in the cavity. MacGregor and Emery (1969) later showed that the differences in aspect ratio of the enclosure had a significant effect on the temperature fields and streamlines inside the cavity. Ostrach (1988) also noted that the natural convection was very sensitive to variations in the enclosure configurations and the thermal boundary conditions. Thus, the discussion of the investigations of natural convection in the rectangular enclosure will be divided into three sections based on the aspect ratio of the cavity investigated. Those where the aspect ratio of the cavity investigated was approximately unity are discussed first. The investigations where the height was significantly larger than the width are then presented. Finally, the investigations in cavities with the height much less than the width are presented.

2.1.1 Natural convection in enclosures with the height approximately equal to the width

The investigations in rectangular cavities with aspect ratio approximately unity are summarized in Table 2.1. The flow pattern and temperature distribution that occur inside the approximately square enclosures with heated and cooled side walls have been characterized for a range of Grashof numbers. For example, MacGergor and Emery (1969) investigated the effect of the temperature difference between the two vertical walls on the flow pattern and heat transfer using numerical simulations. The local flow and heat flux patterns within the enclosure for Grashof numbers ranging from 10^2 to 10^5 are shown in Figure 2.1. The Grashof number here is based on the width of the cavity and is given by

$$Gr_L = \frac{g\beta(T_H - T_C)L^3}{\nu^2}, \tag{2.1}$$

where L is the width of the cavity, and $T_H - T_C$ is the temperature difference between the two vertical walls. For a Grashof number of 10^2, the isotherms are approximately vertical lines that are evenly spaced indicating the heat is transferred primarily by

Investigators	Approach	Study Area	Findings
MacGregor and Emery (1969)	Numerical computations and experiment	Natural convection for isothermal wall and constant-heat-flux wall-boundary conditions.	The effects of Pr, Gr, and aspect ratio on natural convection were described. Experimental measurements of heat transfer, and the velocity and temperature profiles were given.
Newell and Schmidt (1970)	Numerical techniques	Two-Dimensional laminar natural convection in air-filled rectangular enclosure with isothermal walls at different temperatures.	The time-dependent governing differential equations were solved. Steady-state solutions were obtained.
Cormack et al. (1974 a, b)	Theoretical analysis and simulation	Natural convection in a shallow cavity with differentially heated end walls.	The flow consisted of two regimes: a parallel flow in the core region and a second, non-parallel flow near the ends of the cavity.
Ostrach and Raghavan (1979)	Experimental	The effect of stabilizing thermal gradients on natural convection in silicone oils in rectangular cavity with different aspect ratio. $Pr \sim 10^5$; Gr up to 20; and aspect ratios of 1 and 3.	The flow generated by a horizontal gradient was retarded by a stabilizing thermal gradient. The reduction was shown as a function of the relevant parameters.
Sernas and Lee (1981)	Experiment using an interferometer	Heat transfer rates inside rectangular air enclosures of aspect ratios between 0.1 and 1. $2.64\times10^6 < Gr < 5.45\times10^6$.	The heat transfer characteristics and flow patterns within the two types of enclosures were found to be significantly different.
Shiralkar and Tien (1982)	Numerical technique	The flow and heat transfer in an square enclosure subjected to comparable horizontal and vertical temperature differences.	A stabilizing vertical temperature difference was found to decrease the vertical velocities along the hot wall, but increase the horizontal heat transfer.
Briggs and Jones (1985)	Experiment using a laser-doppler velocimeter	Two-dimensional periodic natural convection in a rectangular enclosure of aspect ratio one. The two vertical walls at different temperatures; the two horizontal walls with temperatures varying linearly between the two vertical walls.	Clearly defined the existence of the periodic laminar flow regimes detectable at $Ra > 0.3\times10^7$ .The effect of Ra on frequency of flows was reported.
Bohn and Anderson (1986)	Experimental	Temperature and heat flux distribution in a three-dimensional natural convection enclosure flow.	A three-dimensional enclosure exhibited core stratification. The temperature in the core varied only in the vertical direction.
Viskanta et al. (1986)	Numerical algorithm and experiment	Three-dimensional natural convection heat transfer of a liquid metal in a rectangular cavity with differential side heating.	For the low-Prandtl-number fluids, three-dimensional effects on the convective heat transfer throughout the cavity.
Tian and Karayiannis (2000)	Experimental	Natural convection in an air-filled square cavity with the temperature differential between the two vertical walls.	The temperature and velocity distribution was measured at different locations inside the cavity. A contour plot of the thermal field and a vector plot of the air flow in the cavity were reported.

Table 2.1 Summary of investigations of natural convection in rectangular enclosure with the height approximately equal to the width.

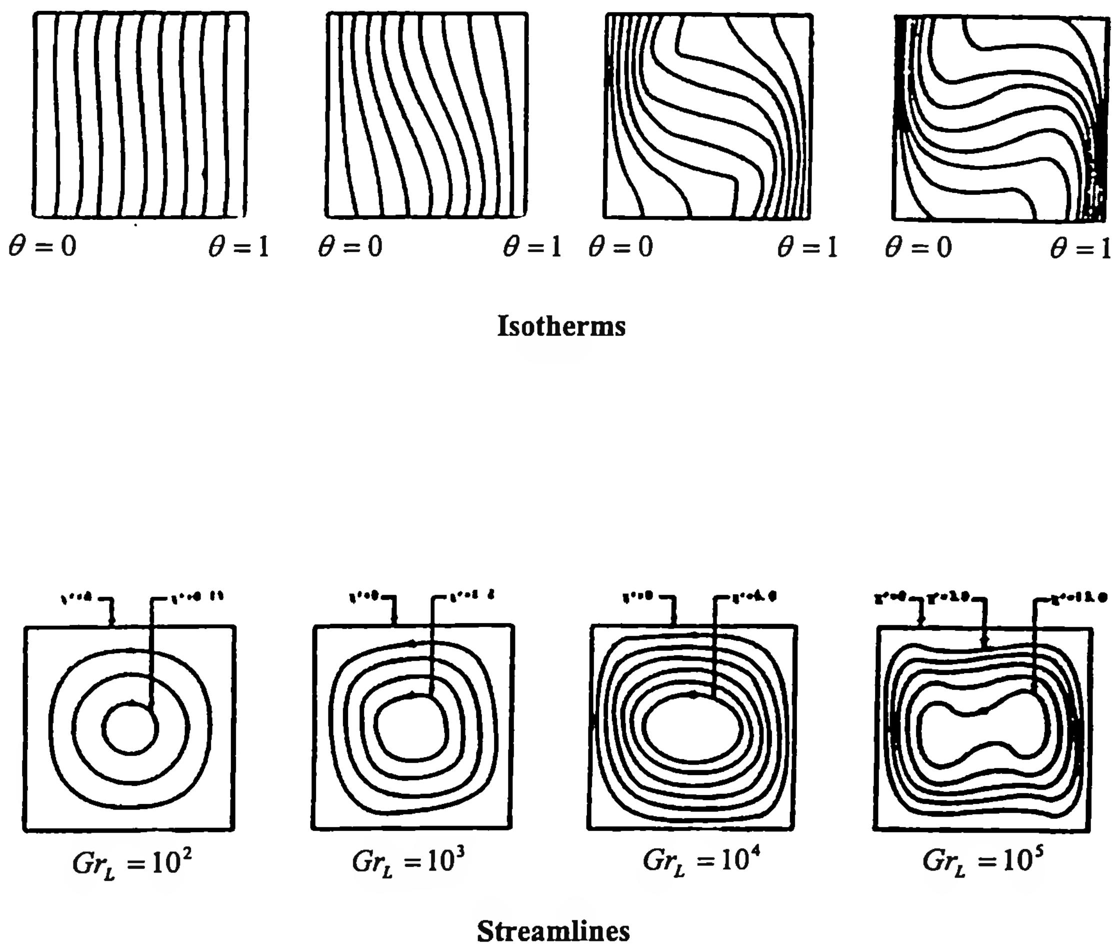

Figure 2.1 Change in the isotherms and streamline patterns with Grashof numbers for enclosures with aspect ratio of 1 and fluid with $\Pr = 1.0$ from MacGergor and Emery (1969). Here $\theta = \dfrac{T - T_C}{T_H - T_C}$ and Gr_L is the Grashof number based on the width of the cavity given in Equation (2.1).

conduction. There is a circulatory motion in the cavity driven by the horizontal temperature difference $T_H - T_C$, but the streamlines are evenly spaced showing there is not a particularly strong natural convection flow near the wall. As the temperature difference between the two vertical walls was increased and the Grashof number increased, the isotherms and the streamlines become distorted indicating that there is heat transfer by convection. There is an obvious change in the isotherms and the fluid motion indicating that the magnitude of the temperature difference has a significant effect on the heat transfer inside the square cavity. For the highest Grashof number ($\sim 10^5$) investigated by MacGergor and Emery (1969), the concentration of the isotherms and streamlines near the walls suggests that the buoyancy forces drive the flows near the walls. Cormack et al. (1974b) later investigated the natural convection in a square cavity with a temperature difference on the vertical walls that gave a similar order of Grashof number and found similar streamlines and isotherms.

Tian and Karayiannis (2000) recently measured the temperature and velocity distributions near the wall, using an E-type thermocouple and a 2D Laser Doppler Anemometer (LDA), in an air filled square cavity with isothermal hot and cold vertical walls and adiabatic top and bottom walls for a Rayleigh number of 1.58×10^9, where the Rayleigh number was based on the width of the cavity L given by

$$Ra = \frac{g\beta(T_H - T_C)L^3}{\alpha\nu}. \tag{2.2}$$

The temperature distribution at different heights and a schematic of the flow structure inside the square cavity obtained by Tian and Karayiannis (2000) are shown in Figure

2.2. In this case, it can be seen that there is a significant change in the temperature profile near the vertical walls indicating there was a boundary layer, and the flow is primarily in boundary layers along the walls driven by the buoyancy force. They found, however, that there were secondary circulation flows just outside of the boundary layer.

The correlation for the heat transfer produced by natural convection in a square enclosure has been reported in a number of investigations. Newell and Schmidt (1970) performed a numerical simulation of the two-dimensional laminar natural convection in an air-filled square enclosure with isothermal walls for a range of temperature differences and found that the correlation for the heat transfer was given by

$$\overline{Nu}_L = 0.145\left(Gr_L'\right)^{0.397}, \tag{2.3}$$

where L is the width of the enclosure, for Grashof numbers ranging from 2×10^3 to 7×10^4. Here the Grashof number is based on the width of the cavity and is defined somewhat different from the standard definition in Equation (2.1), i.e.,

$$Gr_L' = \frac{g\beta\left[T_H - \left(\frac{T_H+T_C}{2}\right)\right]L^3}{\nu^2}. \tag{2.4}$$

The temperature difference in the vertical direction can also affect the natural convection characteristics within the rectangular enclosure that is heated on the two vertical walls. Ostrach and Raghavan (1979) investigated the effect of the temperature difference between the top and bottom walls on the flow patterns inside the enclosure with aspect ratio one for a fluid with a Prandtl number of the order of 10^5. The flow pattern became more asymmetric as the temperature difference in the vertical direction

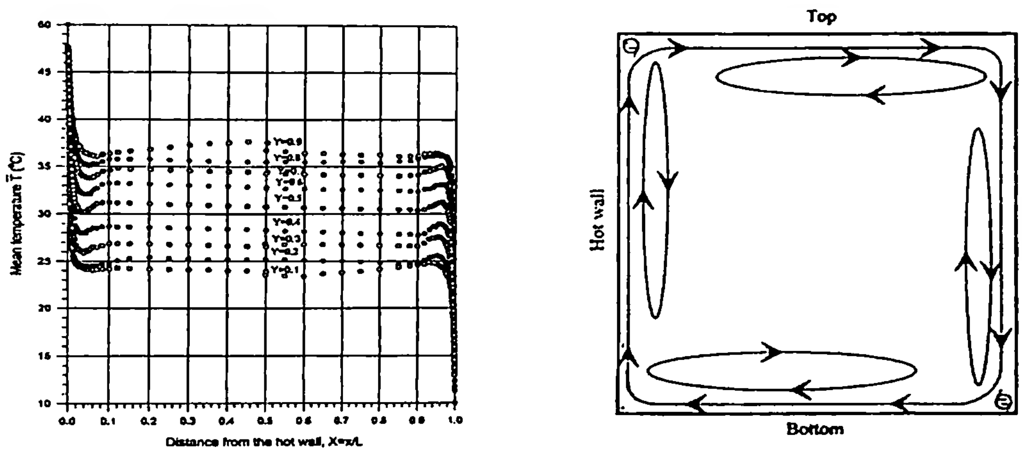

Figure 2.2 Temperature distribution at different heights (on left) and schematic of the flow structure (on right) inside the square cavity from Tian and Karayiannis (2000).

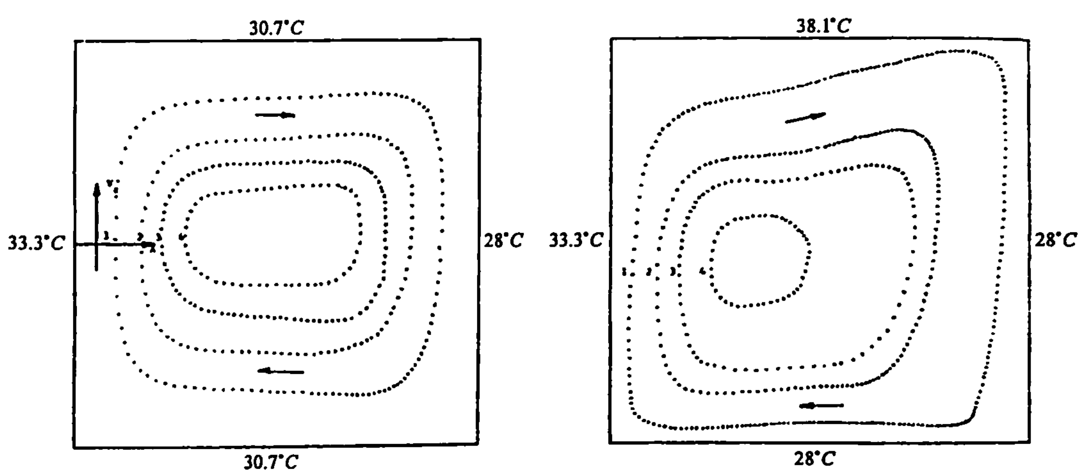

$Gr_H = 0.558$, $Gr_V = 0$
Aspect ratio = 1

$Gr_H = 0.584$, $Gr_V = 1.102$
Aspect ratio = 1

Figure 2.3 Streamline patterns from Ostrach and Raghavan (1979).

was increased for a fixed temperature difference in the horizontal direction as shown in Figure 2.3. Sernas and Lee (1981) compared the local heat flux on the hot vertical wall for a square enclosure with adiabatic top and bottom walls, and for the case where the top and hot vertical walls were at the same temperature, and the bottom wall and cold vertical walls were at the same temperature. The results for the Grashof number based on the width of the enclosure of 5.45×10^6 are shown in Figure 2.4. It is clear that the thermal boundary conditions on the top and bottom walls have a significant effect on the heat transfer from the hot vertical wall, particularly in the region near the bottom wall. Shiralkar and Tien (1982) numerically investigated the flow and heat transfer for the same geometries, and concluded that the stabilizing temperature difference in the vertical direction decreased the vertical velocities along the hot vertical wall, but increased the heat transfer from the hot vertical wall.

2.1.2 Natural convection in enclosures with the height much greater than the width

The flow field in an enclosure where the height is much greater than the width differs from that in cavities that are approximately square in part because the flow along the top and bottom walls plays a much smaller role in retarding the flow. A summary of the investigations for this geometry is contained in Table 2.2. Eckert and Carlson (1961) measured the temperature distribution between two vertical isothermal walls in an enclosure with aspect ratios of 10 and 20, using a Zehnder-Mach interferometer. The top and bottom walls in the enclosure were adiabatic. The temperature profiles at different height are shown in Figure 2.5. When the Grashof number was 4×10^3, the temperature

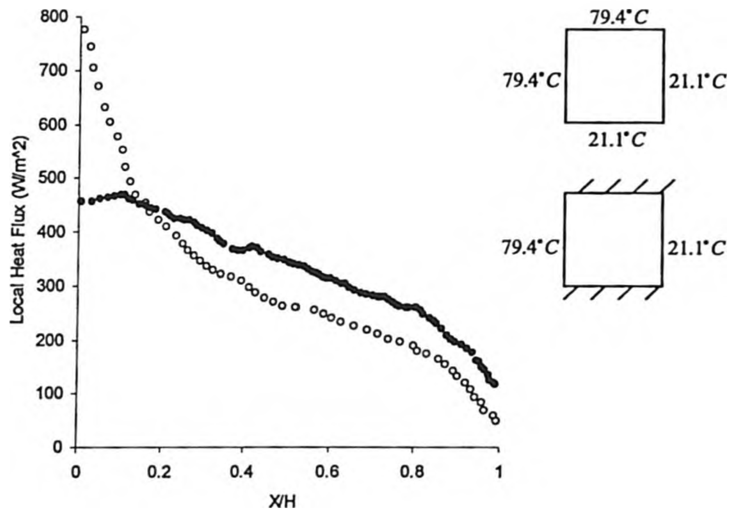

Figure 2.4 Local heat flux distribution along the hot vertical wall for ○ isothermal top wall ($79.4^{\circ}C$) and bottom wall ($21.1^{\circ}C$), and for ● foam top and bottom walls from Sernas and Lee (1981). Enclosure aspect ratio of 1.

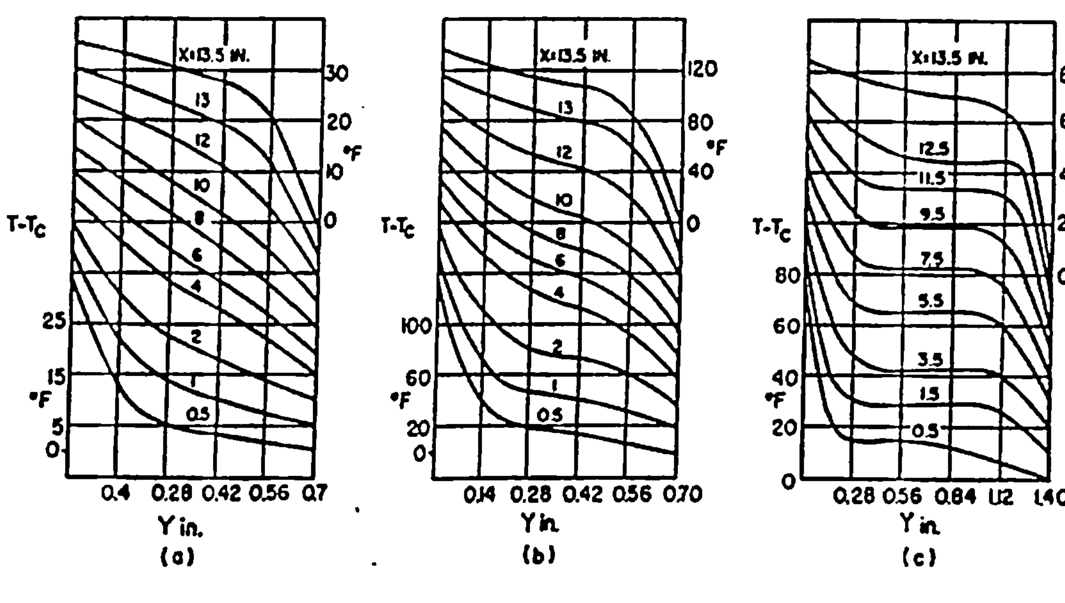

Figure 2.5 Temperature field in air filled cavity with a height of 14 in. and aspect ratios of 10 to 20 from Eckert and Carlson (1961). (a) conduction regime, $Gr_L = 4\times10^3$; (b) transition regime, $Gr_L = 2\times10^4$; (c) boundary layer regime, $Gr_L = 1.6\times10^5$.

Investigators	Approach	Study Area	Findings
Eckert and Carlson (1961)	Experiment using an interferometer	The temperature field in an air-filled enclosure with two different temperature vertical walls.	Local heat transfer coefficients were derived. The range of Grashof numbers and the value of aspect ratio determined the natural convection characters inside the cavity.
Emery and Chu (1965)	Theoretical analysis and experiment	The heat transfer across a vertical layer by natural convection.	The heat transfer was a function of temperature differential in the horizontal direction, and the aspect ratio. Heat transfer coefficients were reported.
Elder (1965)	Experimental	Laminar natural convection in a rectangular cavity with different temperatures on the two vertical walls. Aspect ratio=1-60; Prandtl number = 1000; and $Ra < 10^8$.	With the different range of the Rayleigh numbers, the temperature field and the flow pattern were different.
Gill (1966)	Theoretical analysis	Two-Dimensional convective motion in a rectangular cavity with two vertical walls at different temperatures.	An approximate solution was obtained for the case of large values of the Prandtl number, and found to be in agreement with experimental data.
Seki et al. (1978)	Experimental visualization	Natural convective flow in a narrow rectangular cavity with two vertical walls at different temperature and horizontal walls insulated.	The effects of Prandtl number, the working fluid and the aspect ratios on the flow patterns were discussed qualitatively.
Yin et al. (1978)	Experimental	Natural convection in an air-filled rectangular cavity with temperature differential between the two vertical walls. Aspect ratio from 4.9 to 78.7.	Two Nusselt-Grashof correlations were presented for the measured heat-transfer data. $Nu_L = 0.091 Gr_L^{0.307}$; $Nu_L = 0.210 Gr_L^{0.269} (H/L)^{-0.131}$.
Ostrach and Raghavan (1979)	Experimental	The effect of stabilizing thermal gradients on natural convection in silicone oils in rectangular cavity with different aspect ratio. $\Pr \sim 10^5$, Gr up to 20, and aspect ratio were 1 and 3.	It was found that the flow generated by a horizontal gradient was retarded by a stabilizing thermal gradient. The reduction was shown as a function of the relevant parameters.

Table 2.2 Summary of investigations of natural convection in rectangular enclosure with the height much greater than the width.

profiles in the centre portion of Figure 2.5 (a) were linear, so that was defined as the "conduction regime". On the other hand, as the Grashof number was increased to 1.6×10^5, thermal boundary layers were observed near the two vertical walls as shown in Figure 2.5 (c), and the temperature profiles were horizontal in the central core. The thermal boundary layer increases upward along the hot vertical wall, and increases downward along the cold vertical wall. In this case, the heat was transferred by conduction near the vertical wall, and then by convection across the cavity. For the intermediate Grashof number of 2×10^4, there was a transition regime as shown in Figure 2.5 (b). The temperature profiles were curved throughout the entire height of the enclosure indicating that both convection and conduction contribute to the heat transfer from the hot to the cold vertical wall. Eckert and Carlson (1961) found that the heat transfer correlation for the conduction regime was given by

$$Nu_L = \frac{h_c L}{k} = 1 \quad \text{for } Gr_L \sim 10^3, \tag{2.5}$$

while the heat transfer correlation for the boundary layer regime was given by

$$Nu_L = 0.119(Gr_L)^{0.3}\left(\frac{L}{H}\right)^{0.1} \quad \text{for } Gr_L \sim 10^5. \tag{2.6}$$

Emery and Chu (1965) studied the heat transfer in a similar case with aspect ratios of 10 and 20, and found the correlations for the two regimes were given by

$$Nu_L = 1 \quad \text{for } Ra_L < 10^3, \tag{2.7}$$

$$Nu_L = 0.280\left(\frac{H}{L}\right)^{-1/4} Ra_L^{1/4} \quad \text{for } 10^3 < Ra_L < 10^7. \tag{2.8}$$

Yin et al. (1978) investigated the heat transfer in a cavity with aspect ratios ranging from 4.9 to 78.7 and Grashof number based on layer thickness in the range 1.5×10^{3} to 7.0×10^{6}. They developed the correlation

$$Nu_L = 0.091 Gr_L^{\ 0.307}, \tag{2.9}$$

if the effect of the aspect ratio was neglected, or

$$Nu_L = 0.210 Gr_L^{\ 0.269}\left(\frac{H}{L}\right)^{-0.131}, \tag{2.10}$$

if the effect of the aspect ratio was considered.

Elder (1965) examined the boundary layer flows in a rectangular cavity with aspect ratios of 1 to 60 for medicinal paraffin and silicone oil with Prandtl numbers approximately equal to 1000 by measuring the temperature profiles and observing the flow using aluminum powder suspended in the working fluid. The velocity profiles along the hot vertical wall at various heights for a fixed aspect ratio of 18.6 are shown in Figure 2.6. The velocity is maximum at roughly half of the cavity height, and the velocity profiles at vertical positions of 30, 40 and 50cm collapse, indicating the flow in this region is fully developed. Elder (1965) found that for Rayleigh numbers above 3×10^{5}, there is a transition of the flow in the core region of the cavity as shown in Figure 2.7. In particular, for a Rayleigh number of 3.6×10^{5}, a second cell of circular flow appeared in the core region. More secondary flow cells appeared as the Rayleigh number was increased. Gill (1966) later developed a model to predict the boundary-layer regime for large Prandtl number fluids. The approximate solutions obtained were in agreement with the experimental results obtained by Elder (1965). Seki et al. (1978) observed a similar

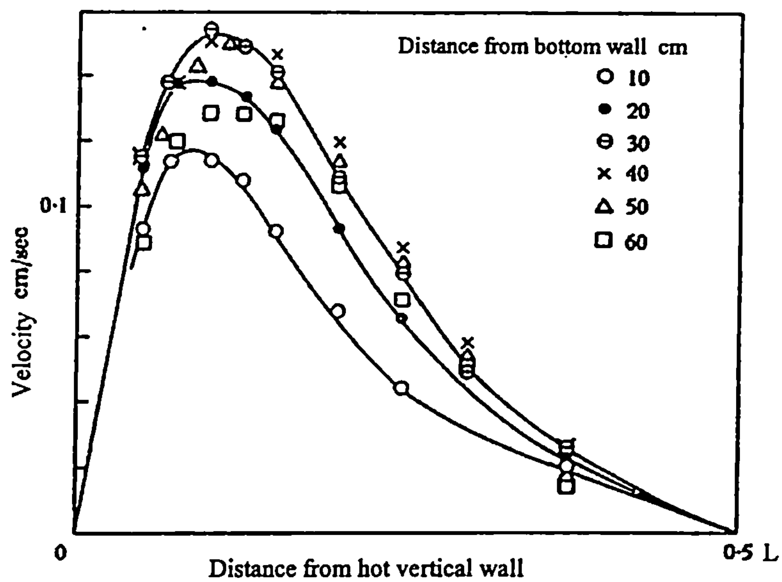

Figure 2.6 Velocity profiles from Elder (1965) for a cavity with L=4.08 cm, H=75.7 cm, and $Ra = 4.0 \times 10^5$ at various distances from the bottom wall.

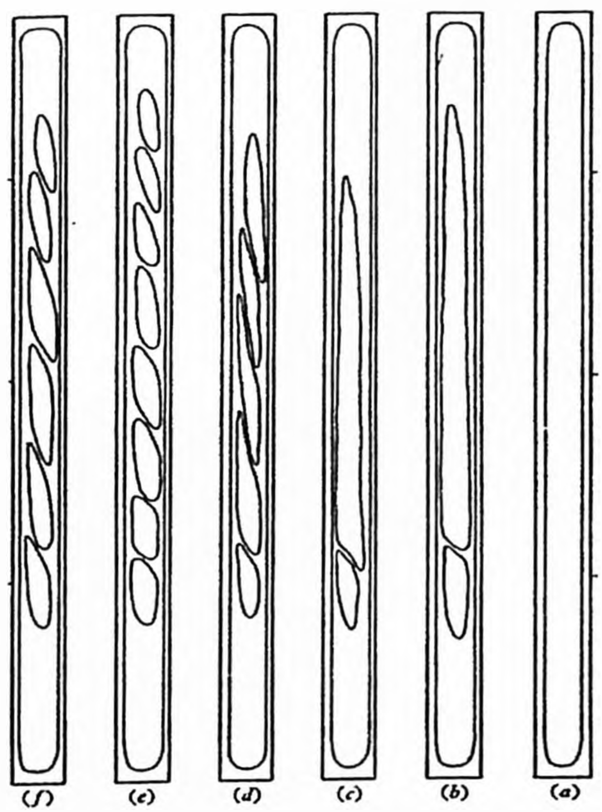

Figure 2.7 Schematic of streamlines of the secondary flow from Elder (1965) at various Ra_L (a) 3.0×10^5, (b) 3.6×10^5, (c) 4.0×10^5, (d) 4.9×10^5, (e) 5.8×10^5, (f) 6.8×10^5. Here the width of the cavity L was 2 cm, and the height H was 38 cm.

phenomenon by experimental visualization of natural convective flow in a cavity with aspect ratio of 15.

Ostrach and Raghavan (1979) investigated the effect of stabilizing thermal gradients on natural convection in silicone oils with Prandtl number of 10^5 in a rectangular enclosure with height to width ratio of 3. The streamline patterns at steady-state for three cases are shown in Figure 2.8. The horizontal Grashof numbers Gr_H based on the width of the enclosure and the temperature difference in the horizontal direction were 0.246, 0.253, and 0.143 respectively, while the vertical Grashof numbers Gr_V based on the height of the enclosure and the temperature difference in the vertical direction for these cases varied from 0 to 28.49. Initially, the flow pattern was approximately symmetric about the horizontal and vertical centerlines. However, when the large vertical stabilizing gradient was imposed with Gr_V/Gr_H of 83, a pronounced elongation towards the upper right corner was noticed. A further increase of Gr_V/Gr_H to 140.3 caused a second counter clockwise rotating cell to appear in the upper left corner. In these cases, the stabilizing gradient initially retarded the velocity of the flow on the hot vertical wall and then caused a secondary recirculating flow near the vertical wall.

2.1.3 Natural convection in enclosures with the height much less than the width

There have been a number of investigations of the effect of the cavity width on the natural convection in enclosures for small aspect ratio as summarized in Table 2.3. Cormack et al. (1974a) analyzed the flow theoretically and found that the flow inside the cavity consisted of a parallel flow in the core region and a second non-parallel flow near

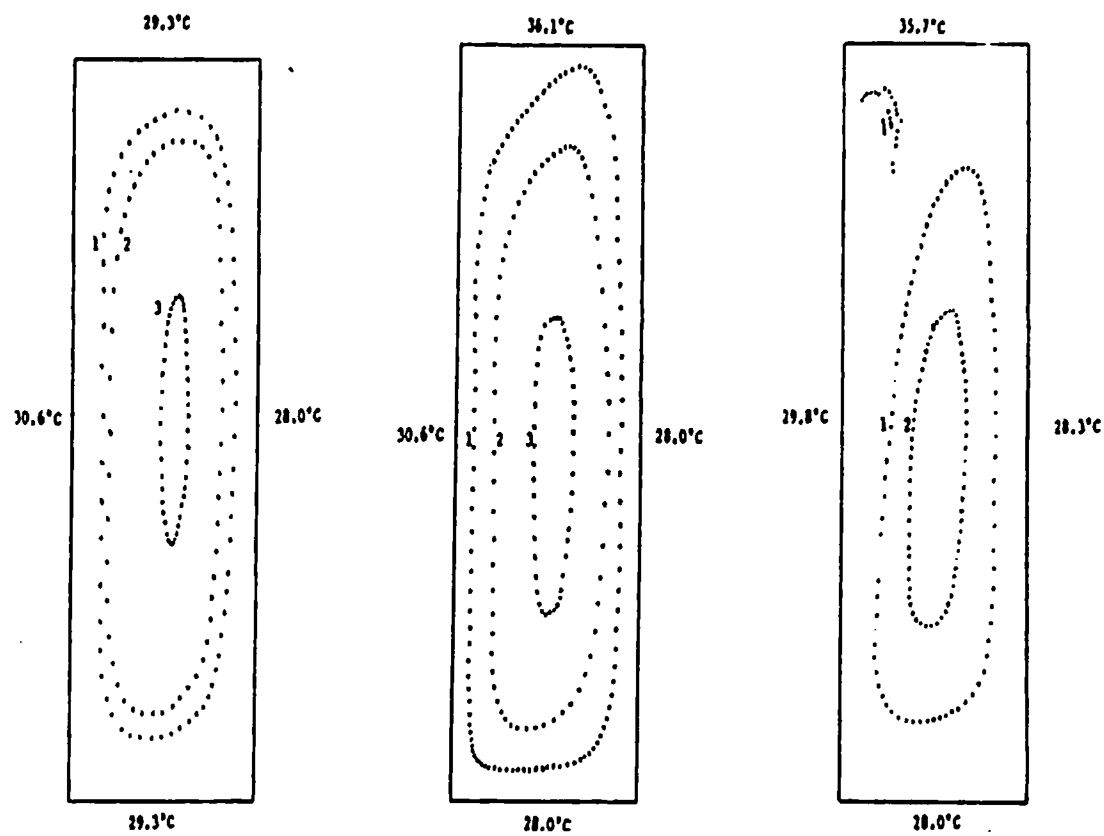

(a) (b) (c)

Figure 2.8 Streamline patterns from Ostrach and Raghavan (1979) for an aspect ratio $(\frac{H}{L})$=3, and (a) $Gr_H = 0.246$, Gr_V=0; (b) $Gr_H = 0.253$, $Gr_V = 21.049$; (c) $Gr_H = 0.143$, $Gr_V = 28.49$.

Investigators	Approach	Study Area	Findings
Cormack et al. (1974 a, b)	Theoretical analysis and simulation	Natural convection in a shallow cavity with differentially heated end walls.	The flow consisted of two regimes: a parallel flow in the core region and a second, non-parallel flow near the ends of the cavity.
Imberger (1974)	Experimental	The steady motion of water in an enclosed rectangular cavity with differentially heated vertical walls with aspect ratio= 10^{-2} & 1.9×10^{-2}	The experimental results were compared with the findings obtained from the theoretical analysis and numerical computations.
Bejan et al. (1981)	Experimental	High-Rayleigh-number convection in a horizontal rectangular cavity with the two vertical walls at different temperatures and the horizontal walls adiabatic. Aspect ratio = 0.0625.	The core flow structure was non-parallel and was dominated by horizontal intrusions flowing along the horizontal walls. The fluid between the two horizontal jets was stagnant and stratified.
Sernas and Lee (1981)	Experiment using an interferometer	Heat transfer rates inside rectangular air enclosures of aspect ratios between 0.1 and 1. $2.64\times10^6 < Gr < 5.45\times10^6$.	The heat transfer characteristics and flow patterns within the two types of enclosures were found to be significantly different.
Yewell et al. (1982)	Experimental	Transient natural convection in enclosures at high Rayleigh number (1.28×10^9,1.49×10^9) and low aspect ratios (0.0625, 0.112).	The thin intrusion layers along the horizontal adiabatic surfaces were observed. The core was thermally stratified. The equation for the time to reach the steady state was given.
Hart (1983)	Theoretical analysis	Two-dimensional convection in a horizontal cavity with two vertical walls at different temperatures.	Found the conditions for which a parallel core flow will exist at low Pr.
Ozoe et al. (1983)	Experimental	Natural convection inside a rectangular enclosure with the temperature differential at the vertical walls.	The horizontal and vertical velocity profiles near a heated vertical wall were measured. The horizontal temperature profiles were measured.
Drummond and Korpela (1987)	Numerical technique	Natural convection in a shallow enclosure heated from a side.	For fluids of small Prandtl number, the differences in the flow patterns in the two cases with different thermal boundary conditions on the top and bottom walls were slight.
Khalifa (2001)	Review paper	Natural convective heat transfer coefficients on surfaces in two- and three-dimensional enclosures.	Comparison between the correlations for the heat transfer coefficients showed that large discrepancies could occur. The discrepancies were found to be up to a factor of 5 for vertical walls.

Table 2.3 Summary of investigations of natural convection in rectangular enclosure with the height much less than the width.

the vertical walls. Cormack et al. (1974b) later simulated natural convection flows with Rayleigh number ranging from 70 to 1.4×10^5 for cavities with aspect ratio varying from 0.05 to 1. The streamlines and isotherms for cavities with a Rayleigh number of 1.4×10^5 and aspect ratios ranging from 0.05 to 0.2 are shown in Figure 2.9. The horizontal length scales have been compressed in these figures. As the aspect ratio of the cavity decreased, the streamlines become more parallel to the top and bottom walls and the isotherms became parallel to the vertical walls. Thus, the natural convection flow in the cavity was reduced as the aspect ratio of the cavity decreased and the viscous force on the top and bottom walls became more prevalent. The change in the streamlines and isotherms for Rayleigh numbers from 70 to 1.4×10^4 in a cavity with an aspect ratio of 0.1 are shown in Figure 2.10. It is clear that the streamlines are increasingly parallel to the horizontal walls as the Rayleigh number decreased and the isotherms are vertical at the lowest Rayleigh number. Thus, the heat was transferred mainly by conduction at the lowest Rayleigh number.

Imberger (1974) measured the steady motion of water in a shallow cavity with differentially heated vertical walls for Rayleigh number ranging from 1.31×10^6 to 1.11×10^8 and aspect ratios of 10^{-2} to 1.9×10^{-2}. The streamlines measured for these cases are shown in Figure 2.11. The results were in qualitative agreement with the results obtained by Cormack et al. (1974b). Imberger (1974) found that the heat transfer from the hot vertical wall to the opposite cold vertical wall was given by

$$\overline{Nu} \sim \left(H/L\right)^{-1} Ra^{1/4}, \tag{2.11}$$

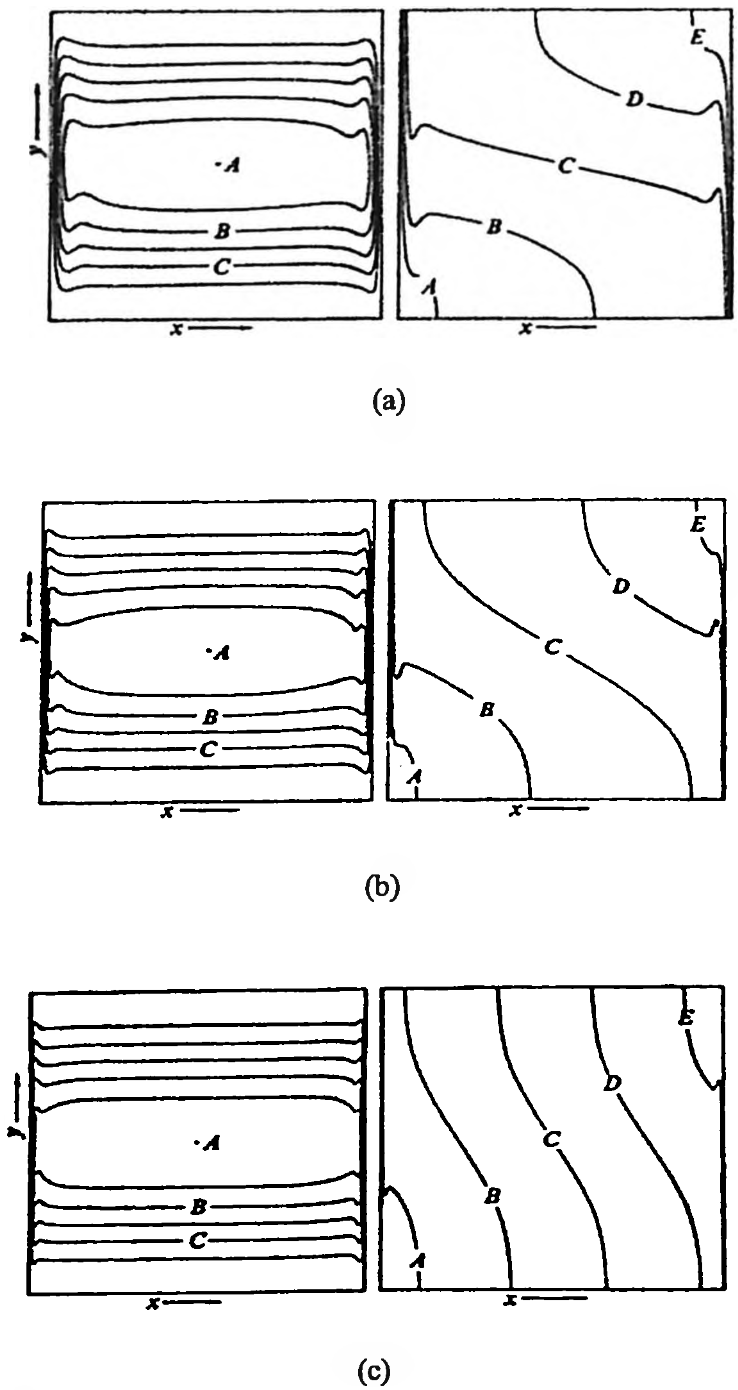

Figure 2.9 Comparison of the streamlines (on left) and isotherms (on right) in cavities with aspect ratios of (a) 0.2, (b) 0.1, and (c) 0.05 for natural convection in cavities with $Ra = 1.4\times10^5$ from Cormack et al. (1974b).

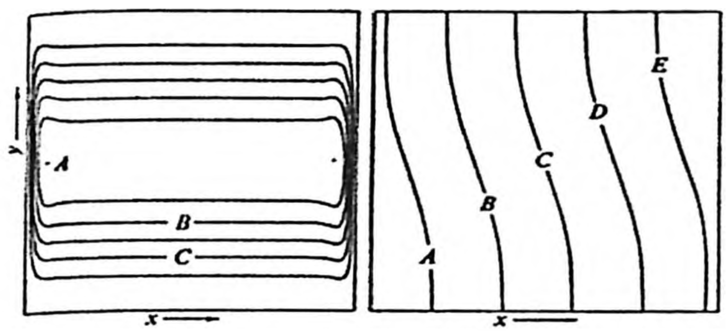

(a)

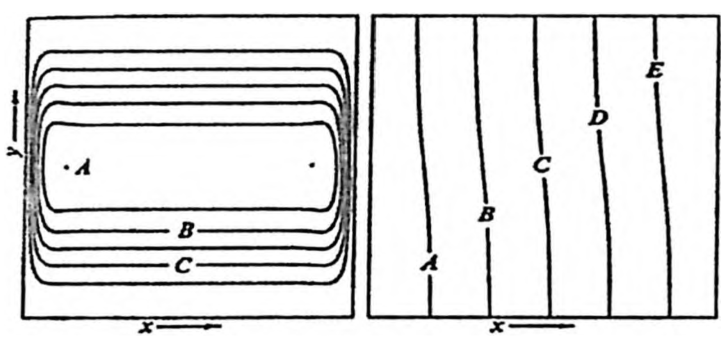

(b)

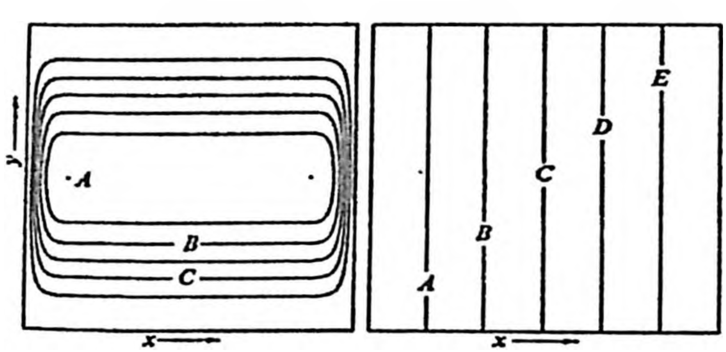

(c)

Figure 2.10 Comparison of the streamlines (on left) and isotherms (on right) in cavities with Rayleigh numbers of (a) 1.4×10^{4}, (b) 3500, and (c) 70 for natural convection in cavities with aspect ratio of 0.1 from Cormack et al. (1974b).

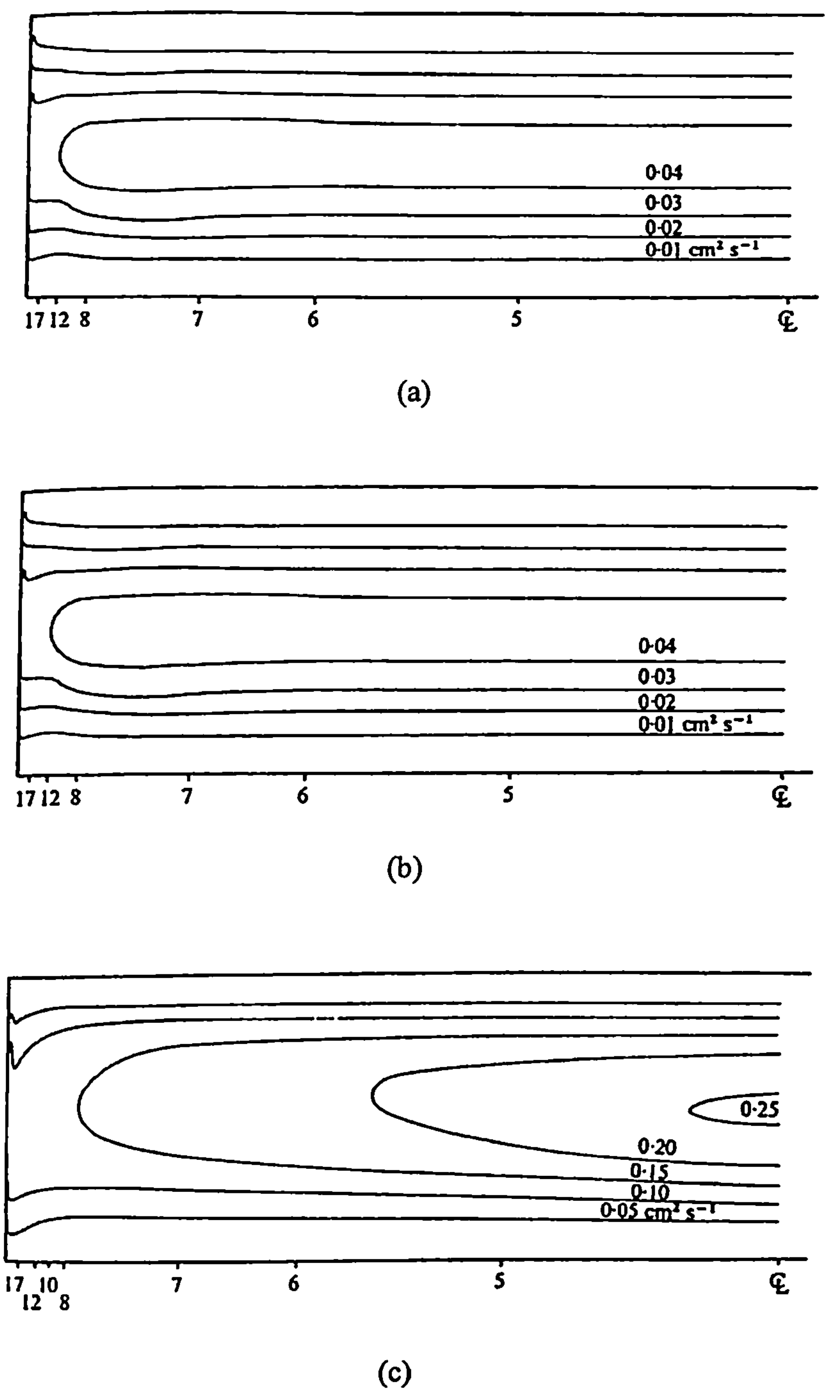

Figure 2.11 Streamlines from Imberger (1974) for (a) $Ra = 2.34\times10^{6}$, (b) $Ra = 8.04\times10^{6}$, and (c) $Ra = 1.11\times10^{8}$.

where H/L is the aspect ratio of height/width.

Bejan et al. (1981) also measured natural convection in shallow enclosures with higher Rayleigh numbers (based on the height of the enclosure) of 2×10^8 to 2×10^9 and aspect ratio of 0.0625. This investigation focused on the flow and temperature patterns in the core region. The results of flow visualization experiments are shown in Figures 2.12 and 2.13. The flow patterns indicate that, contrary to lower Rayleigh number flows, the core flow structure was not parallel to the horizontal walls. There were horizontal wall jet flows along the two insulated horizontal walls, but similar to larger aspect ratio cavities there were two secondary flows outside of these wall jets. The results also indicate there is a lack of symmetry between the two ends of the core flow. The convective heat transfer correlation between the two ends was given by

$$Nu = 0.014Ra^{0.38}. \tag{2.12}$$

Yewell et al. (1982) later observed similar horizontal velocity profiles in experiments in a shallow enclosure at a high Rayleigh number of 1.28×10^9.

When the aspect ratio of an enclosure is less than one, the area of the top and bottom walls begin to account for the majority of the enclosure surface area. In this case, the design of the top and bottom walls can influence the heat transfer characteristic of the flow inside the enclosure. Sernas and Lee (1981) investigated the heat transfer rates inside rectangular air enclosures with top and bottom walls made from low thermal conductivity foam rubber and constant temperature plates kept at the vertical wall temperatures. The schematic of the geometry of the enclosures are shown in Figure 2.14. The enclosure aspect ratios were between 0.1 and 1. Figure 2.15 shows the local heat flux

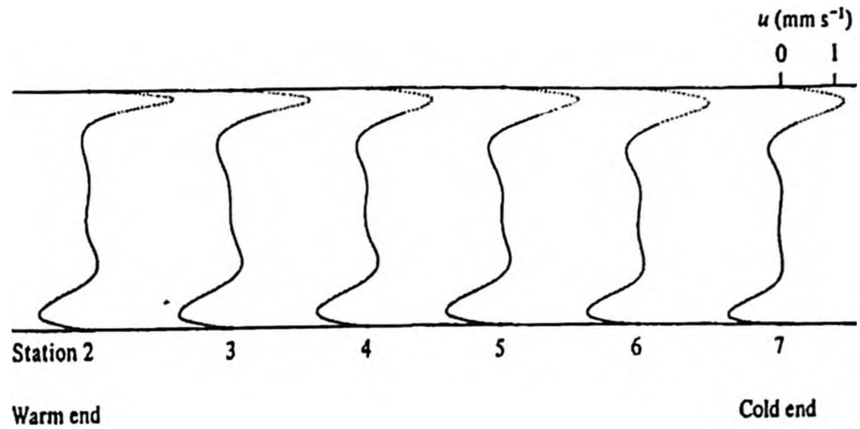

Figure 2.12 Horizontal velocity profiles from Bejan et al. (1981) for $Ra = 1.59 \times 10^9$ and aspect ratio of 0.0625.

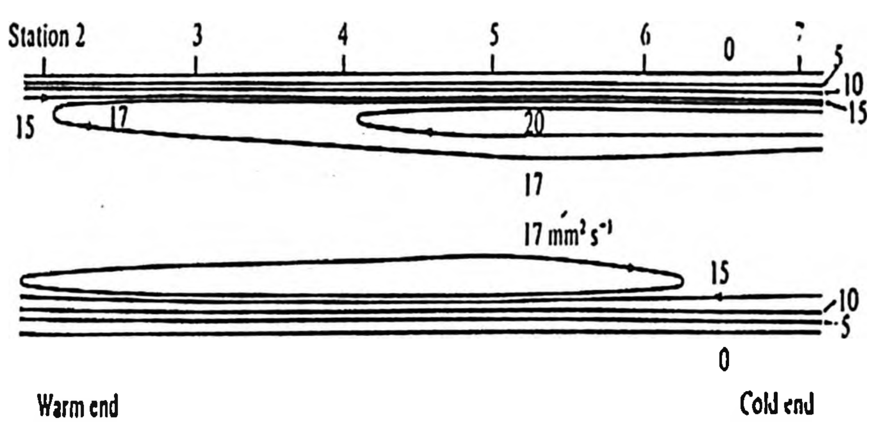

Figure 2.13 Streamline pattern for the core region from Bejan et al. (1981) for $Ra = 1.59 \times 10^9$ and aspect ratio of 0.0625.

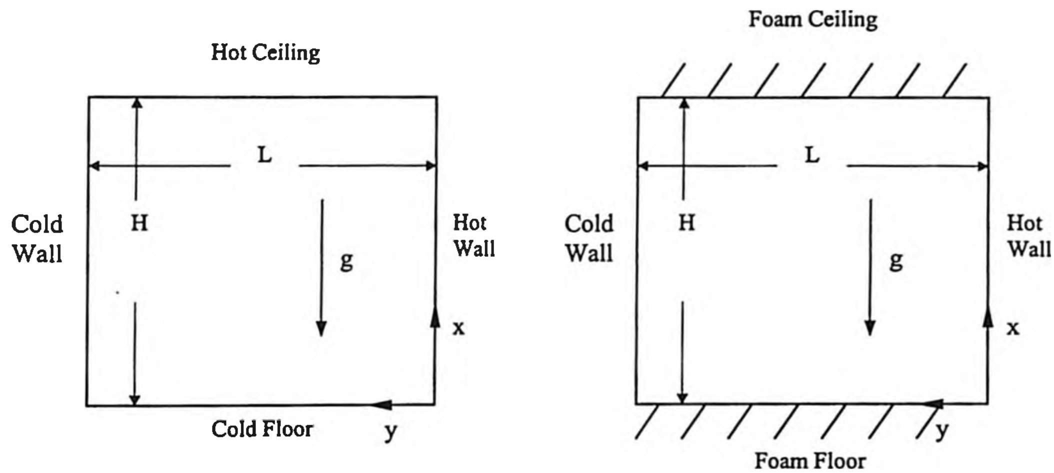

Figure 2.14 Schematic of the geometry of the enclosures investigated by Sernas and Lee (1981).

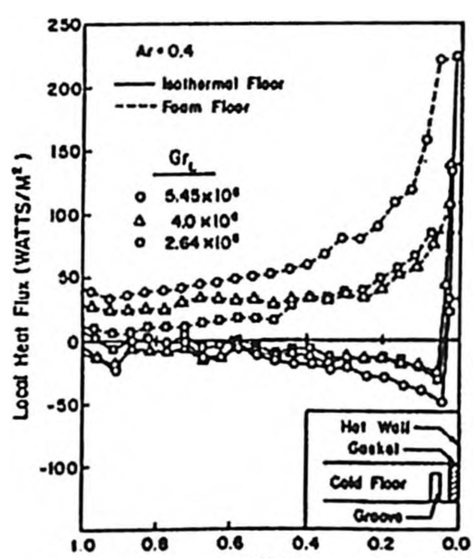

Figure 2.15 Heat flux distribution along the floor from Sernas and Lee (1981) for an aspect ratio of 0.4.

distribution along the floor of the enclosures with aspect ratio 0.4. They found that the amount of heat entering into the cavity from the foam floor was larger than the heat taken up by the isothermal floor from the cavity. This indicates that for this aspect ratio, the isothermal floor that was kept at the same temperature as the cold vertical wall is more like an adiabatic floor than the foam floor. The magnitude of the average heat flux at the floor as a function of Grashof number and aspect ratio is shown in Figure 2.16. They found that in the aspect ratio range of 0.4 to 1, the isothermal floor approximates the adiabatic boundary condition much better than the foam floor, and at aspect ratios less than 0.2 the foam floor seems to produce a better adiabatic condition. A comparison of the average heat flux from the hot vertical wall for all the isothermal and foam enclosures is shown in Figure 2.17. Sernas and Lee (1981) found that the Nusselt number is a function of Grashof number, and the thermal boundary conditions on the top and bottom wall influence the heat transfer characteristic of the cavity significantly.

Drummond and Korpela (1987) also investigated the effect of thermal boundary conditions of the top and bottom wall on the natural convection in a shallow cavity. However, they focused on the difference of the conducting and insulated top and bottom boundaries. The authors found that for fluids of small Prandtl number, the differences in the flow patterns in these two cases were small and the strength of the circulation in the cells was weaker when the boundaries were insulated.

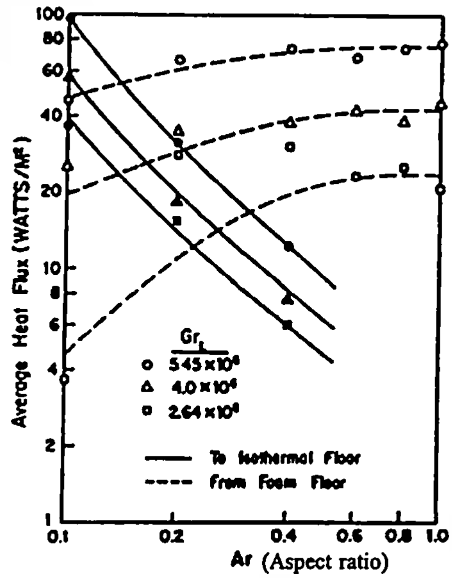

Figure 2.16 Average heat flux to isothermal floor and from the foam floor from Sernas and Lee (1981).

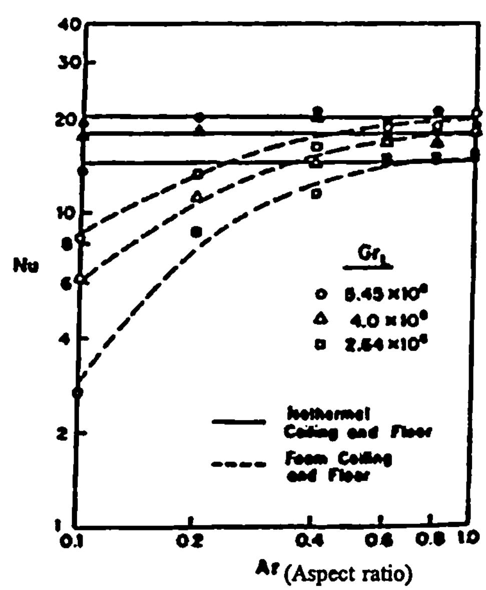

Figure 2.17 Comparison of Nusselt numbers, based on hot wall average heat flux, in isothermal and foam enclosures from Sernas and Lee (1981).

2.2 Natural convection in a horizontal cylinder

Brooks and Ostrach (1970) investigated the natural convection of silicone oil inside a horizontal cylinder with imposed temperatures at two fixed points on the circumference of the cylinder. They found that the motion of the interior core region consisted of two small counter clockwise rotating cells as shown in Figure 2.18. The temperature profiles across the cylinder at four different cross sections are shown in Figure 2.19. They found that the fluid was thermally stratified in the central region of the cylinder with a constant temperature gradient.

Kimura and Bejan (1980) examined the natural convection in a horizontal cylindrical cavity with a diameter to length ratio of 0.112 filled with distilled water that was heated and cooled at the two ends. The Rayleigh number based on diameter was 10^8 to 10^{10}. They found a flow pattern similar to the rectangular enclosure with two horizontal wall jets driven by natural convection. The warm jet moves toward the cold end along the top of the cylinder, while the cold jet travels in the opposite direction along the bottom. The fluid in the central region was stagnant and stratified with a temperature profile that varied linearly with the depth. The temperatures on the horizontal planes were uniform except close to the vertical end-walls. At high Rayleigh number, the temperature difference between the top and bottom was of the same order of magnitude as the temperature difference between the two ends. The overall Nusselt number for end-to-end heat transfer through the pipe was found to weakly depend on the Rayleigh number.

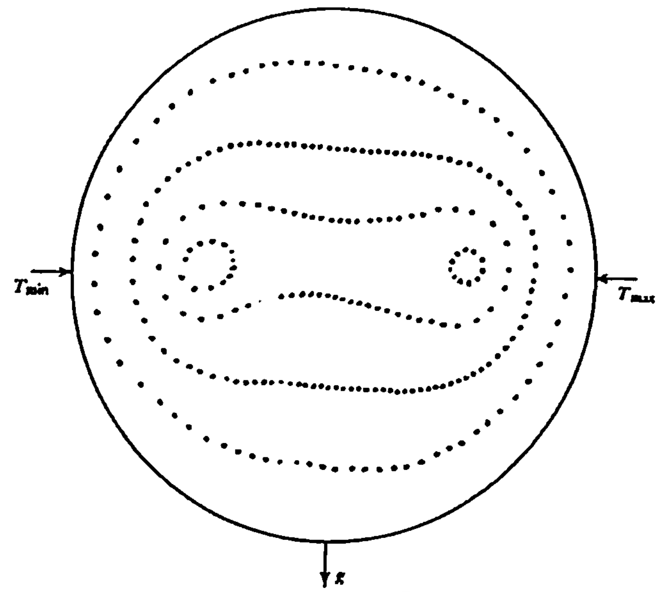

Figure 2.18 Streamline pattern inside a horizontal cylinder with imposed temperatures at two fixed points on the circumference of the cylinder from Brooks and Ostrach (1970).

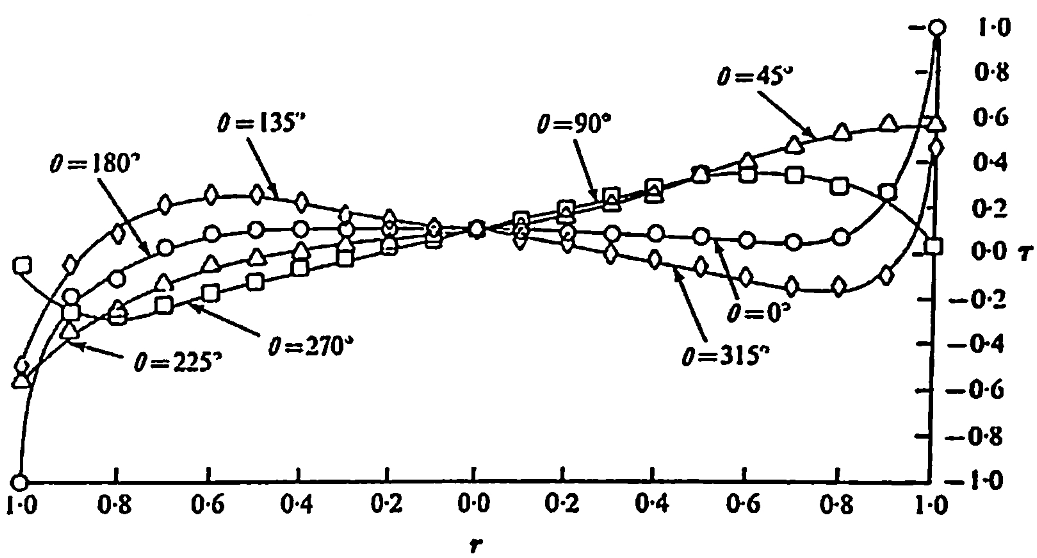

Figure 2.19 Temperature profiles along four diameters from Brooks and Ostrach (1970), where □ is the vertical diameter, and r is radius of the cylinder, θ is the angle from the horizontal line to the radius, and $\tau = [2T - (T_{max} + T_{min})]/(T_{max} - T_{min})$.

2.3 Natural convection in tilted enclosures or other configurations

There have been a number of investigations that have focused on natural convection in cavities with other geometries, including cavities with tilted surfaces or particular thermal boundary conditions. A summary of these investigations is shown in Table 2.4. For example, Dropkin and Somerscales (1965) performed an experiment to examine the natural convection heat transfer in tilted rectangular cavities as shown in Figure 2.20 for Rayleigh number ranging from 5×10^4 to 7.17×10^8 and aspect ratios varying from 4.41 to 16.56. The cavities had two parallel copper plates and four insulated plates. The working fluids for the experiments were water, silicone oils, and mercury with Prandtl numbers ranging from 0.02 to 11,560. The authors developed a correlation for confined working fluids given by

$$Nu = C(Ra)^{1/3}(\mathrm{Pr})^{0.074}, \tag{2.13}$$

where Nu is Nusselt number based on the distance between the copper plates L, and C is a constant that depends on the angle of inclination. They found that the values of C varied from 0.069 for the horizontal case with the hot wall below the cold wall to 0.049 for the vertical orientation. They found that a change in the aspect ratio from 4.41 to 16.56 did not affect the correlation for the vertical case.

Randall et al. (1979) performed an experimental investigation of natural convection in tilted rectangular enclosures with Grashof numbers of 4×10^3 to 3.1×10^5, aspect ratios of 9 to 36 and inclination angles relative to the horizontal of 45° to 90°. They found that the empirical correlation for the heat transfer in inclined enclosures

Investigators	Approach	Study Area	Findings
Dropkin and Somerscales (1965)	Experimental	Convective heat transfer in liquids confined by two parallel plates and inclined at various angles. $5\times10^4 < Ra < 7.17\times10^8$, 0.02<Pr<11,560	The heat transfer coefficients at the different angles can be determined from the relationship $Nu = C(Ra)^{1/3}(\Pr)^{0.074}$
Ozoe et al. (1974)	Finite-difference methods and experiment	Two-dimensional natural circulation in an inclined cavity heated on one side and cooled on the opposing side.	The mode of circulation changed with the angle of inclination and aspect ratio.
Arnold et al. (1976)	Experimental	The effect of angle of inclination on heat transfer across a rectangular cavity. $10^3 < Ra < 10^6$; aspect ratio=1,3,6 and 12.	Comparison was made with previous theoretical analysis; a scaling law was derived that was valid for tilt angles varying from 0° to 90°.
Chu et al. (1976)	Numerical	The effect of heater size, location, aspect ratio, and boundary conditions on the 2-D laminar natural convection in rectangular cavity.	The computed flow patterns were found to be in agreement with experimental results.
Flack et al. (1979)	Experiment using an interferometer	The heat transfer rates of a laminar convection air flow in 2-D triangular enclosure. $2.9\times10^6 < Gr < 9.0\times10^6$.	Results approximately agreed with rectangular enclosure results.
Meyer et al. (1979)	Experiment using an interferometer	Local and average heat transfer coefficients for natural convection between two parallel walls separated by slats. Ra up to 7×10^4.	The effects of Rayleigh number, tilt and slat angles, as well as aspect ratio on Nusselt number were determined.
Randall et al. (1979)	Experiment using an interferometer	The natural convective heat transfer in a rectangular enclosure with various tilt angles. $4\times10^3 < Gr < 3.1\times10^5$, aspect ratio between 9 and 36.	Correlations were developed for local and average Nusselt number. The tilt angle influenced the average heat transfer. Based on heat transfer mechanisms, a method for characterizing the flow regimes was proposed.
Flack (1980)	Experimental	The natural convective heat transfer in triangular air-filled enclosures heated or cooled from below wall.	The geometry was able to represent the conventional attic space of a house during winter and summer conditions.
Turner and Flack (1980)	Experiment using an interferometer	The heat transfer rates of laminar convective air flow in rectangular cavity with one isothermal hot vertical wall, a concentrated cooling strip on the opposing wall.	Correlations were obtained. Measuring data indicated the dependence of heat transfer rates on the geometric parameters.
Anderson and Bejan (1981)	Theoretical analysis and experiment	The heat transfer across a single or double partition that divided a fluid-filled rectangular cavity into two differentially-heated chambers.	The relationship between overall heat transfer and the degree of the thermal stratification on both sides of the partitions was determined. The net heat transfer $\propto (1+n)^{-0.61}$.
Bajorek and Lloyd (1982)	Experiment using an interferometer	Natural convection heat transfer inside a 2-D, partitioned rectangular enclosure of aspect ratio 1. $1.7\times10^5 < Gr < 3.0\times10^6$.	The partitions significantly influenced the convective heat transfer. The unsteady core region affected the flow along the vertical isothermal walls.
Elsherbiny et al. (1982)	Experimental	The natural convection heat transfer across vertical and inclined air layers. Aspect ratio between 5 and 110, $10^2 < Ra < 2\times10^7$.	Correlation equations were obtained that allowed the heat transfer across the inclined cavity to be calculated.
Lin and Bejan (1983)	Experimental	Natural convective heat transfer in a rectangular enclosure with internal partition.	The heat transfer rate and flow pattern were influenced by the aperture ratio.
Poulikakos and Bejan (1983)	Experimental	Steady natural convective heat transfer in a triangular space (attic-shaped). $10^6 < Ra < 10^9$.	Aspect ratio played a minor role in the Nu. And Nu depended on the Ra.
Filis and Poulikakos (1986)	Experimental	Natural convection in a parallelepipedal enclosure driven by a single wall with a cold and a hot region. $10^{10} < Ra < 5\times10^{10}$.	The velocity field in the cavity consisted of four cells. Non-uniform wall temperature affected the heat and flow characteristics.
Hamady and Lloyd (1989)	Experiment and simulation	The effect of inclination on the natural convection heat transfer in an air-filled enclosure. $10^4 < Ra < 10^6$.	The heat flux in the hot and cold boundaries depended on the angle of inclination and the Rayleigh number.
Elsherbiny (1996)	Experimental	Natural convection heat transfer in an inclined air-filled rectangular enclosure. $10^2 < Ra < 2\times10^6$.	Some correlations expressing the effect of tilt angle on the average Nusselt number were obtained.
Aydin et al. (1999)	Numerical analysis	Natural convection of air in a 2-D enclosure heated from one side and cooled from the ceiling. $10^3 \le Ra \le 10^7$. The aspect ratios ranged from 0.25 to 4.0.	The effect of Ra on heat transfer was significant when the aspect ratio more than1; and the influence of aspect ratio was strong when it less than 1 and Ra was high.
Leong et al. (1999)	Experimental	Natural convection Nusselt number for a cubical, air-filled cavity. One pair of opposing walls were kept at different temperatures (T_h and T_c) and the remaining walls had a linear variation from T_c to T_h.	The Nusselt number results were obtained. The results were intended to provide data for a benchmark problem in CFD.

Table 2.4 Summary of investigations of natural convection in enclosures with tilt angle, particular thermal boundary conditions, or other configurations.

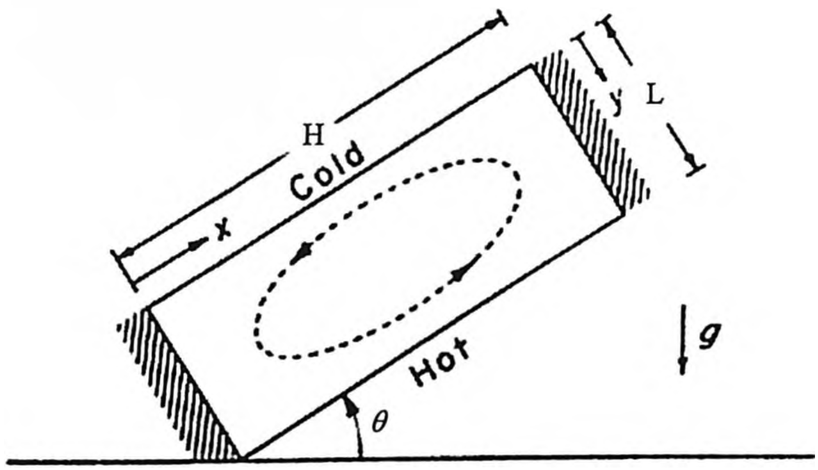

Figure 2.20 Schematic of the experimental configuration investigated by Dropkin and Somerscales (1965).

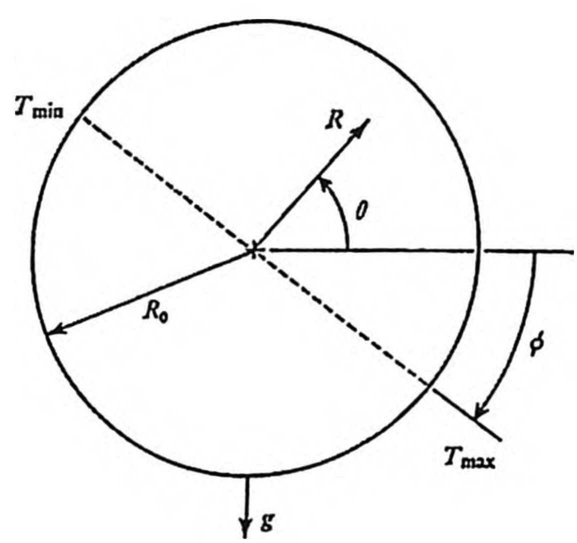

Figure 2.21 Schematic of the geometry from Brooks and Ostrach (1970).

could be represented by

$$\overline{Nu_L} = 0.118\left[Gr_L \Pr\cos^2(\theta - 45)\right]^{0.29}, \tag{2.14}$$

for the parameter range investigated in their experiment.

Elsherbiny (1996) investigated the natural convection heat transfer in a similar inclined rectangular enclosure with an aspect ratio of 20 and Rayleigh number of 10^2 to 2×10^6. They reported the correlation given by

$$Nu_L = \left[1 + \left(0.212 Ra_L^{\ 0.136}\right)^{11}\right]^{1/11}, \quad \text{for } \theta{=}180^{\circ}, \tag{2.15}$$

$$Nu_L = \left[1 + \left(0.0566 Ra_L^{\ 0.332}\right)^{4.76}\right]^{1/4.76}, \quad \text{for } \theta{=}120^{\circ}, \tag{2.16}$$

and

$$Nu_L(\theta) = Nu_L(180^{\circ}) + \frac{180-\theta}{60}\left[Nu_L(120^{\circ}) - Nu_L(180^{\circ})\right], \quad \text{for } 120^{\circ} \le \theta \le 180^{\circ}. \tag{2.17}$$

Brooks and Ostrach (1970) also investigated the natural convection inside a horizontal cylinder with varying heating angle ϕ as shown in Figure 2.21. They found that for small heating angles ϕ, the core region consisted of two small, slowly moving cells similar to the case where the cylinder was heated and cooled on the horizontal points. For large heating angles, the motion consisted of one cell located to the cold side of the cylinder. The core region was thermally stratified in these cases, but the temperature gradient decreased with the increase of the heating angle.

Lin and Bejan (1983) examined the natural convective heat transfer in rectangular cavities fitted with an incomplete internal partition with Rayleigh number ranging from 10^9 to 10^{10} and aperture ratios varying from 0 to 1. They found that the aperture ratio (aperture height / enclosure height) had a strong effect on both the heat transfer rate and the flow pattern. Flack et al. (1979) examined the laminar natural convection flows in two-dimensional triangular enclosures consisting of a heated wall, a cooled wall and an adiabatic bottom with Grashof number varying from 2.9×10^6 to 9.0×10^6 and aspect ratios (enclosure height/base width) ranging from 0.29 to 0.87. They found that the angle between the hot and cold walls had almost no effect on the local Nusselt numbers, and the overall Nusselt numbers were in approximate agreement with the data obtained from a rectangular enclosure.

Chapter 3 Experimental Methodology

The objective of this investigation was to characterize how the heat transfer inside a square cavity heated and cooled on the side walls was affected by changes in the thermal boundary conditions on the top and bottom walls. The experimental facilities used in the investigation are presented first. The experimental procedure and the data analysis procedure are then discussed in detail.

3.1 Experimental Facility

The experiments were performed for the cavity shown in Figures 3.1 – 3.4. The cavity was designed with a height of 304.8 mm (1'). The right vertical wall of the cavity was designed to be movable so that the width of the cavity could be adjustable from 0 to 609.6 mm (2'). The experiments were performed here for a cavity with a width of 304.8 mm (1') so the height was equal to the width. The depth of the cavity was 914.4 mm (3') so that the flow in the cavity should be approximately two-dimensional. The cavity was designed so that the left vertical wall and the top wall could be maintained at high temperatures using heaters. The right vertical wall, that was movable, and the bottom wall were designed with cooling channels so that the heat could be removed from the two walls and these walls could be maintained at low temperatures. The ends of the cavity were sealed with clear glass windows. The cavity was insulated using OFI-48 insulation

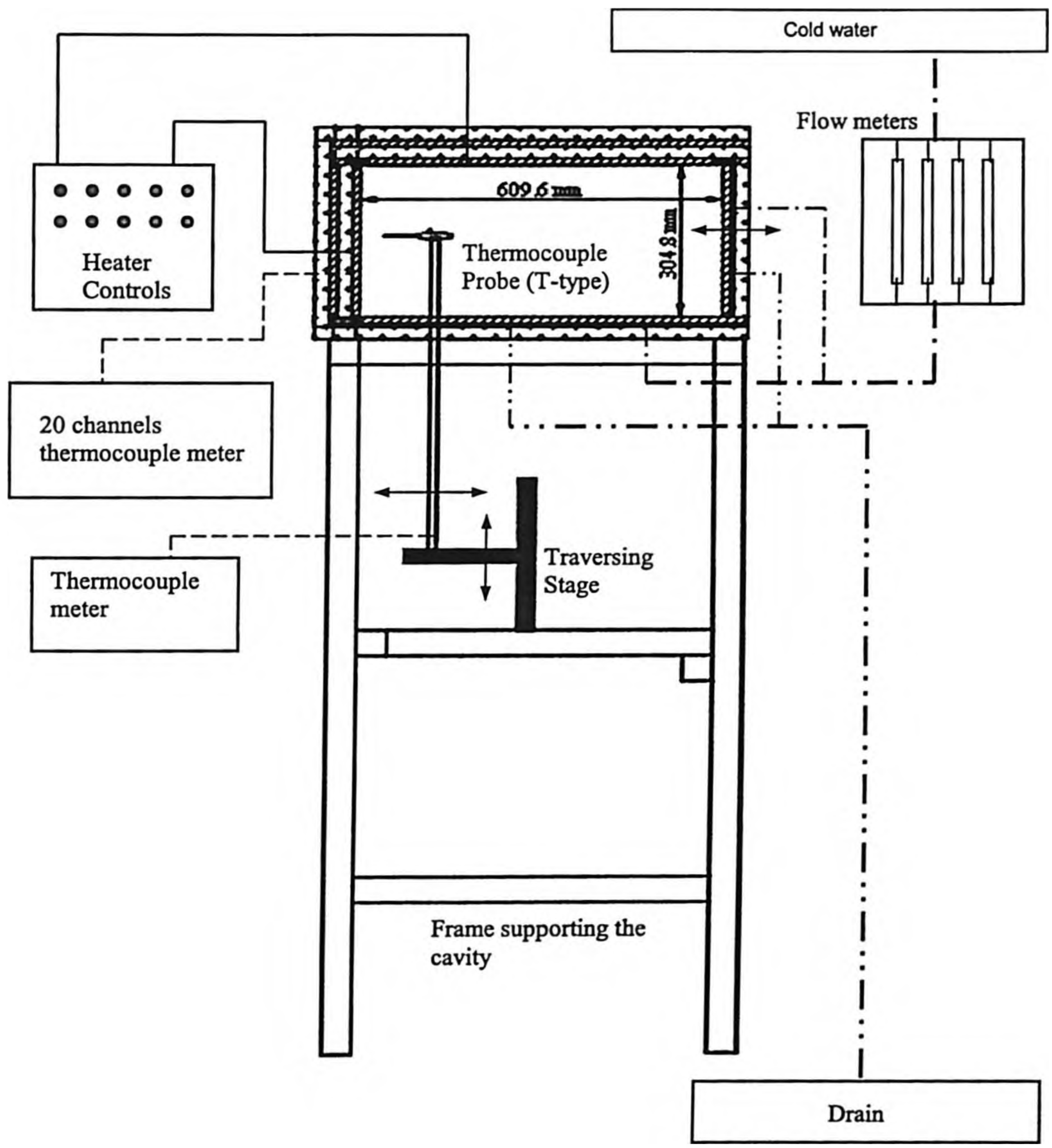

Figure 3.1 Schematic of the experimental facility.

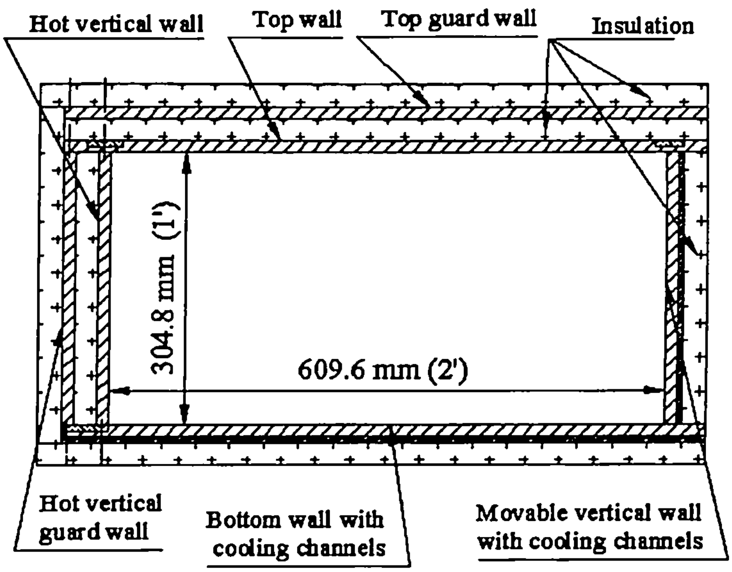

Figure 3.2 Detailed cross section of the cavity.

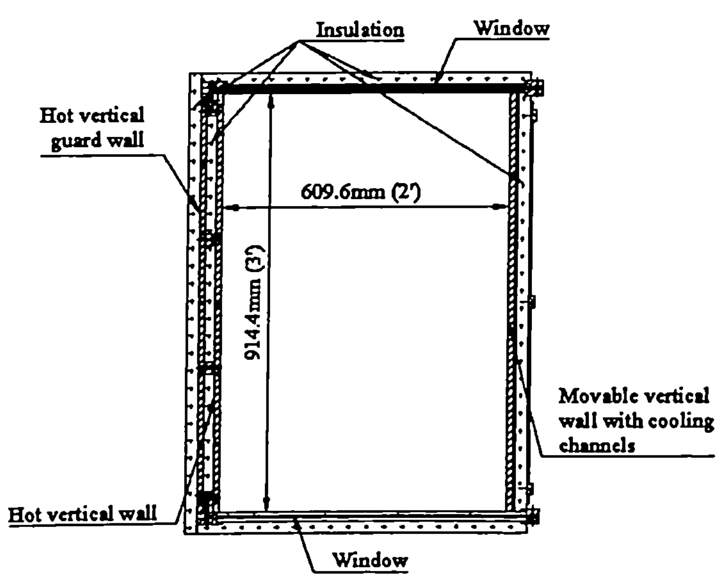

Figure 3.3 Detailed top view of the cavity.

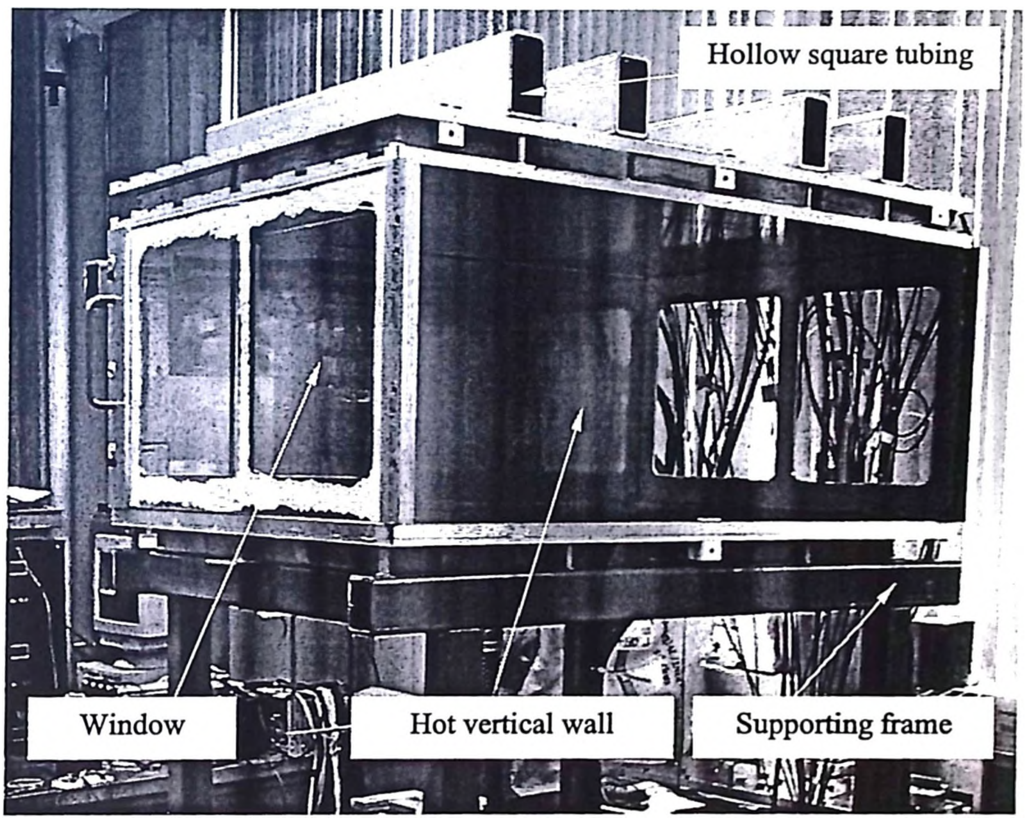

Figure 3.4 Photograph of the cavity.

to reduce heat transfer to the ambient. The cavity was supported on a 1.5m (5') high frame constructed from rectangular tubing. A traversing system was mounted on this frame that was used to move a thermocouple in both horizontal and vertical directions to measure the temperature distribution in the cavity.

The vertical walls and the horizontal walls were constructed from a series of sections and instrumented using thermocouples that were used to measure the surface temperature. For example, the top wall and the hot vertical wall were constructed from two aluminium plates with a thickness of 12.7mm (0.5"). It was estimated that the Biot numbers, Bi, of these plates given by (Holman, 1986)

$$Bi = \frac{hs}{k}, \tag{3.1}$$

were on the order of $10^{-3} \sim 10^{-4}$ so that the temperature distributions in these plates should be approximately uniform. Here h is the heat transfer coefficient for natural convection to the cavity, k is the thermal conductivity, and s is the thickness of the plate. For both walls, a second guard heater wall was attached to the back of these walls to minimize the heat transfer to the ambient. This made it easier to control the temperature of the heated walls and estimated the heat flux into the cavity from the hot vertical wall and the top wall. A layer of OFI-48 with a thickness of 25.4mm (1") was positioned between the inner surfaces and the guard walls to further reduce the heat transfer by conduction.

Schematics of the inner portion of the top wall and the hot vertical wall are shown in Figures 3.5 and 3.6. The plates were divided into sections, with independent heaters,

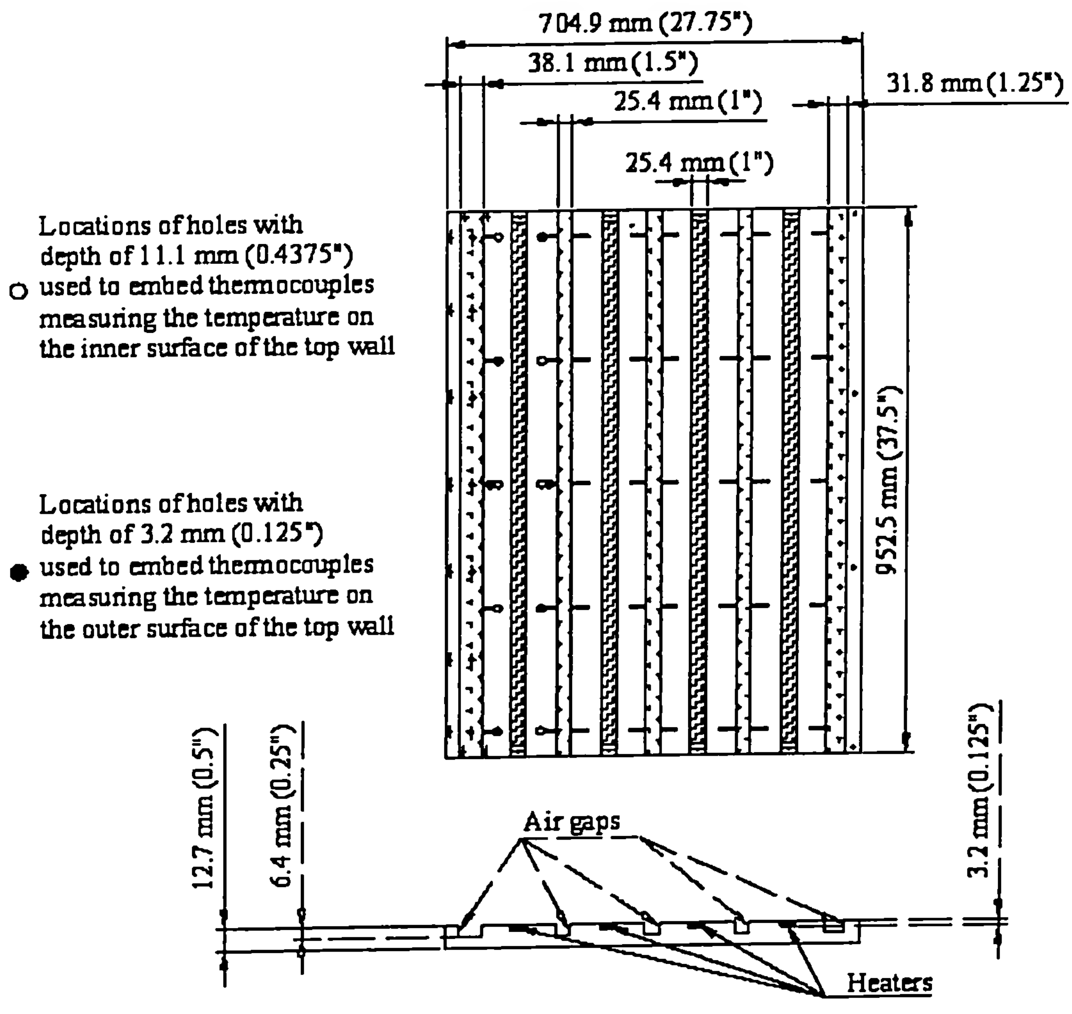

Figure 3.5 Schematic of the top wall.

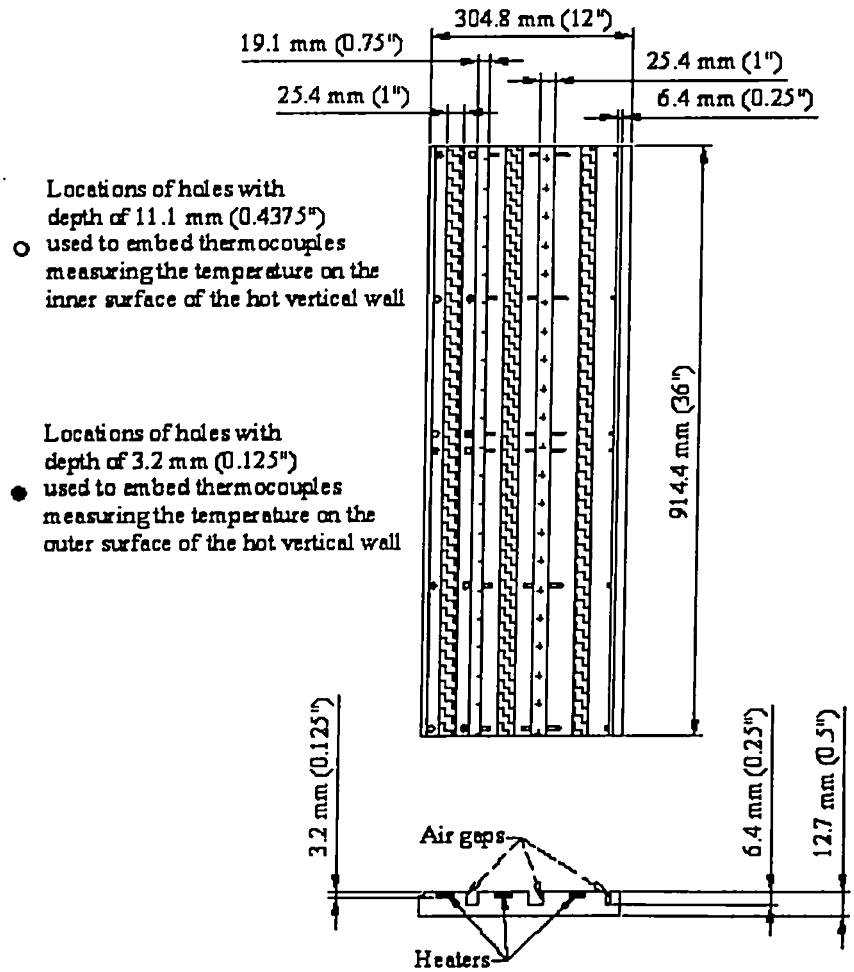

Figure 3.6 Schematic of the hot vertical wall.

by milling grooves with a depth of 6.4mm (0.25") into the back of these plates. The top wall was divided into equally sized sections. For the hot vertical wall, the section on the bottom of the wall was smaller than the rest because the heat flux into the cavity was largest in this region. The size of the other sections on the hot vertical wall increased along the height of the wall. Flexible silicone rubber heaters were embedded into grooves with a width of 25.4mm (1") and a depth of 3.2mm (0.125") machined in the center of these sections. The heaters were adhered using a layer of thermally conductive epoxy adhesive cured at $121^{\circ}C$ for 8 hours. The heaters could provide 0 to 180 W with a maximum temperature of $232^{\circ}C$.

The heaters were powered using a multi-channel variable duty controller that could vary the duty cycle for each of the heaters independently. The voltage and duty cycle for each heater was measured using an oscilloscope and the power for each heater was given by

$$Q = \frac{u^2}{R} \times \textit{duty cycle}, \tag{3.2}$$

where u is the voltage across the resistive heater and R is the resistance of the heater.

The temperature distribution on the both sides of the top wall and the hot vertical wall were measured using T-type thermocouples embedded in the surfaces at the locations shown in Figures 3.5 and 3.6. Each section of the walls contained 12 thermocouples. Six thermocouples embedded in holes with a depth of 3.2mm (0.125") from the back of the walls were used to measure the outside temperature of the plates, while six embedded in holes with a depth of 11.1mm (0.4375") were used to measure the temperature of the inner surfaces of the walls. The detailed schematic showing how the thermocouples were embedded in the surface is shown in Figure 3.7. The thermocouples were bare wire thermocouples with a diameter of 0.254mm (0.010"). They were insulated using ceramic tubing and Teflon tubing as shown in Figure 3.7. The thermocouple was held in the wall using thermally conductive epoxy adhesive that was used to fill the hole. The thermocouple leads were connected to 24 AWG T-type thermocouple wire at a phenolic terminal block as shown in Figure 3.8 that can withstand temperatures up to $150^{\circ}C$. The six thermocouples located on the outer surface in each section were connected together to determine the average outside temperature of the wall and then connected to a 20-channel thermocouple meter. This was used to estimate the heat transfer from the top wall and the hot vertical wall to their respective guard walls. The thermocouples mounted on the inside of the wall were connected individually to the thermocouple meter.

The structure of the guard walls for the top wall and the hot vertical wall, shown in Figures 3.9 and 3.10, are similar to the structure of the inner surfaces. The guard walls were heated using flexible silicone rubber heaters distributed in four sections on the back of the top guard wall, and in three sections on the back of the hot vertical guard wall. The heaters on the top guard wall were connected in parallel and powered using a variable transformer with maximum current of 10 amps. The output voltage of the transformer was adjusted so that the average temperature on the inner surface of the guard wall was approximately equal to the average temperature on the outside of the top wall. Similarly, the three heaters on the hot vertical guard wall were connected in parallel to a transformer

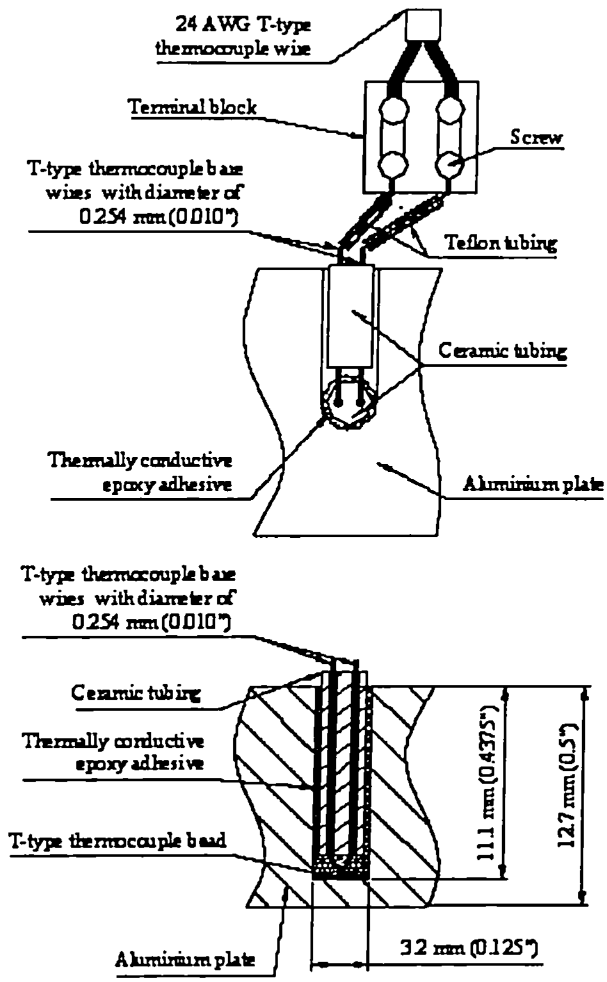

Figure 3.7 Detailed structure of thermocouple embedded in the wall.

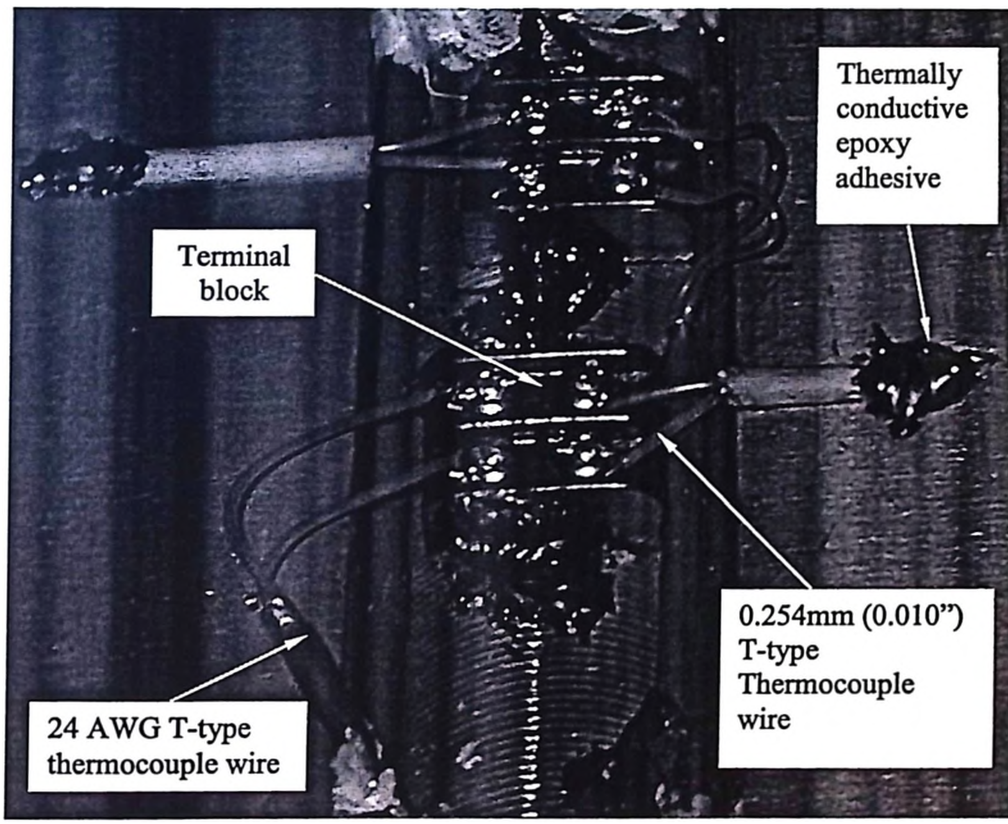

Figure 3.8 Photograph of thermocouple arrangement on the back of the top wall.

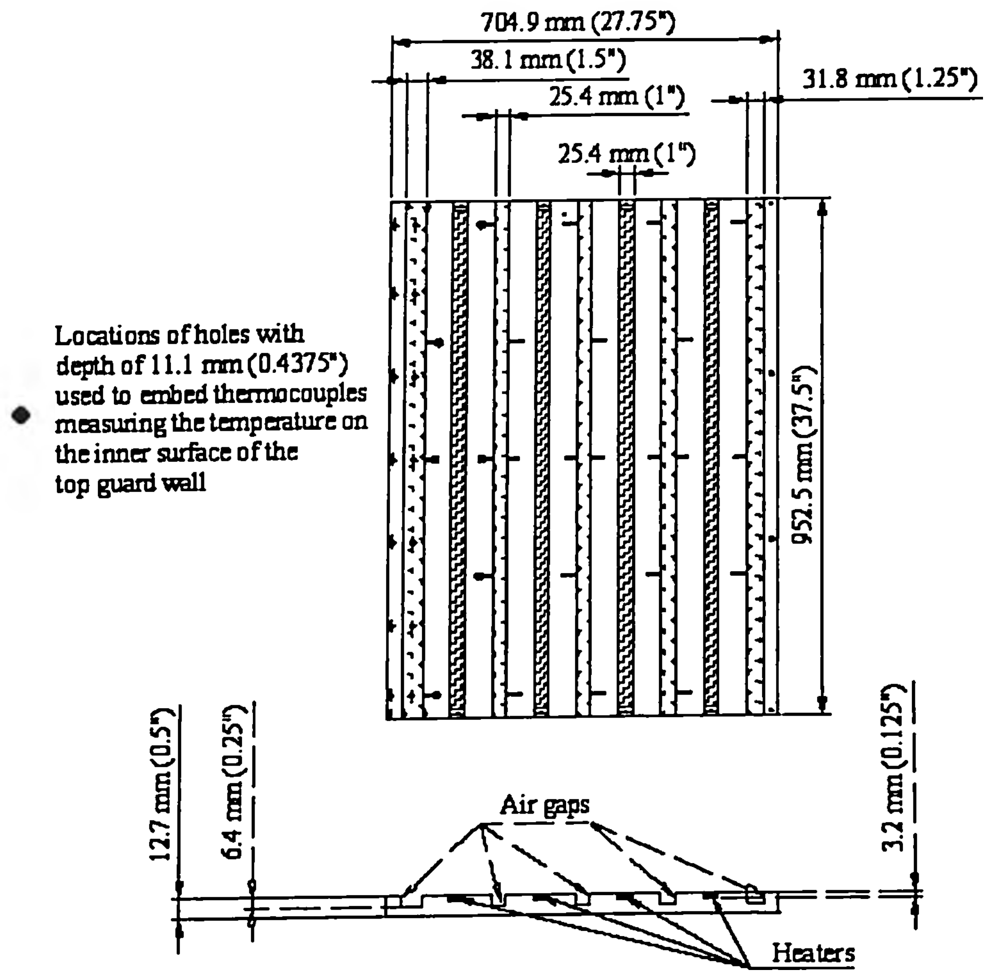

Figure 3.9 Schematic of the top guard wall.

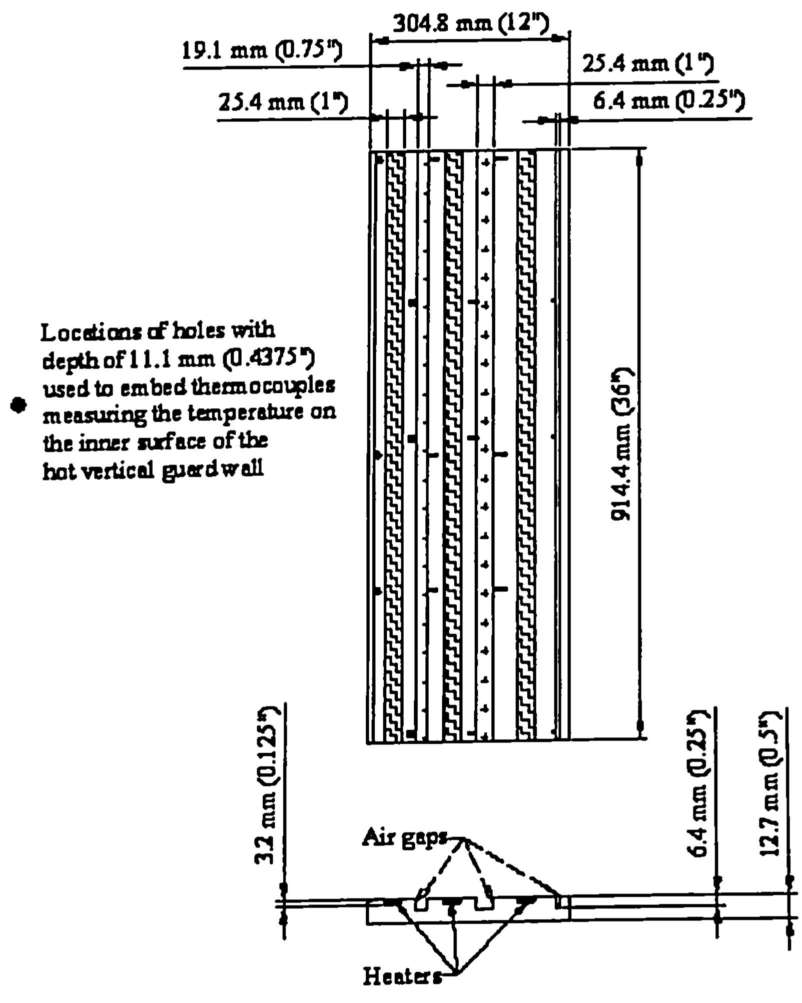

Figure 3.10 Schematic of the hot vertical guard wall.

with maximum current of 7.5 amps. The guard walls included six T-type thermocouples embedded in each of the sections at the same locations as the thermocouples on the outside of the top wall, or the outside of the hot vertical wall. The six thermocouples in each of the sections were connected together and then connected to the 20-channel thermocouple meter so that the average temperature of each section could be determined.

The bottom wall and the movable vertical wall with cooling channels were constructed from two sections as shown in Figures 3.11 and 3.12. The cooling channels were serpentine grooves with a width of 25.4 mm (1") and depth of 6.4 mm (0.25") machined into a 12.7 mm (0.5") thick aluminium plate. A 6.4 mm (0.25") thick aluminium plate was screwed to the back of the plate to close the channels. A thin layer of Epoxy adhesive was used to seal the plates. The 6.4mm thick aluminium plate contained four 12.7 mm (0.5") diameter holes that were inlets and outlets of the water channels as shown in Figures 3.11 and 3.12. Two slots with width of 14 mm (0.55") were machined into the bottom wall so the frame for the movable thermocouple probe could pass through the wall.

The temperature of the bottom wall was measured using 16 T-type thermocouples. These thermocouples were embedded using the same approach as in the heated walls. Four of these thermocouples were located in the centerline of the bottom wall and the other thermocouples were distributed throughout the remaining area. The temperature on the movable vertical wall was measured using 11 T-type thermocouples, three of which were on the centerline.

Municipal water was used for the cooling channels. The cold water first passed

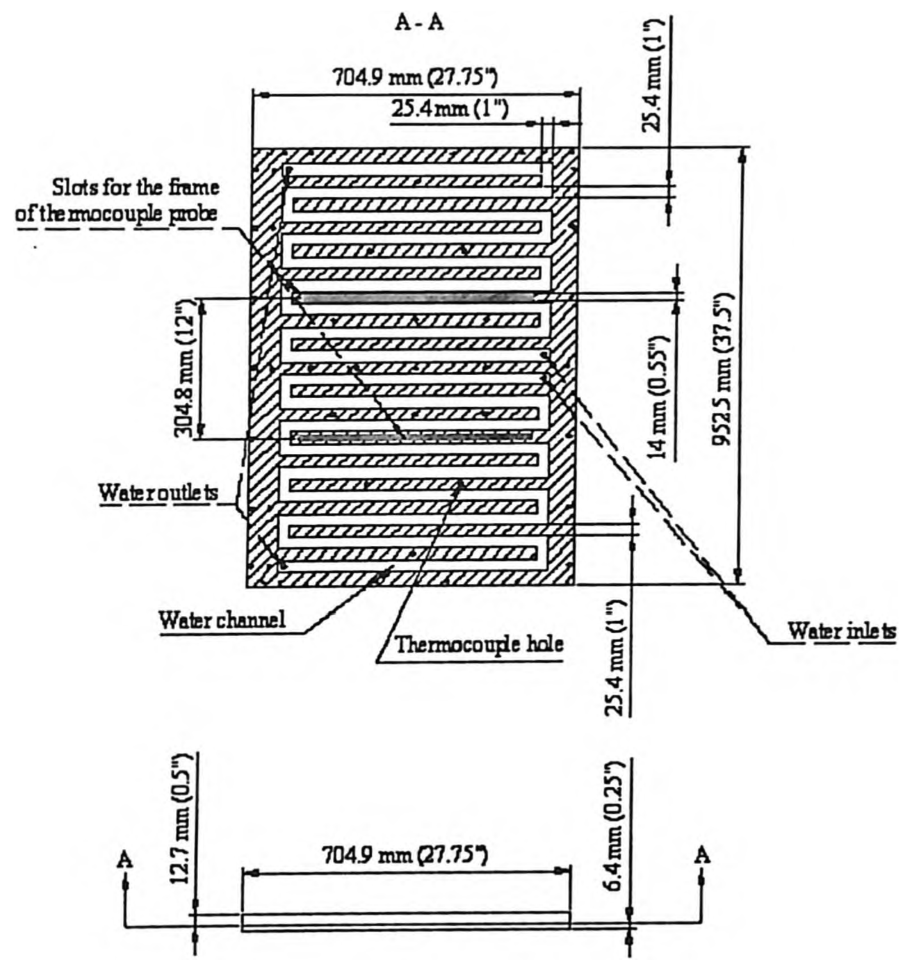

Figure 3.11 Schematic of the bottom wall with cooling channels.

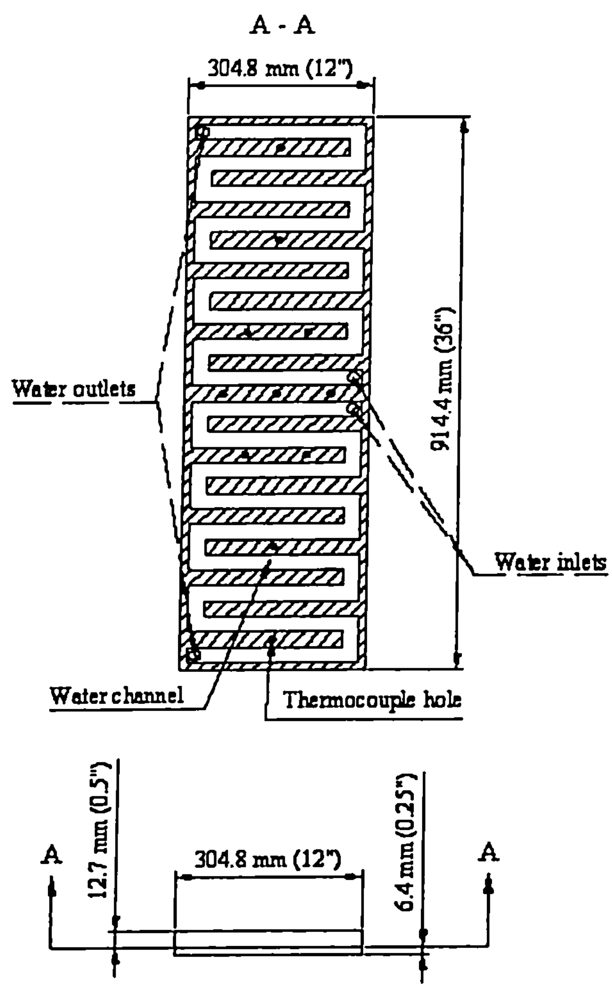

Figure 3.12 Schematic of the movable vertical wall with cooling channels.

through a bank of four COLE-PARMER EW-03227-30 flow meters that were mounted on the supporting frame of the cavity. The maximum flow rate of these flow meters was $8.43\times10^{-3}\,L/s$ and their accuracy was $\pm1.69\times10^{-4}\,L/s$. The flow from two of the flow meters then passed through the two cooling channels on the bottom wall, while the flow from the other two passed through the cooling channels on the movable vertical wall. The water leaving the water channels discharged to the drain. The water temperature at the inlet and outlet of the channels was measured using eight T-type thermocouples mounted at the beginning and the end of the flow loops. The energy removed from the cavity was estimated as

$$Q=\dot{m}\,c_P\left(T_{w,o}-T_{w,i}\right), \tag{3.3}$$

where $\dot{m}$ is the mass rate of the water and c_P is the specific heat of the water, while $T_{w,o}$ and $T_{w,i}$ are the outlet and inlet temperatures of the water, respectively.

The design of the end walls containing the glass windows is shown in Figure 3.13. The frame for the windows was machined from aluminum plate with a thickness of 6.4 mm (0.25") so the frame was strong enough to support the weight of the top wall. The outside dimensions of both frames were 686 mm (27") × 305 mm (12"). Two panes of glass with a thickness of 6.4 mm (0.25") were attached to each frame using a thin layer of Epoxy adhesive (RTV 108). This allowed an air gap of 6.4 mm (0.25") between the two panes of glass to reduce the heat loss from both ends of the cavity.

The walls were connected using screws. The junctions of the walls were sealed by inserting and compressing a thin layer of mineral fiber paper with conductivity of

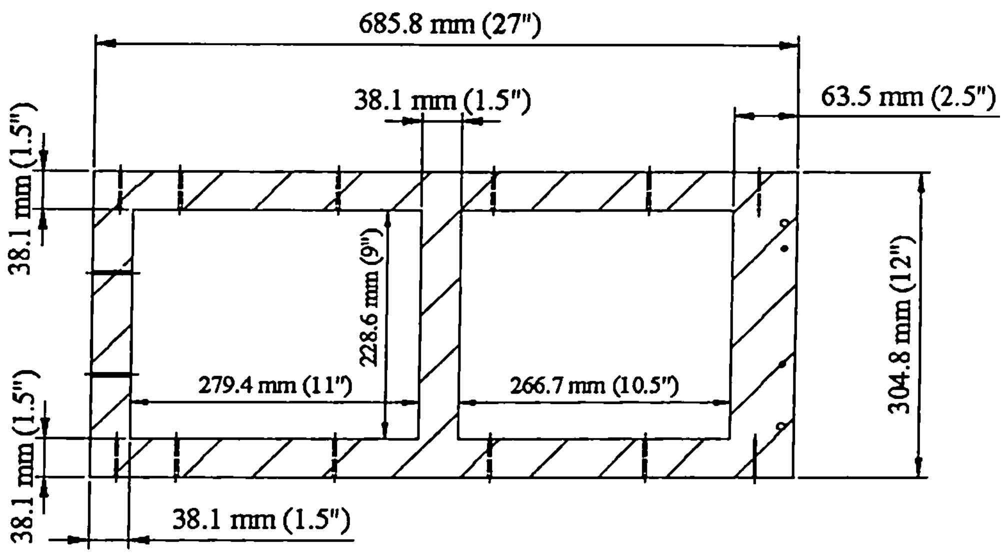

Figure 3.13 Structure and dimensions of the frame of the end glass windows.

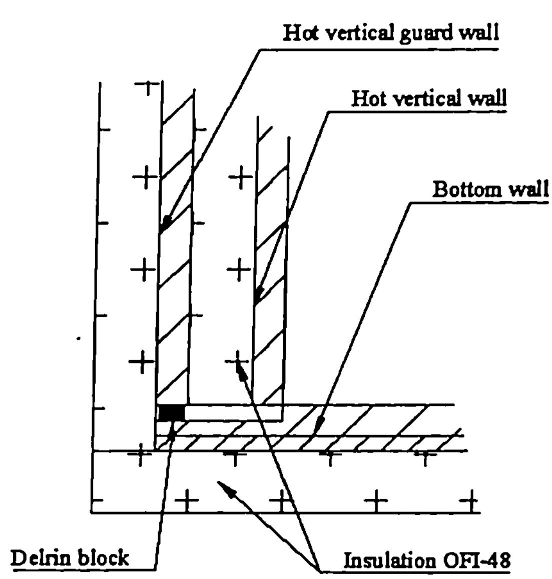

Figure 3.14 Detailed structure of the corner between the hot vertical wall, hot vertical guard wall and the bottom wall with cooling channels.

$0.05 W/m\cdot^{\circ}C$ between them. In order to minimize the heat transfer between the heated walls and the bottom wall, a small air gap was left as shown in Figure 3.14. The hot vertical guard wall was supported by 4 Delrin blocks that were 19.1 mm (0.75") × 10.2 mm (0.4") × 6.86 mm (0.27"). Since the cross sectional area of these blocks was small and the conductivity of them was low, the corner was approximately insulated.

The movable vertical wall was fixed by six aluminum rods. One end of these rods were connected to the back of the movable vertical wall and the other end of the rods were attached to three aluminum bars connected to the edges of the top and bottom walls. The position of the movable vertical wall with cooling channels could be changed by varying the length of these rods. The gap between the movable vertical wall and the other walls was less than 1 mm. This allowed the vertical wall to be moved and minimized the heat transfer among these walls, while not affecting the flow inside the cavity.

The temperature distribution inside the cavity was measured using a thermocouple probe mounted on a frame that was fixed on a traversing stage shown in Figure 3.15. The frame passed through the slots on the bottom wall so that the thermocouple probe inserted into the cavity could move horizontally and vertically. The detailed structure and dimensions of the thermocouple probe is shown in Figures 3.16 and 3.17. Since the thermal boundary layer was very thin, a T-type thermocouple with diameter of 0.051 mm ($0.002''$) was used in the probe. The bare wires of the thermocouple were passed through a thermocouple support that was constructed from two stainless steel tubes with diameters of 1.6 mm (0.0625"). A 26 AWG Teflon tubing was inserted between the bare wire and the inner surface of the stainless steel tubes. The length of the stainless steel

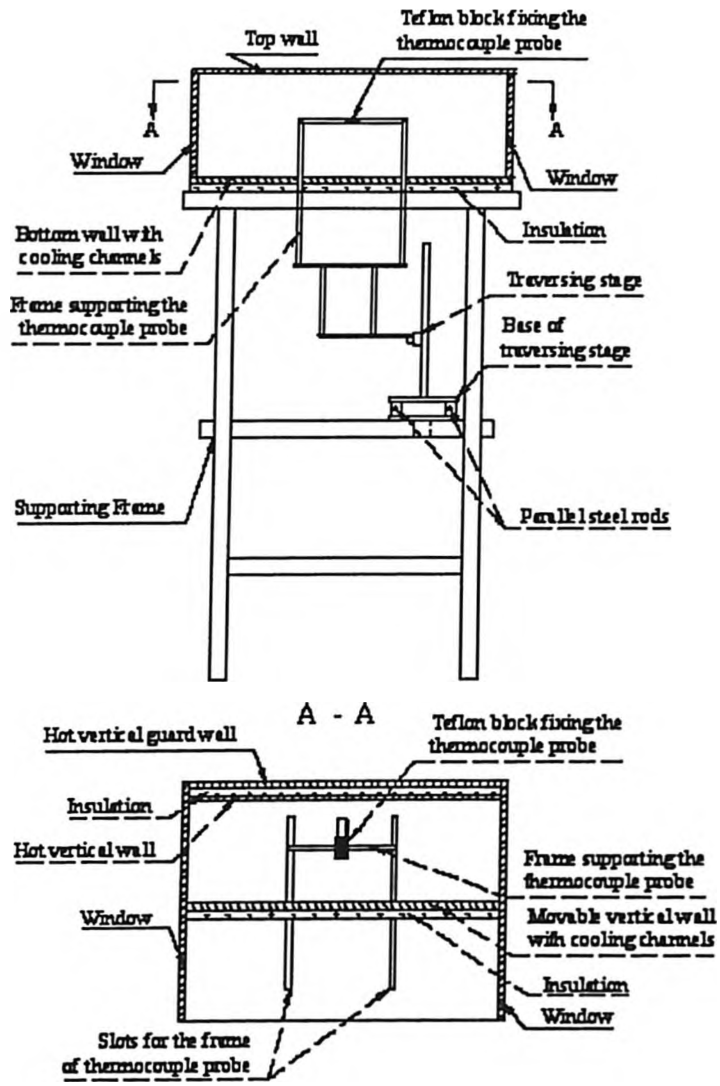

Figure 3.15 Schematic of the measurement traverse for the thermocouple.

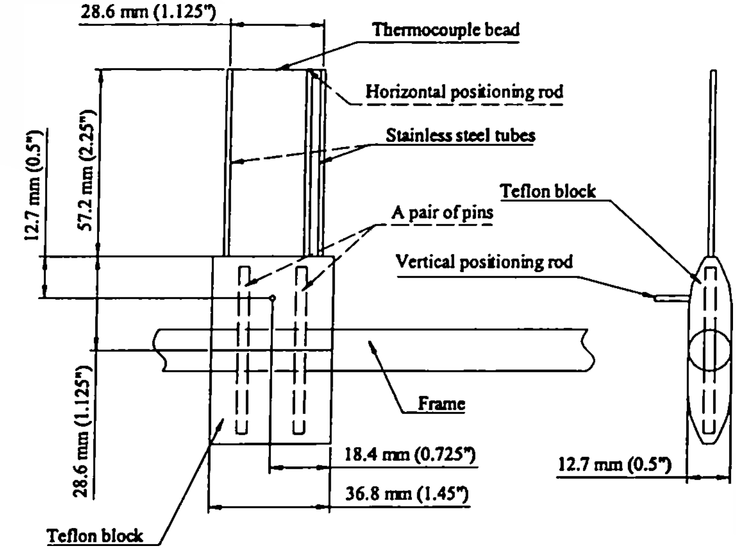

Figure 3.16 Structure and dimensions of the thermocouple probe.

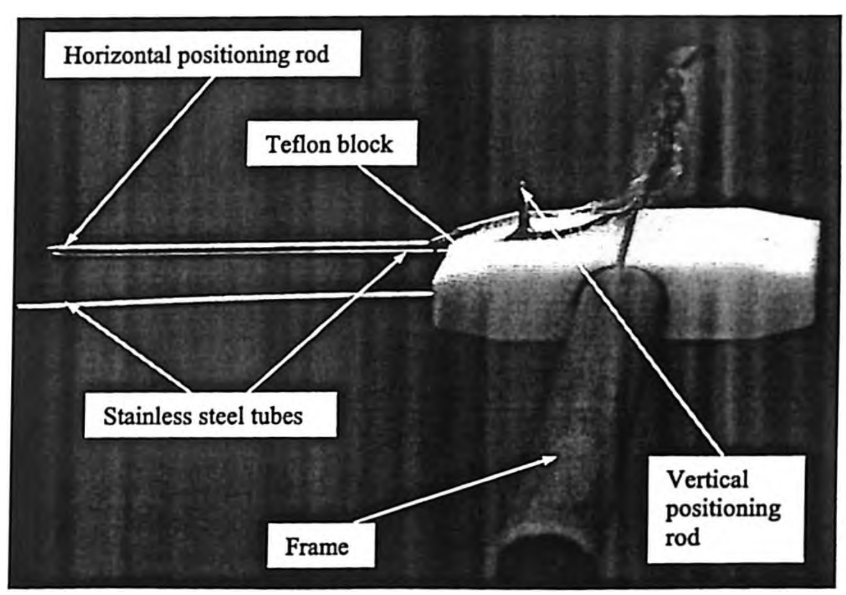

Figure 3.17 Photograph of the thermocouple probe.

tubes was 57.2 mm (2.25") to keep the frame out of the thermal boundary layer. The distance between the two stainless steel tubes was 28.6 mm (1.125") so they would not block the flow near the measurement point. The support was mounted into a Teflon block. The leads from the bare thermocouple wire were connected to a 24 AWG T-type thermocouple wire inside the Teflon block. The entire junction was surrounded and anchored to the Teflon block using an electrically conductive epoxy, Circuitworks CW2400. The 24 AWG T-type thermocouple wires were then connected to a Fluke 52 II thermocouple meter.

The position of the thermocouple bead relative to the hot vertical wall and the top wall was determined using horizontal and vertical positioning rods, that were made from stainless steel rod with diameter of 1.6 mm (0.0625") and mounted into the Teflon block. These rods were connected to electrical leads that could be used to determine when the tips contacted the walls. The distance between the thermocouple bead and the tip of the vertical positioning rod was $17.5mm$. The distance between the thermocouple bead and the tip of the horizontal positioning rod measured using a microscope was found to be 0.7mm. The tension of the thermocouple probe wire was tested using a heat gun as shown in Figure 3.18. Comparison of the position of the thermocouple bead with and without airflow showed no apparent difference as shown in Figure 3.19.

The thermocouple probe was fixed on the frame as shown in Figures 3.16 and 3.17 using a pair of steel pins with diameter of 3.2mm (0.125"). The frame shown in Figure 3.20 consisted of five pieces of stainless steel tubes with diameter of 12.7 mm (0.5") and two pieces of aluminum bars with thickness of 6.4 mm (0.25"). The height of

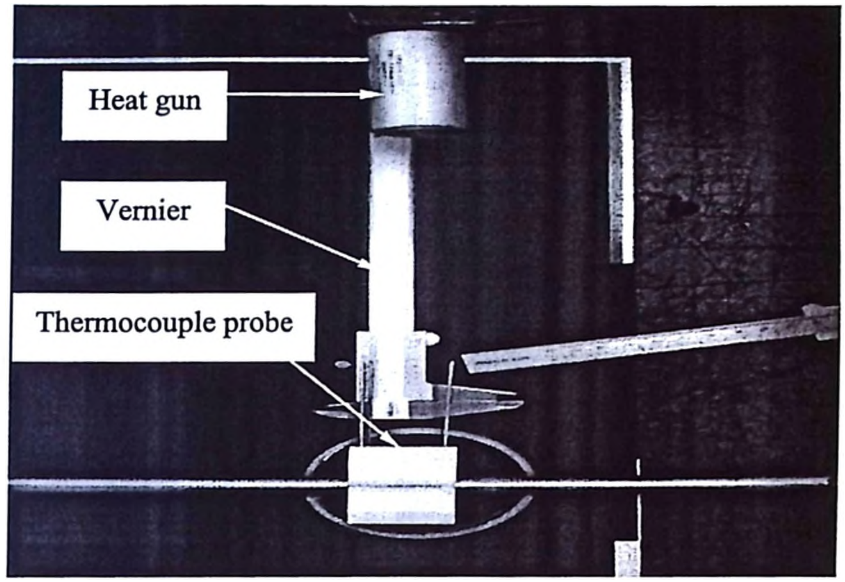

Figure 3.18 Testing the tension of the thermocouple probe wire using a heat gun.

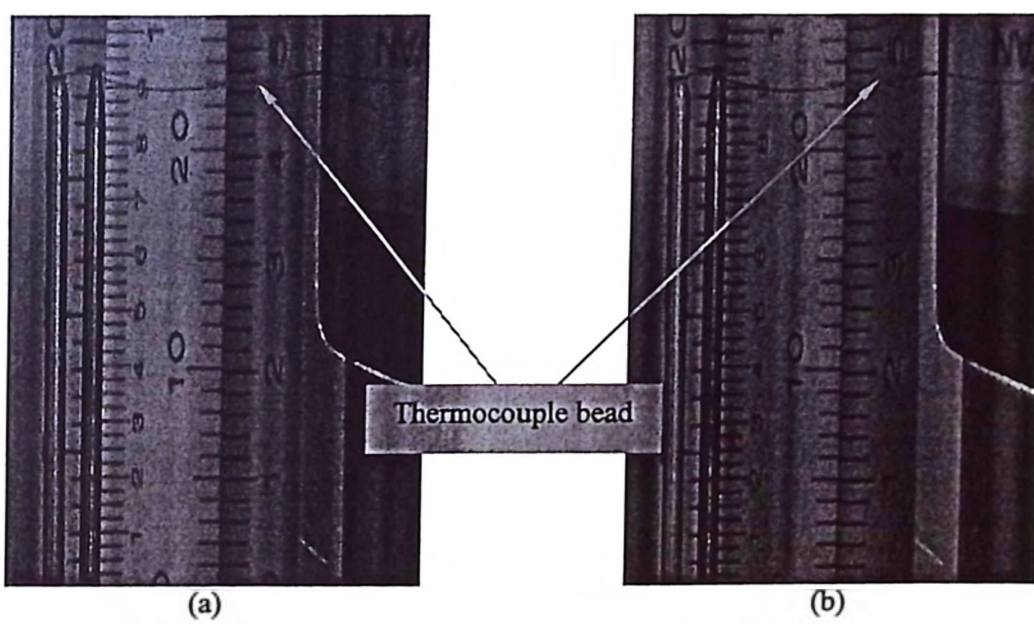

Figure 3.19 Comparison of the thermocouple bead position (a) with airflow blown by a head gun, and (b) without airflow blowing.

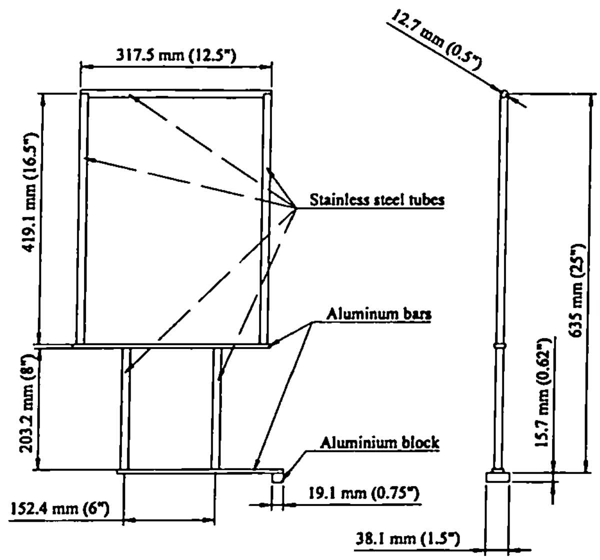

Figure 3.20 Structure and dimensions of the frame supporting the thermocouple probe.

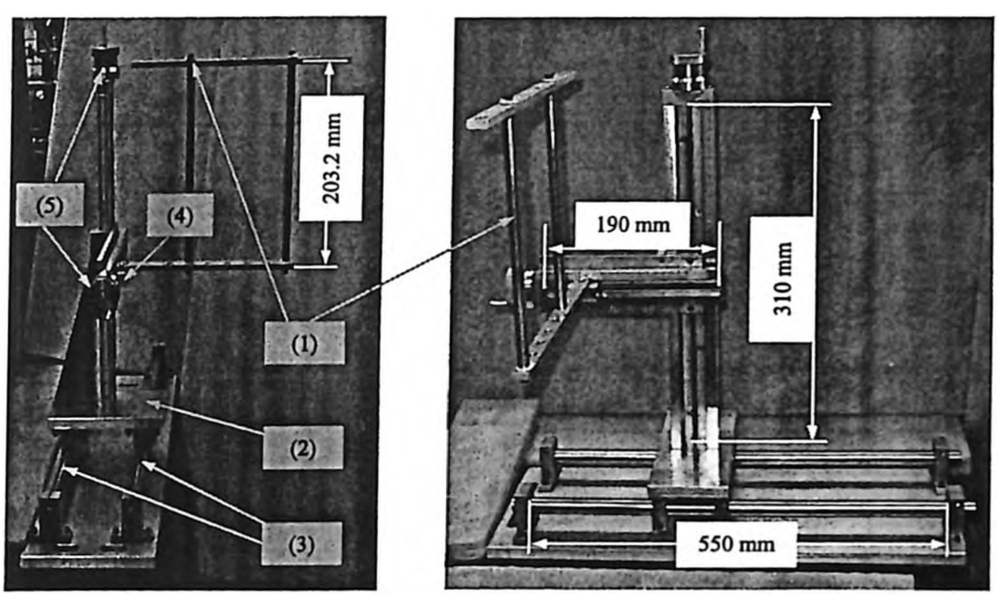

(1) A section of the frame supporting the thermocouple probe; (2) Base of the traversing stage; (3) Parallel steel rods; (4) Aluminium block; (5) Handles with minimum graduation of 0.01mm.

Figure 3.21 Photograph of the traversing stage.

the frame was 635 mm (25"). The frame was mounted on a traversing stage as shown in Figure 3.21 using an aluminum block with the outside dimensions of 38.1 mm (1.5") × 19.1 mm (0.75") × 15.7 mm (0.62"). This traversing stage could move the thermocouple probe through 190 mm in the horizontal direction and 310 mm in the vertical direction by turning the handles shown in Figure 3.21. The base of the traversing stage was mounted on the parallel steel rods that were set on a movable hollow tubing as shown in Figure 3.22. This base could be moved so the thermocouple probe can, in principle, reach any position on the central plane of the cavity. The thermocouple probe moved 1mm for each full turn on the traverse and the minimum graduation in the measurement of the position was 0.01mm. In the experiments, the minimum step size of the thermocouple probe was 0.25mm and the accuracy of the location of the probe was found to be approximately 0.02 mm to 0.03 mm.

3.2 Experimental procedure

A typical thermocouple of the type embedded in the walls (diameter of 0.254mm or 0.010") and the movable thermocouple probe (diameter of 0.051 mm or $0.002^{"}$) were calibrated before the experiments by placing them in a container filled with heated water along with an alcohol thermometer with accuracy $\pm 1^{\circ}C$. The temperature of the water was decreased gradually by adding ice into the container, until the temperature was close to $0^{\circ}C$. A comparison of temperature determined from the $0.010^{"}$ thermocouple and $0.002^{"}$ thermocouple to the reading from the alcohol thermometer is shown in Figure

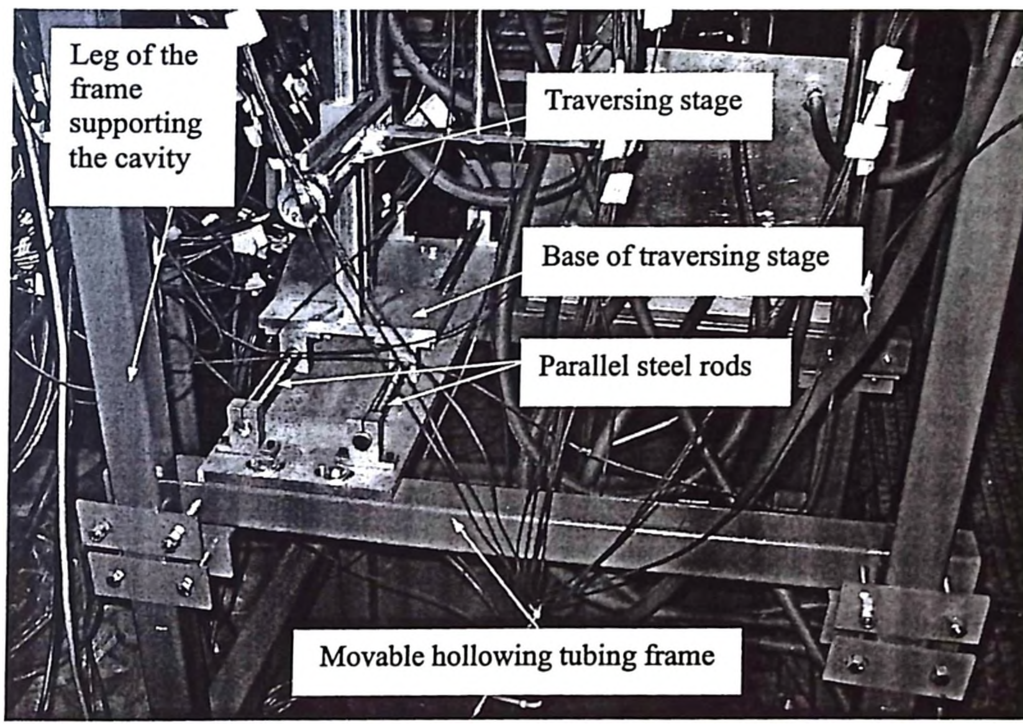

Figure 3.22 Arrangement of the traversing stage.

3.23. The results were curve fit to determine the calibration for the $0.002''$ thermocouple and $0.010''$ thermocouple as shown in Figure 3.23. These calibration equations were then used in the data analysis for all experiments.

In each experiment, the heaters and the cooling flow rate were adjusted to achieve the desired temperatures on the four walls of the cavity. Steady state was assumed to be reached when the variation in surface temperature was within $\pm 0.5^{\circ}C$ for one hour, similar to the approach used by Chinnakotla et al. (1996). In general, it required approximately 10 hours to reach steady state. Once the boundary conditions had reached steady state, the temperature profiles in the cavity were measured at 9 different heights. The distance from the bottom wall and the top wall to the nearest measurement location was 25.4mm ($1''$) or 0.1 of the cavity height, and the distance between the measurement locations was 25.4 mm ($1''$) as well. At each height, the probe was initially moved to the point nearest the hot vertical wall using the positioning rod. The probe was then moved away from the wall in steps of 0.25 mm for the first 13.5 mm, and then in steps of 0.5 mm between 13.5 mm to 23.5 mm from the hot vertical wall. Finally, the probe was moved from 23.5 mm to roughly 88.5 mm away from the hot vertical wall in steps ranging from 1 to 10 mm to determine the temperature profile outside of the thermal boundary layer. It was found that even for the thinnest thermal boundary layer, there were at least seven measurement points in the near wall region of the boundary layer where the heat transfer is predominated by conduction. In all the cases, the number of measurements in this region varied from 7 to 25.

At some measurement points close to the top wall the temperature was found to

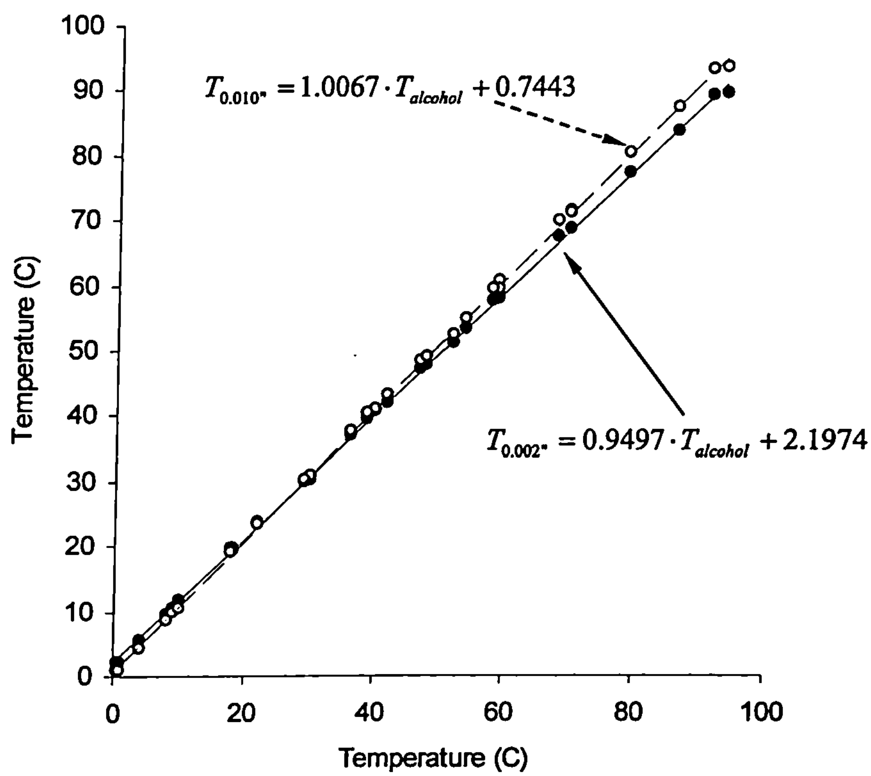

Figure 3.23 Change in the temperature measured with the ○ 0.010" thermocouple and the ● 0.002" thermocouple with temperature measured by an alcohol thermometer.

fluctuate, which was likely due to a change in the flow in this region. The temperature was averaged over a time period of 20 seconds, and the variance in the average temperature over this time period was less than $\pm 0.2^{\circ}C$.

3.3 Data analysis procedure

A typical set of temperature profiles along the hot vertical wall measured in the square cavity is shown in Figure 3.24. The heat transfer from the hot vertical wall was determined by taking the slope of the profile in the conduction layer where the slope is constant. The conduction layer is typically about one third of the thickness of the natural convection thermal boundary layer (Holman, 1986). The boundary layer thickness was estimated from the profile based on the value of $(T_H - T)/(T_H - T_\infty) = 0.95$. A best linear fit of the data over approximately the first third of the boundary layer thickness was then used to determine the slope of the temperature profile as shown in Figure 3.25. The local heat flux was estimated from the product of the thermal conductivity and the slope using the equation

$$q^{\bullet} = -k\frac{\partial T}{\partial x}, \tag{3.4}$$

where k is the thermal conductivity of air at the average temperature in the conduction layer and the $\frac{\partial T}{\partial x}$ is the slope of the temperature profile.

In many cases, it was found that the temperature was not uniform in the central region of the cavity near the top wall. A typical set of temperature profiles is shown in

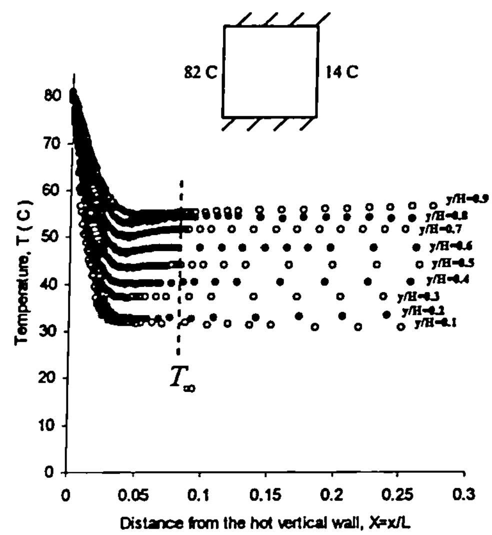

Figure 3.24 Temperature profiles in the first case where the top and bottom walls were insulated, the temperatures of the vertical walls were kept at 82°C and 14°C, respectively.

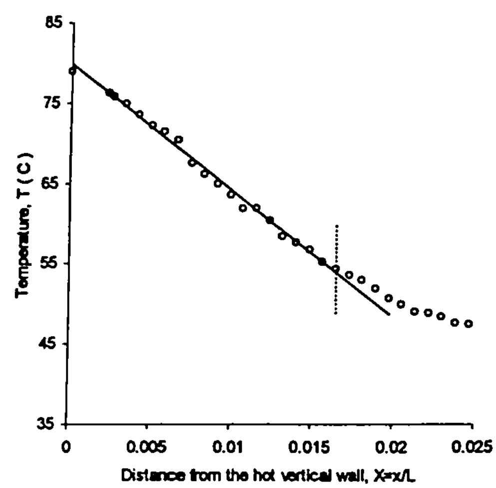

Figure 3.25 Best linear fit used to determine the slope of the temperature profile at the mid-height of the cavity in the first case where the top and bottom walls were insulated, the temperatures of the vertical walls were kept at 82°C and 14°C, respectively.

Figure 3.26. In these cases, the ambient temperature used to evaluate the heat transfer coefficient was determined in the region nearest to the hot vertical wall where the temperature was approximately uniform. Thus, the local heat transfer coefficient was computed from the equation given by

$$h = \frac{\dot{q}}{(T_H - T_\infty)}, \tag{3.5}$$

where T_∞ is the ambient temperature outside of the thermal boundary layer measured by the movable thermocouple probe, and T_H is the hot vertical wall temperature estimated from the projection of curve fit to the hot vertical wall. It was found that there was a consistent discrepancy between the wall temperature determined from the temperature profile and that measured from the thermocouple embedded in the hot vertical wall. The difference was typically less than 3% of the temperature difference across the thermal boundary layer, but in some cases was as large as 6.2%.

The local Nusselt number along the hot vertical wall was obtained by

$$Nu = \frac{h \cdot y}{k}, \tag{3.6}$$

where y is the local height and k is the thermal conductivity of air at the average temperature in the thermal boundary layer. Finally, the local Rayleigh number along the hot vertical wall was estimated from

$$Ra = \left(\frac{\beta}{\alpha\nu}\right) \cdot g \cdot (T_H - T_\infty) \cdot y^3, \tag{3.7}$$

where β, α and ν are the properties of air at the temperature of $(T_H + T_\infty)/2$.

The normalized uncertainty of the local heat flux is given by

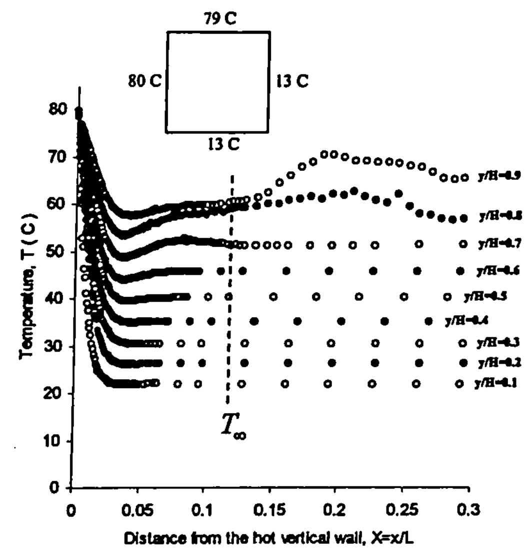

Figure 3.26 Temperature profiles in the square cavity when the top and bottom walls were kept at $79^\circ C$ and $13^\circ C$, respectively.

$$\frac{\Delta q^{\bullet}}{q^{\bullet}} = \sqrt{\left(\frac{\sqrt{\Delta T_H^{\ 2} + \Delta T_{edge}^{\ 2}}}{T_H + T_{edge}}\right)^2 + \left(\frac{\Delta\left(\frac{\partial T}{\partial x}\right)}{\left(\frac{\partial T}{\partial x}\right)}\right)^2}, \tag{3.8}$$

where ΔT_H is the uncertainty of the hot vertical wall temperature and was determined to be $\pm 1^{\circ}C$, ΔT_{edge} is the uncertainty of the temperature at the edge of the conduction layer T_{edge} measured by the thermocouple probe and was $\pm 1^{\circ}C$, and $\Delta(\partial T/\partial x)$ is the uncertainty of the slope of the temperature profile.

The normalized uncertainty of the local heat transfer coefficient is given by

$$\frac{\Delta h}{h} = \sqrt{\left(\frac{\Delta q^{\bullet}}{q^{\bullet}}\right)^2 + \left(\frac{\sqrt{\Delta T_H^{\ 2} + \Delta T_{\infty}^{\ 2}}}{T_H - T_{\infty}}\right)^2}, \tag{3.9}$$

where ΔT_{∞} is the uncertainty of the ambient temperature outside of the thermal boundary layer T_{∞} determined by the thermocouple probe and was $\pm 1^{\circ}C$.

Finally, the normalized uncertainty of the local Nusselt number is given by

$$\frac{\Delta Nu}{Nu} = \sqrt{\left(\frac{\Delta h}{h}\right)^2 + \left(\frac{\Delta y}{y}\right)^2 + \left(\frac{\sqrt{\Delta T_H^{\ 2} + \Delta T_{edge}^{\ 2}}}{T_H + T_{edge}}\right)^2}, \tag{3.10}$$

where Δy is the uncertainty of the position of the measurement point in the vertical direction y and was ± 0.03 mm.

The average normalized uncertainties of the local heat flux were $3\% - 5\%$, and the average normalized uncertainties of the local heat transfer coefficient and the local Nusselt number were $5\% - 8\%$. The detailed results for all the measurements have been included in the Appendix.

The accuracy of the local heat flux q^{*} computed from the temperature profiles were checked by applying an energy balance for the hot vertical wall. This was done only in the central area of the hot vertical wall as shown in Figure 3.27 because it was difficult to estimate the heat transfer on the edges of the wall. The equations to express the total energy into and leaving the control volume are given, respectively, by

$$Q_{in(a)} = Q_H + Q_T, \tag{3.11}$$

and

$$Q_{out(a)} = Q_C + Q_G + Q_B + Q_R + Q_L. \tag{3.12}$$

The subscripts represent the different sources of energy into or leaving the area. For example, Q_H is the energy input by the heater and Q_C is the energy into the thermal boundary layer along the hot vertical wall. The discrepancy in the energy balance was 14% to 25% and the detailed results are given in the Appendix.

The energy balance for the whole system was also calculated. A control volume was chosen as shown in Figure 3.28 to estimate the energy balance for the whole system. The control volume included the hot vertical wall, the movable vertical wall, partial top wall, and partial bottom wall. The total energy into and leaving the control volume are given, respectively, by

$$Q_{in(CV)} = Q_{h,H} + Q_{h,T} + Q_{G-T} + Q_{G-B}, \tag{3.13}$$

and

$$Q_{out(CV)} = Q_{H-G} + Q_{T-G} + Q_{T-T} + Q_{w,M} + Q_{M,O} + Q_{B-B} + Q_{B,O} + Q_{w,B}. \tag{3.14}$$

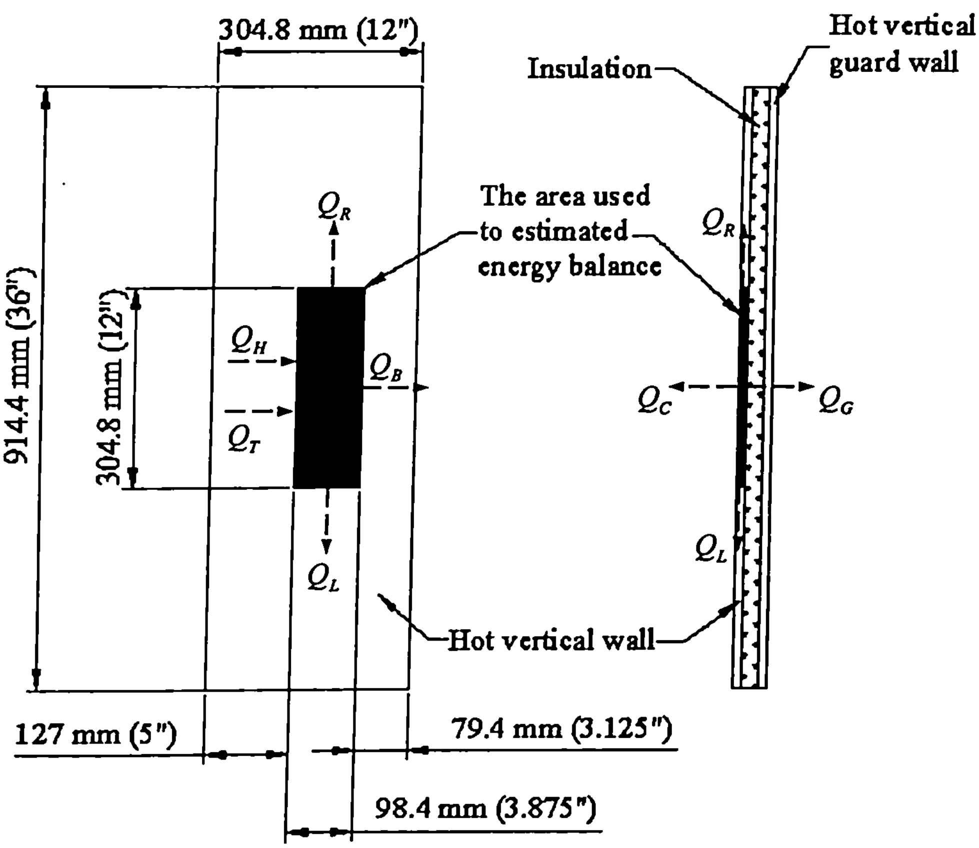

Figure 3.27 Schematic of the area of the hot vertical wall used to estimate energy balance.

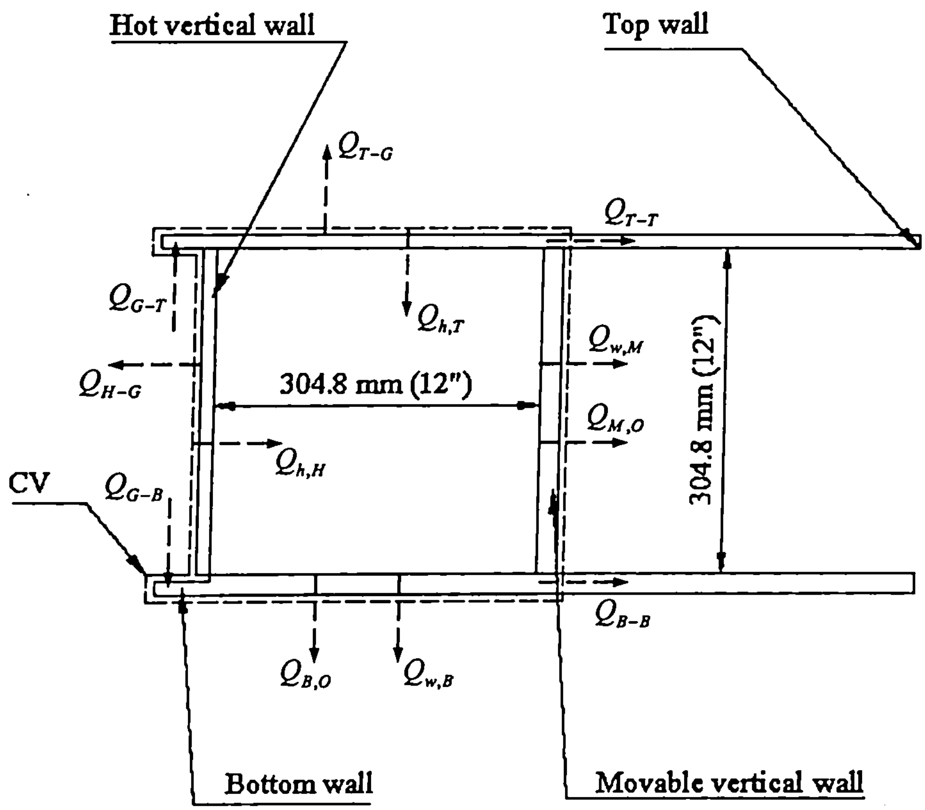

Figure 3.28 Schematic of the control volume used to estimate energy balance for the whole system.

The discrepancy in the energy balance in five cases was 5% to 12%; and in the other two cases the discrepancy was 14% and 22%, respectively. The specific results for all the cases are shown in the Appendix.

Chapter4 Results

4.1 Natural convection in a square enclosure with adiabatic top and bottom walls

The natural convection in the square enclosure shown in Figure 4.1 was examined first for the case where the top and bottom walls were adiabatic. The temperatures of the vertical walls were maintained at $82^{\circ}C$ and $14^{\circ}C$, and the average temperatures of the insulated top and bottom walls were $51^{\circ}C$ and $31^{\circ}C$, respectively. The temperature of the top and bottom insulated walls decreased approximately linearly from the side close to the hot vertical wall to the side close to the cold vertical wall. The variation in the temperature on the top wall was about $5^{\circ}C$ and on the bottom wall was about $3^{\circ}C$. The horizontal Grashof number Gr_H given by

$$Gr_H = \left(\frac{\beta}{\nu^2}\right) g(T_H - T_C)L^3, \tag{4.1}$$

was 1.9×10^8 and the Rayleigh number based on the width of the cavity given by

$$Ra = \left(\frac{\beta}{\alpha\nu}\right) g(T_H - T_C)L^3, \tag{4.2}$$

was 1.3×10^8. Here β, ν and α are the volume expansion coefficient, kinematic viscosity and thermal diffusivity of the air at $(T_H + T_C)/2$. The vertical Grashof number

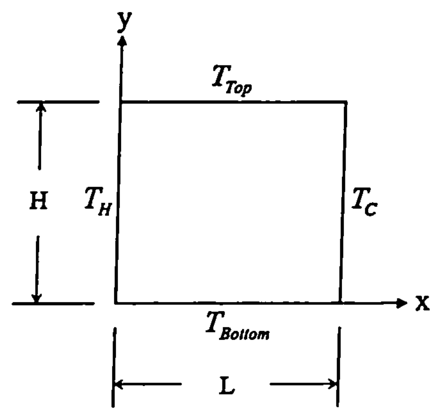

Figure 4.1 Schematic of the square cavity.

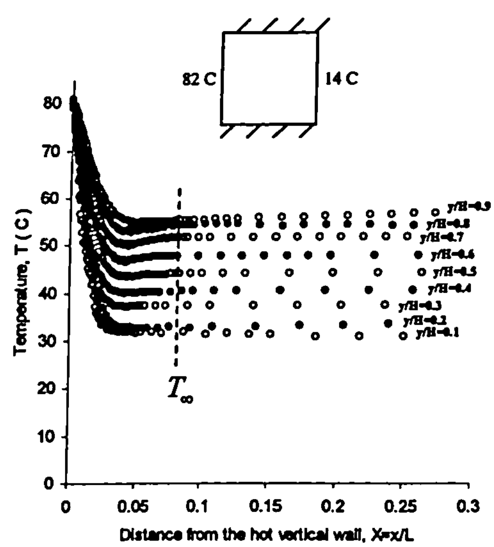

Figure 4.2 Temperature profiles with top and bottom walls insulated, and the vertical walls at $82^\circ C$ and $14^\circ C$.

Gr_V given by

$$Gr_V = \left(\frac{\beta}{\nu^2}\right) g\left(T_{Top} - T_{Bottom}\right) H^3, \tag{4.3}$$

was 6.1×10^7, where β and ν were determined at $\left(T_{Top} + T_{Bottom}\right)/2$.

The temperature profiles along the hot vertical wall for this case are shown in Figure 4.2. There is a significant change in the profile near the hot vertical wall indicating the presence of a boundary layer. The temperature profiles normalized by the temperature difference between the hot vertical wall and core region are presented in Figure 4.3, and shows the increase in thermal boundary layer thickness as the flow develops along the wall. The increase in the thermal boundary layer thickness along the hot vertical wall for this case is shown in Figure 4.4.

The temperature profiles non-dimensionalized by the temperature difference across the enclosure are compared to the data of Tian and Karayiannis (2000) in Figure 4.5. The non-dimensionalized temperature profiles along the hot vertical wall are similar in the two cases, however, the temperature in the core region is lower in the present case. The change in the normalized ambient temperature outside of the thermal boundary layer region with height are compared in Figure 4.6. In both cases, the core region is stably stratified, however, the temperature of the core region for the present measurements is lower than the results of Tian and Karayiannis (2000). The rate of the change in the non-dimensional ambient temperature is 0.51 for the measurements performed here and 0.43 for Tian and Karayiannis (2000) results. The average non-dimensionalized bottom wall temperature is 0.25 for the current experiment and is lower than the value of 0.39 for Tian

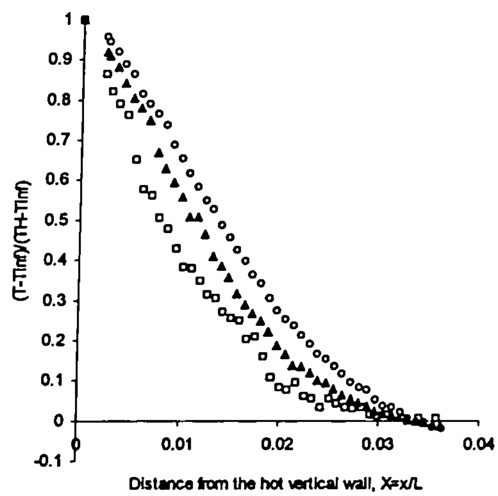

Figure 4.3 Non-dimensionalized temperature profiles along the hot vertical wall with top and bottom walls insulated at ○ y/H=0.9, ▲ y/H=0.5, and □ y/H=0.1.

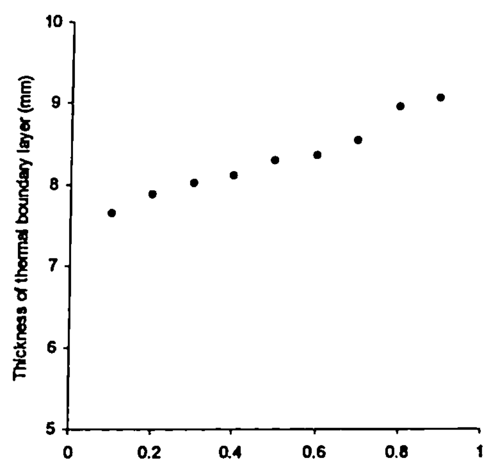

Figure 4.4 Change in thickness of the thermal boundary layer δ_T along the hot vertical wall with top and bottom walls insulated.

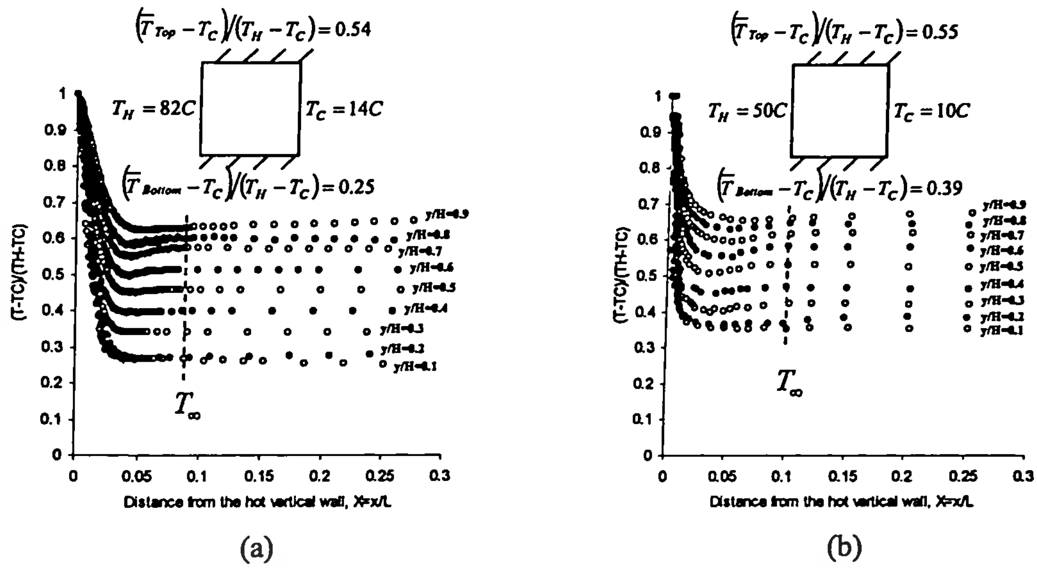

Figure 4.5 Comparison of the temperature profiles in the square cavity. (a) measured here with top and bottom walls insulated, and (b) reported by Tian and Karayiannis (2000).

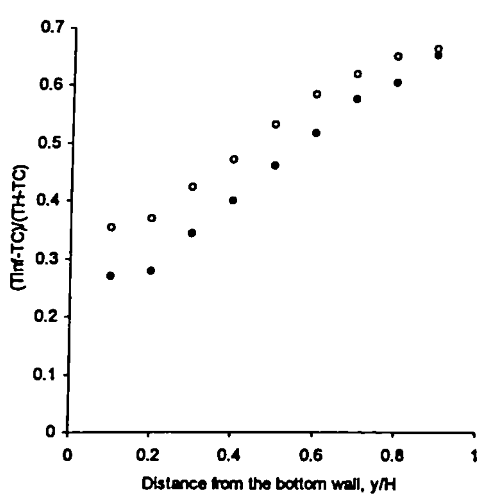

Figure 4.6 Comparison of the non-dimensionalized ambient temperature $(T_\infty - T_C)/(T_H - T_C)$. • measured here with top and bottom walls insulated, and ○ reported by Tian and Karayiannis (2000).

and Karayiannis (2000), while the average non-dimensionalized temperatures on the top wall are the same. This suggests that the differences may be due to the differences in the way the bottom walls were insulated.

A comparison of the local heat flux from the hot vertical wall q^* computed from the temperature profiles from the two experiments is shown in Figure 4.7. It is clear the local heat flux into the cavity from the hot vertical wall decreases as the flow develops along the wall. The heat transfer here was approximately 80% larger than in the case of Tian and Karayiannis (2000) because the temperature difference ($T_H - T_\infty$) was larger in the current experiment as shown in Figure 4.8 (a). The heat flux and the temperature difference were then used to compute the local natural convection heat transfer coefficient h for the hot vertical wall shown in Figure 4.8 (b). In both cases the heat transfer coefficient decreases along the wall due to the increase in boundary layer thickness. In general, there is good agreement in the heat transfer coefficients in the two cases.

The local Nusselt number Nu and local Rayleigh number Ra based on the distance from the bottom wall are shown in Figure 4.9. The range of the Rayleigh number investigated in this experiment is smaller than for Tian and Karayiannis (2000). The local Rayleigh number in the current experiment varied from 8.6×10^4 to 2.5×10^7 and from 8.8×10^5 to 3.1×10^8 for Tian and Karayiannis (2000) results. In both cases, these are below the critical value for transition from laminar to turbulent flow.

The change in the local Nusselt number with the Rayleigh number for the two cases are shown in Figure 4.10. The slopes of both lines that fit the data are 0.315

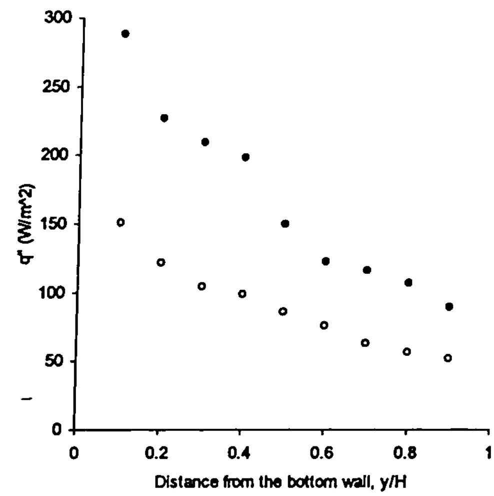

Figure 4.7 Comparison of the local heat flux along the hot vertical wall $q^{"}$. ● measured here with top and bottom walls insulated, and ○ reported by Tian and Karayiannis (2000).

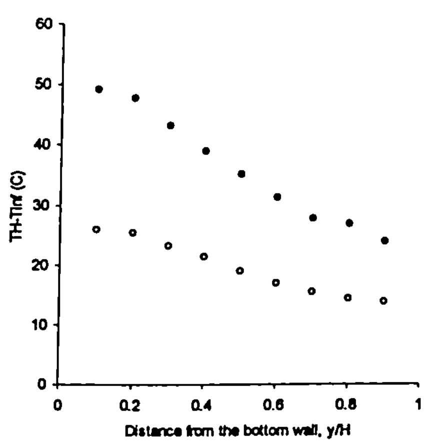

(a)

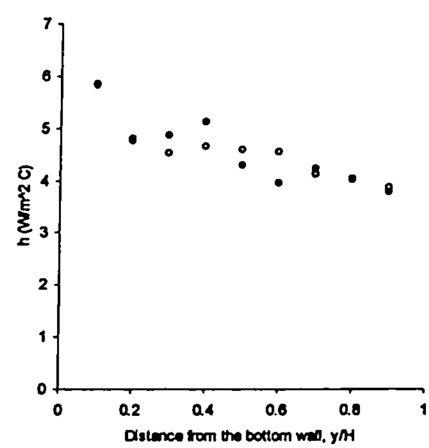

(b)

Figure 4.8 Comparison of (a) the temperature difference along the hot vertical wall $T_H - T_\infty$, and (b) the heat transfer coefficient for the hot vertical wall h. ● measured here with top and bottom walls insulated, and ○ reported by Tian and Karayiannis (2000).

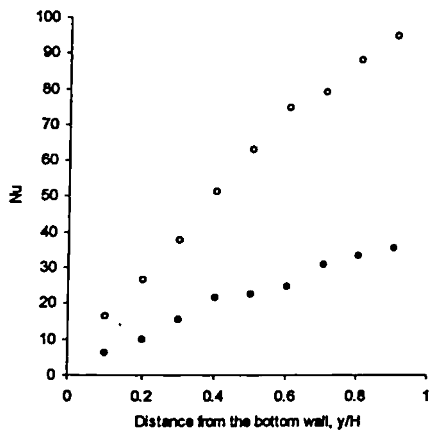

(a)

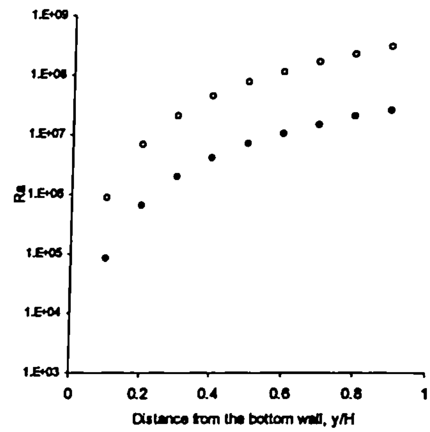

(b)

Figure 4.9 Comparisons of (a) the Nusselt numbers for the hot vertical wall *Nu*, and (b) the local Rayleigh numbers along the hot vertical wall *Ra*. ● measured here with top and bottom walls insulated, and ○ reported by Tian and Karayiannis (2000).

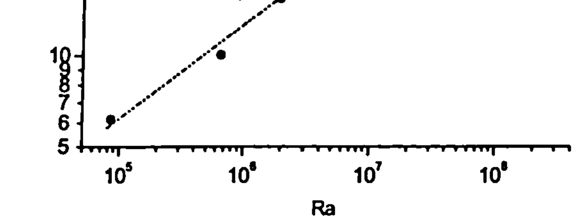

Figure 4.10 Comparison of the change in the local Nusselt number with the Rayleigh number for ● ----- measured here with top and bottom walls insulated, and ○ —— reported by Tian and Karayiannis (2000).

indicating the data can be correlated as

$$Nu = C \cdot Ra^{0.315}, \tag{4.4}$$

The constant C is 0.162 for the measurements with the current facility, and 0.2 for the results by Tian and Karayiannis (2000). It was thought that this difference may be due to the difference in the temperature of the bottom wall.

4.2 Effect of stable stratification on the natural convection in the enclosure

The effect of stable stratification on the natural convection was examined by changing the temperatures of the top and bottom walls independently of the vertical walls. The temperatures of the vertical walls were maintained at $81.5^{\circ}C \pm 1.5^{\circ}C$ and $14.5^{\circ}C \pm 1.5^{\circ}C$ for all cases investigated here.

Initially, the temperatures of the top and bottom walls were maintained at $79^{\circ}C$ and $13^{\circ}C$ to approximately match the temperatures of the vertical walls that were at $80^{\circ}C$ and $13^{\circ}C$ for this test. The vertical Grashof number Gr_V was 1.9×10^{8}. The temperature profiles in the enclosure for this case are shown in Figure 4.11 (a). The temperature profiles measured for the adiabatic top and bottom walls are also shown in Figure 4.11 (b) to facilitate comparison. In both cases, there is evidence of a thermal boundary layer near the hot vertical wall. The change in the ambient temperature in the vertical direction increased when the top and bottom walls were maintained at $79^{\circ}C$ and $13^{\circ}C$. In addition, there is a significant difference in the temperature distribution in the

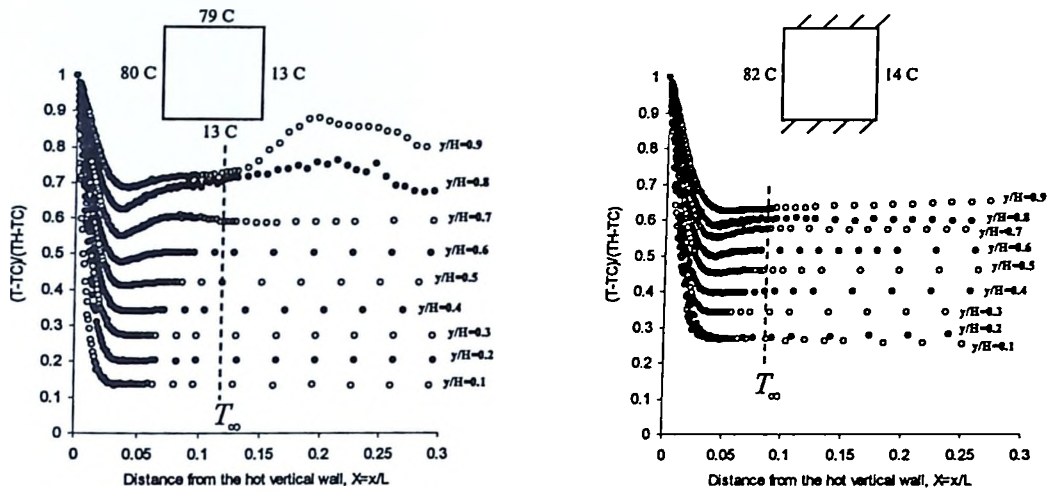

(a) (b)

Figure 4.11 Temperature profiles in the square cavity. (a) with top and bottom walls at $79^{\circ}C$ and $13^{\circ}C$, and (b) with top and bottom walls insulated.

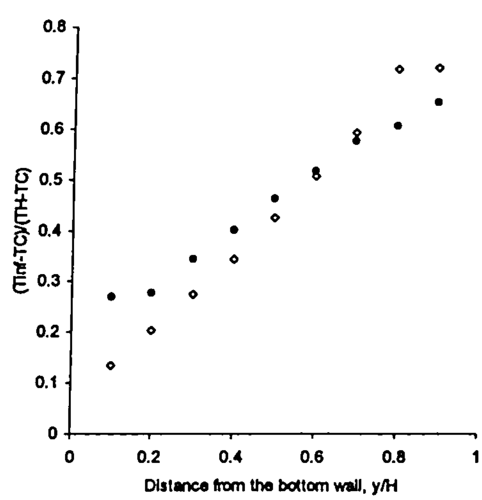

Figure 4.12 Comparison of the non-dimensionalized ambient temperatures near the hot vertical wall $(T_\infty - T_C)/(T_H - T_C)$. ● with top and bottom walls insulated, and ◇ with top and bottom walls at $79^{\circ}C$ and $13^{\circ}C$.

core region at y/H=0.8 and 0.9 when the top wall was heated. The variation of the temperature in the central region was small at y/H=0.8 but was quite large at y/H=0.9, and is likely due to a recirculatory flow in this region similar to that proposed by Tian and Karayiannis (2000). A comparison of the non-dimensionalized ambient temperatures near the hot vertical wall in the two cases is shown in Figure 4.12. The non-dimensionalized ambient temperature gradient is greater with heating and cooling the top and bottom walls resulting in a more stably stratified core region. With the top wall heated, the non-dimensionalized ambient temperature in the region near the top wall was nearly constant.

A comparison of the local heat flux along the hot vertical wall computed from the temperature profiles is shown in Figure 4.13 (a). In both cases, the local heat flux into the cavity decreases with increasing height. The heating and cooling of the top and bottom walls changes the heat transfer characteristics from the hot vertical wall. The local heat flux near the bottom wall (at y/H=0.1) increases by about 50%, while it decreases by about 10% very close to the top wall (at y/H=0.9). This trend is similar to that measured by Sernas and Lee (1981) in an air-filled square cavity with Gr_H of 5.5×10^6 shown in Figure 4.13 (b). The difference in the values from the current measurements and the measurements of Sernas and Lee (1981) is likely due to differences in the Grashof number, and the way the top and bottom walls were insulated.

Comparisons of the temperature difference across the boundary layer ($T_H - T_\infty$) along the hot vertical wall and the local heat transfer coefficient h computed from this temperature difference for the two cases are shown in Figures 4.14. The local heat

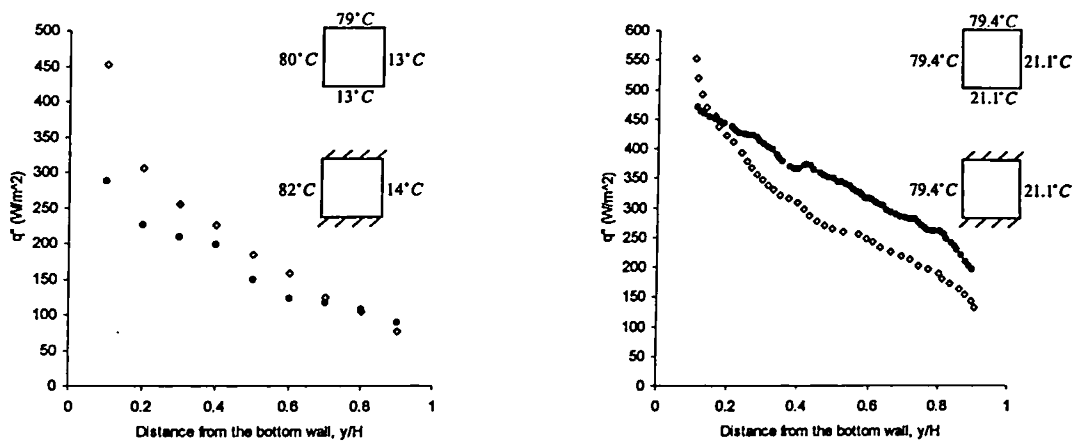

(a) (b)

Figure 4.13 Comparison of the local heat flux along the hot vertical wall q^{*}. (a) measured here • with top and bottom walls insulated, and ◇ with top and bottom walls at $79^{\circ}C$ and $13^{\circ}C$, and (b) reported by Sernas and Lee (1981) • foam top and bottom walls, and ◇ isothermal top wall at $79.4^{\circ}C$ and bottom wall at $21.1^{\circ}C$.

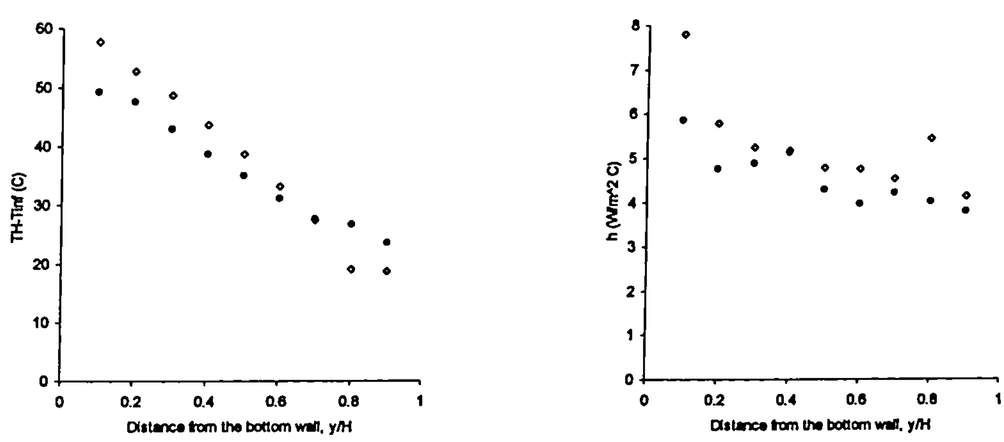

(a) (b)

Figure 4.14 Comparison of (a) the temperature difference along the hot vertical wall $T_H - T_{\infty}$, and (b) the heat transfer coefficient for the hot vertical wall h. • with top and bottom walls insulated, and ◇ with top and bottom walls at $79^{\circ}C$ and $13^{\circ}C$.

transfer coefficient was always larger in the second case where the top wall was heated and the bottom wall was cooled. The difference, however, was not uniform along the hot vertical wall. In particular, the heat transfer coefficient at y/H=0.1 was significantly increased when the bottom wall was cooled so that not all the increase in the heat transfer was caused by the reduction in the ambient temperature. This change in the local heat transfer coefficient may be due in part to the fact that the flow approaching the hot vertical wall along the bottom wall was initially cooled below the ambient temperature near the bottom wall. There was also a large increase in the local heat transfer coefficient at y/H=0.8 when the top wall was heated that may suggest a change in the flow in this region.

The local Nusselt and Rayleigh numbers for the two cases are compared in Figure 4.15. The local Nusselt number was larger when the top wall and bottom wall were heated and cooled as expected, with a particularly large increase at the location y/H=0.8. The local Rayleigh number was larger up to about y/H=0.7 because the ambient temperature was lower in this region, so that the buoyancy force on the boundary layer would be larger. The local temperature near the top wall was much larger when the top wall was heated so the temperature difference across the boundary layer and the buoyancy force near the top wall were reduced. Thus, the local Rayleigh number was smaller close to the top wall.

The correlation between the local Nusselt number and local Rayleigh number for the two cases is shown in Figure 4.16. The slopes of the lines are both roughly 0.315 indicating that the power in the correlation is not affected by the change in the

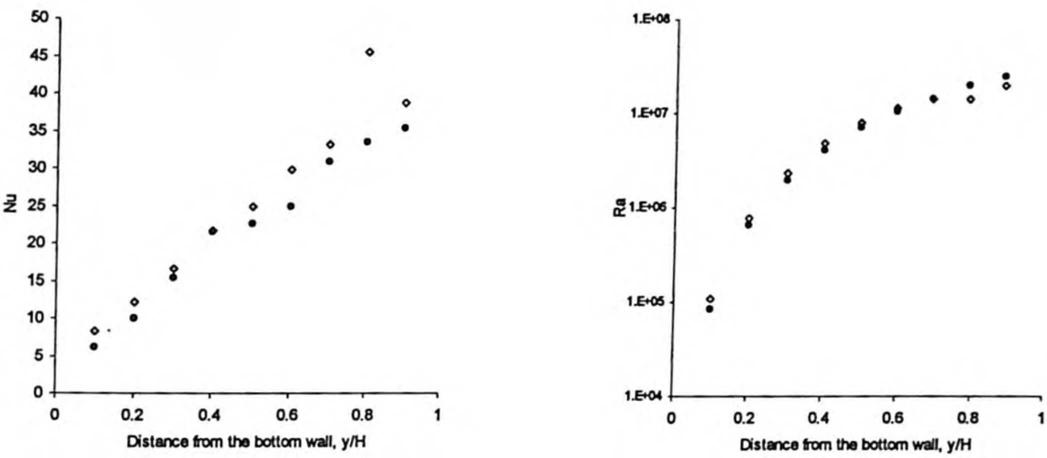

(a) (b)

Figure 4.15 Comparisons of (a) the Nusselt numbers for the hot vertical wall *Nu*, and (b) the local Rayleigh numbers along the hot vertical wall Ra. ● with top and bottom walls insulated, and ◇ with top and bottom walls at $79^{\circ}C$ and $13^{\circ}C$.

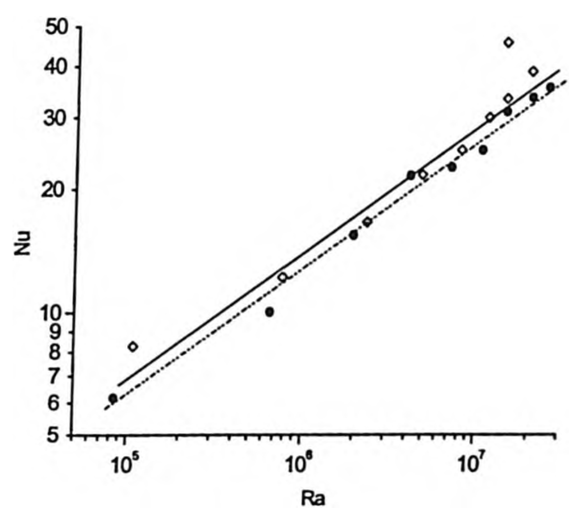

Figure 4.16 Comparison of the change in local Nusselt number with Rayleigh number for ● -·-·- with top and bottom walls insulated, and ◇ —— with top and bottom walls at $79^{\circ}C$ and $13^{\circ}C$.

stratification. The intercept, or the value of the constant *C*, in the correlation for the second case is 0.185 and is larger than the first case. In the second case, the data at y/H=0.8 is significantly higher than the correlation indicating that there may be a change of flow in this region.

4.3 Effect of changing the temperature of the top wall

The results in the previous section suggested that the change in the top wall temperature affected the natural convection flow, particularly in the region near the top wall. This was investigated further by measuring the heat transfer in a series of cases where the temperature of the top wall was changed from $52^{\circ}C$ to $109^{\circ}C$ as shown in Figure 4.17, with global vertical Grashof number in the range of 1.2×10^{8} to 2.2×10^{8}. The temperatures on the other three walls were maintained at $81.5^{\circ}C\pm1.5^{\circ}C$, $14.5^{\circ}C\pm1.5^{\circ}C$, and $14^{\circ}C\pm2^{\circ}C$, respectively, as summarized in Table 4.1. A comparison of the temperature profiles measured along the hot vertical wall for these five cases are shown in Figure 4.18. It is clear that the temperature profiles near the top wall changes as the temperature of the top wall increases. When the top wall was insulated ($T_{Top}=52^{\circ}C$), the temperature in the center of the enclosure outside of the thermal boundary layer was essentially constant at each height. This suggests the air in the core region of the cavity was approximately stationary. In the other four cases, the ambient temperatures outside of the thermal boundary layer at the heights of y/H=0.8 and 0.9 varied significantly across the enclosure. This suggests there is a secondary circulation

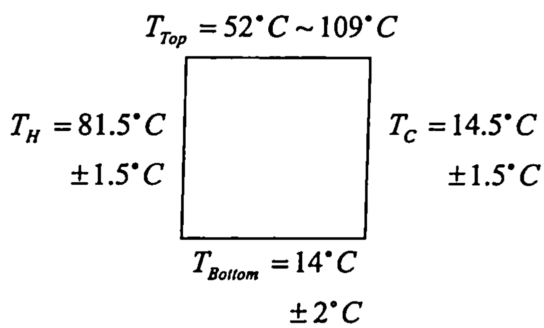

Figure 4.17 Schematic of the thermal boundary conditions for the cases which were used to investigate the effect of changing the top wall temperature

Case No.	Temperature on the Top Wall (C) T_{Top}	Temperature on the Bottom Wall (C) T_{Bottom}	Temperature on the Hot Vertical Wall (C) T_H	Temperature on the Movable Vertical Wall (C) T_C	Vertical Grashof Number Gr_V
1	Insulated (52)	16	83	16	1.2×10^8
2	71	12	83	13	1.8×10^8
3	79	13	80	13	1.9×10^8
4	89	13	80	13	2.0×10^8
5	109	14	82	14	2.2×10^8

Table 4.1 Detailed thermal boundary conditions and vertical Grashof numbers for the cases which were used to investigate the effect of changing the top wall temperature.

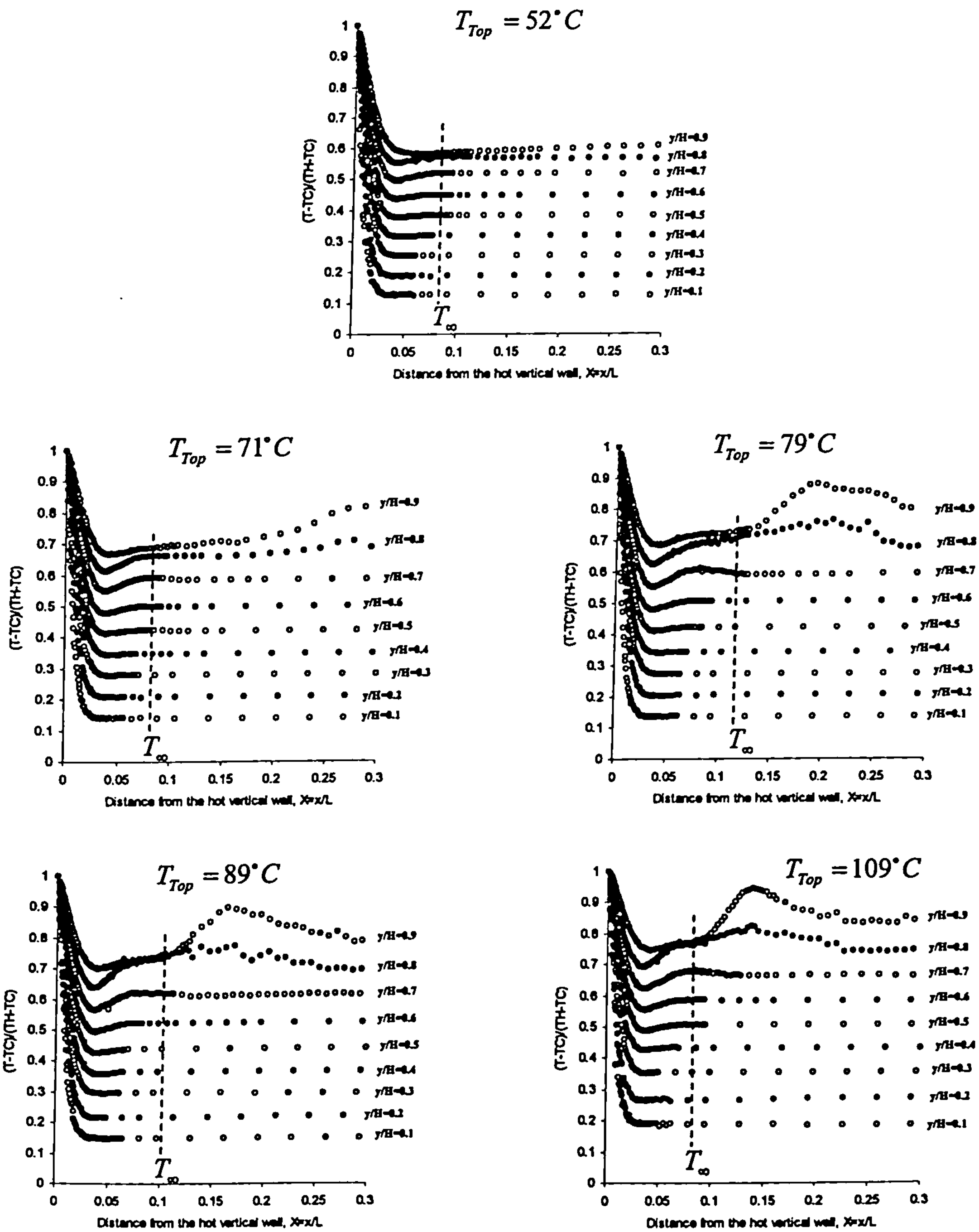

Figure 4.18 Temperature profiles for the cases where the temperature of the top wall was changed from $52^{\circ}C$ (insulated) to $109^{\circ}C$.

outside of the thermal boundary layer along the top wall similar to that observed by Tian and Karayiannis (2000). Further, when the temperature of the top wall was increased from $71^{\circ}C$ to $109^{\circ}C$, the lateral position where the change in the ambient temperature occurs moved toward the hot vertical wall, indicating the region of the secondary circulation was shifting toward the hot vertical wall.

The change in the non-dimensionalized ambient temperature near the hot vertical wall with the height for the five cases is shown in Figure 4.19. In all cases, the ambient temperature increased linearly with the height except at the locations closest to the top wall. The rate of change of non-dimensionalized ambient temperature with height increased from 0.65 to 0.79 as the top wall temperature increased indicating increased stratification in the central region of the enclosure.

The change in the local heat flux along the hot vertical wall q^{*} in the five cases is shown in Figure 4.20. On the top half of the hot vertical wall, from y/H=0.5 to 0.9, the local heat flux decreased as the temperature at the top wall increased and the local ambient temperature was increased. The difference increased as the top wall was approached. For example, at y/H=0.9, the local heat flux decreased by approximately 40% when the top wall temperature increased from $52^{\circ}C$ to $109^{\circ}C$. There was no obvious trend in the data in the region near the bottom wall.

The changes in the temperature difference between the hot vertical wall and the fluid outside of the boundary layer $T_H - T_{\infty}$, and the local heat transfer coefficient for the five cases are shown in Figures 4.21 and 4.22. The results indicate, somewhat surprisingly, that the heat transfer coefficient in the region y/H=0.5 to 0.8 increased as the

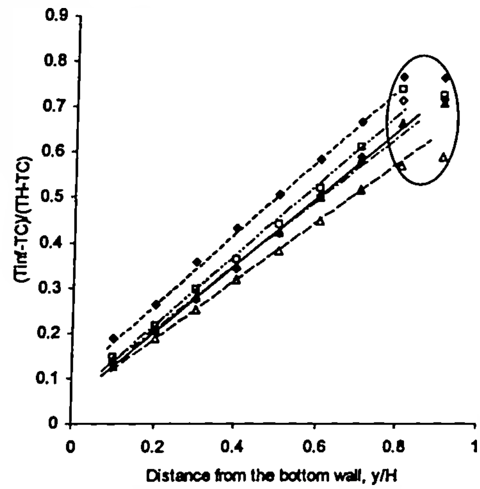

Figure 4.19 Comparison of the non-dimensionalized ambient temperature near the hot vertical wall $(T_\infty - T_C)/(T_H - T_C)$ where the top wall was Δ $52^\circ C$ (insulated), ▲ $71^\circ C$, ◇ $79^\circ C$, □ $89^\circ C$, and ◆ $109^\circ C$.

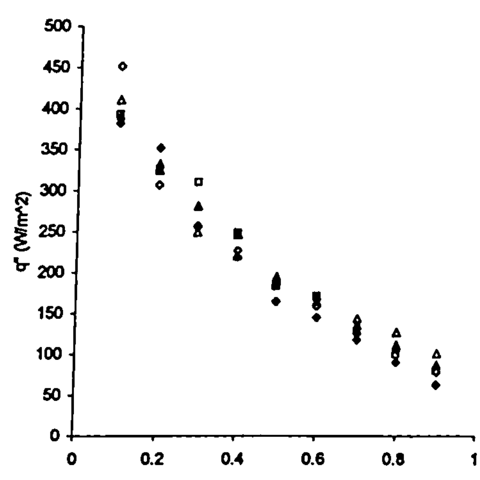

Figure 4.20 Comparison of the local heat flux along the hot vertical wall q'' where the top wall was Δ $52^\circ C$ (insulated), ▲ $71^\circ C$, ◇ $79^\circ C$, □ $89^\circ C$, and ◆ $109^\circ C$.

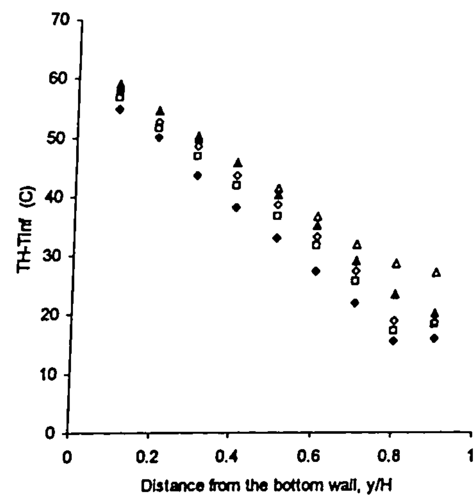

Figure 4.21 Comparison of the temperature difference along the hot vertical wall $T_H - T_\infty$ where the top wall was Δ $52^\circ C$ (insulated), ▲ $71^\circ C$, ◇ $79^\circ C$, □ $89^\circ C$, and ◆ $109^\circ C$.

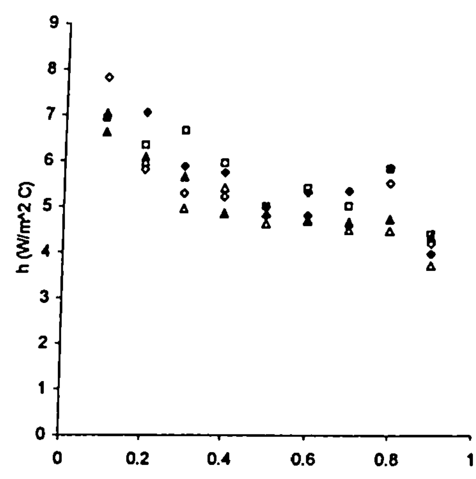

Figure 4.22 Comparison of the heat transfer coefficient for the hot vertical wall h where the top wall was Δ $52^\circ C$ (insulated), ▲ $71^\circ C$, ◇ $79^\circ C$, □ $89^\circ C$, and ◆ $109^\circ C$.

top wall temperature increased. The difference in heat transfer coefficient became larger as the height increased. In all cases, there is a local maximum in the heat transfer coefficient at y/H=0.8.

The changes in the local Nusselt number and the local Rayleigh number for the five cases are shown in Figure 4.23. In the region y/H=0.5 to 0.8, the local Nusselt number increased while the local Rayleigh number decreased as the top wall temperature increased. The change in the local Nusselt number with the Rayleigh number for the five cases with different upper wall temperatures is shown in Figure 4.24. The change in the Nusselt number with Rayleigh number can be fit with a line with a slope of 0.315 ± 0.005 on this log-log plot indicating the correlations for the different cases are given by $Nu = C \cdot Ra^{0.315}$. The exception is in the region near the top wall at y/H=0.8 where the flow appears to be affected by the top wall. The intercept of the correlation lines, and hence the constant *C*, increased from 0.150 to 0.212 as the top wall temperature increased. The values of the exponent *n* and constant *C* for the correlation $Nu = C \cdot Ra^{n}$ for each case are shown in Table 4.2.

4.4 Effect of changing the temperature of the bottom wall

The effect of changing the bottom wall temperature was investigated by measuring the heat transfer for a series of cases where the bottom wall was insulated or cooled. It was not possible to vary the bottom wall temperature in controlled steps in the current configuration so the effect of the bottom wall temperature was examined with the

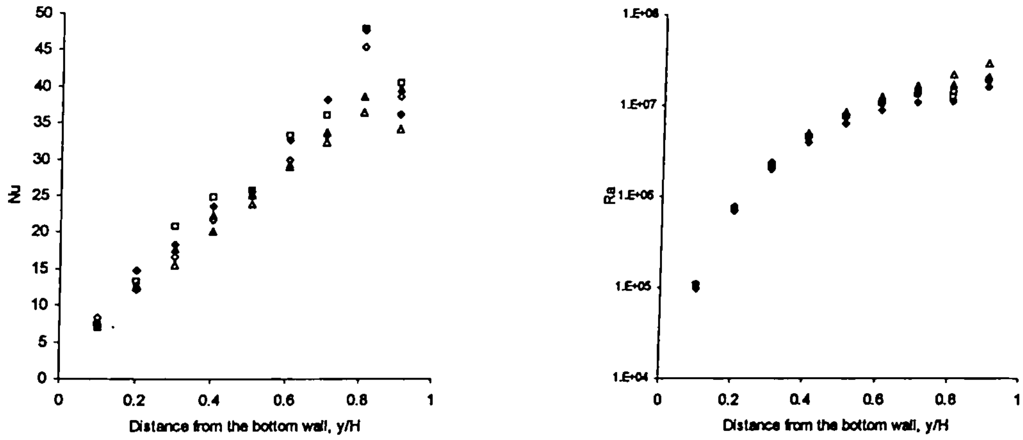

(a) (b)

Figure 4.23 Comparisons of (a) Nusselt number for the hot vertical wall *Nu*, and (b) Rayleigh number along the hot vertical wall *Ra* where the top wall was Δ $52^{\circ}C$ (insulated), ▲ $71^{\circ}C$, ◇ $79^{\circ}C$, □ $89^{\circ}C$, and ◆ $109^{\circ}C$.

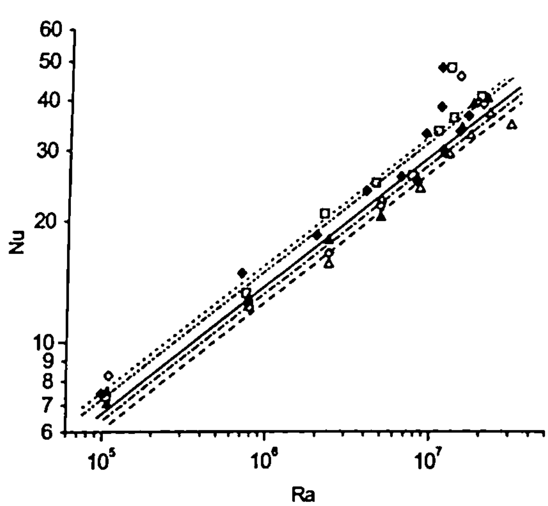

Figure 4.24 Comparison of the change in the local Nusselt number with Rayleigh number where the top wall was Δ---- $52^{\circ}C$ (insulated), ▲-·-·- $71^{\circ}C$, ◇—— $79^{\circ}C$, □-··-·· $89^{\circ}C$, and ◆······ $109^{\circ}C$.

Temperatures of the top wall ($^{\circ}C$), T_{Top}	Temperatures of the bottom wall ($^{\circ}C$), T_{Bottom}	Values of the exponent n	Values of The constant C
Insulated (52)	16	0.32	0.150
71	12	0.32	0.157
79	13	0.31	0.185
89	13	0.31	0.202
109	14	0.31	0.212

Table 4.2 Values of the exponent n and constant C for the form of the Nusselt Rayleigh number correlation $Nu = C \cdot Ra^n$ in the cases when the temperature of the top wall was changed from $52^{\circ}C$ (insulated) to $109^{\circ}C$.

Case No.	**Temperature on the Top Wall (C)** T_{Top}	**Temperature on the Bottom Wall (C)** T_{Bottom}	**Temperature on the Hot Vertical Wall (C)** T_H	**Temperature on the Movable Vertical Wall (C)** T_C	**Vertical Grashof Number** Gr_V
1	Insulated (51)	Insulated (31)	82	14	6.1×10^7
2	Insulated (52)	16	83	16	1.2×10^8
3	80	Insulated (32)	80	15	1.2×10^8
4	79	13	80	13	1.9×10^8

Table 4.3 Detailed thermal boundary conditions and vertical Grashof numbers for the cases which were used to investigate the effect of changing the bottom wall temperature.

wall insulated or cooled for different top wall temperatures as summarized in Table 4.3. The temperatures on the vertical walls were maintained at $81.5^{\circ}C \pm 1.5^{\circ}C$ and $14.5^{\circ}C \pm 1.5^{\circ}C$. A comparison of the temperature profiles for the four cases is shown in Figure 4.25. The temperature profiles near the top wall changed as the top wall temperature changed, as in the previous results, and were relatively independent of the bottom wall temperature. The non-uniformity in the temperature profiles near the top wall in the heated cases is relatively independent of the temperature of the bottom wall indicating the change in this region is a local phenomenon. Similarly, the ambient temperature near the bottom wall was relatively independent of the top wall temperature for these cases. The change in the non-dimensionalized ambient temperature near the hot vertical wall with the height for the four cases is shown in Figure 4.26. The rate of change of temperature with height increased as the bottom wall was cooled for both upper wall temperatures indicating the core region of the flow was more stratified as the bottom wall temperature decreased.

The change in the local heat flux along the hot vertical wall q^{*} for the four cases is shown in Figure 4.27. The heat flux near the bottom of the hot vertical wall was increased 40% to 50% when the bottom wall was cooled for both upper wall temperatures. The local heat flux at heights y/H≥0.3 was also increased when the bottom wall was cooled, though only by 10% to 20%.

The changes in the temperature difference between the hot vertical wall and the fluid outside of the boundary layer $T_H - T_\infty$, and the heat transfer coefficient for the four cases are shown in Figures 4.28 and 4.29. In the region y/H=0.1 to 0.2, the heat transfer

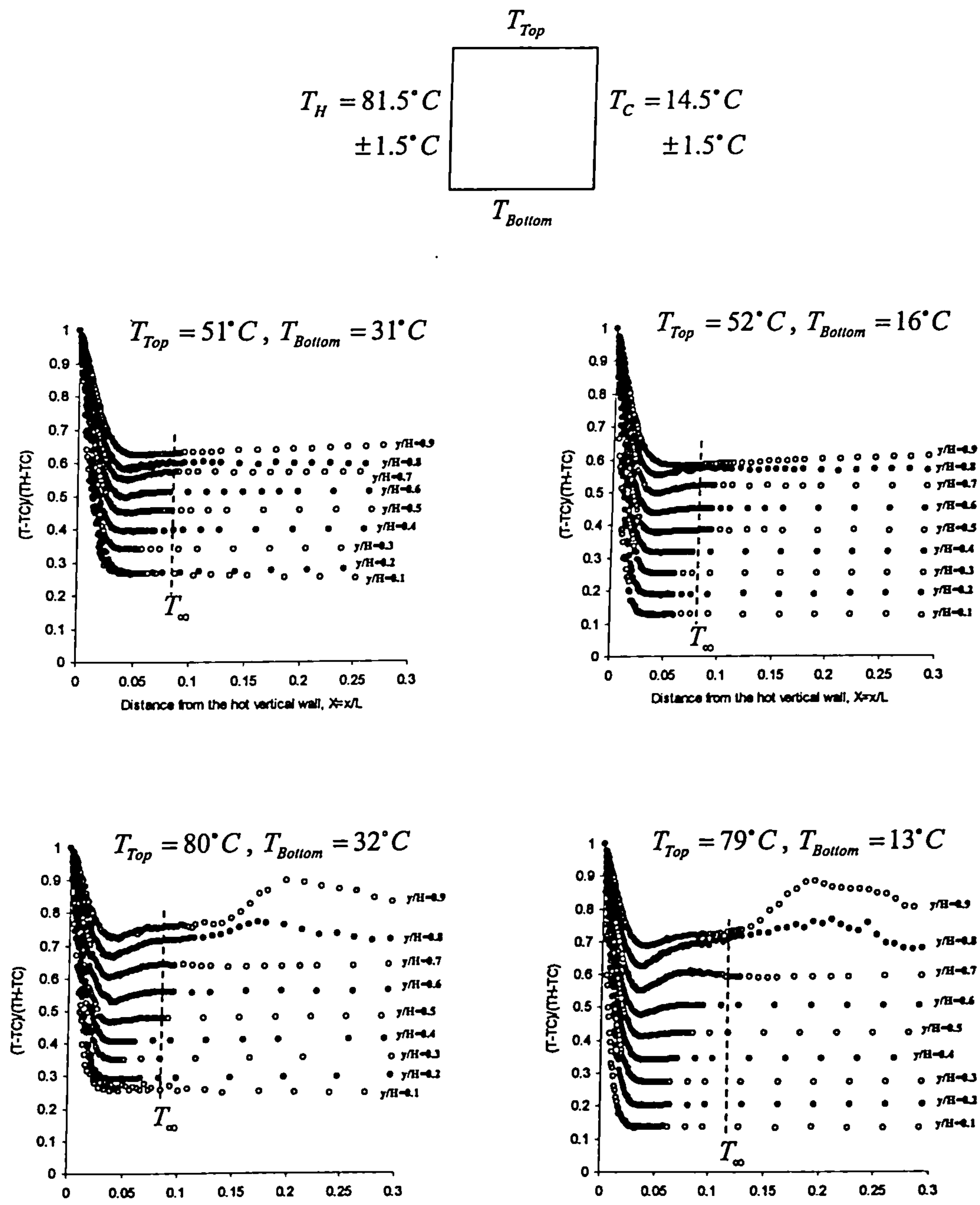

Figure 4.25 Temperature profiles for the cases where the thermal boundary condition of the bottom wall was changed from being insulated to cooled.

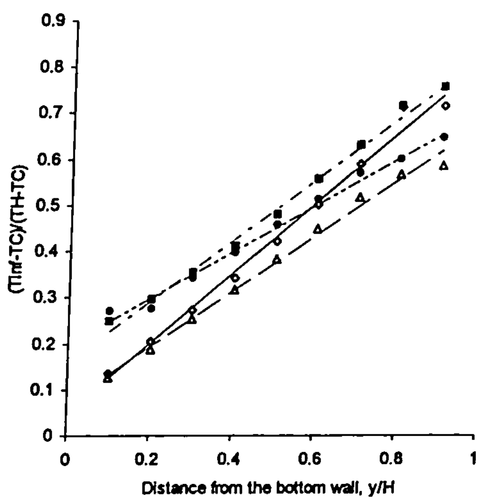

Figure 4.26 Comparison of the non-dimensionalized ambient temperature near the hot vertical wall $(T_\infty - T_C)/(T_H - T_C)$ where the top and bottom walls were • $51^\circ C$ and $31^\circ C$ (both insulated), Δ $52^\circ C$(insulated) and $16^\circ C$, ■ $80^\circ C$ and $32^\circ C$(insulated), ◇ $79^\circ C$ and $13^\circ C$.

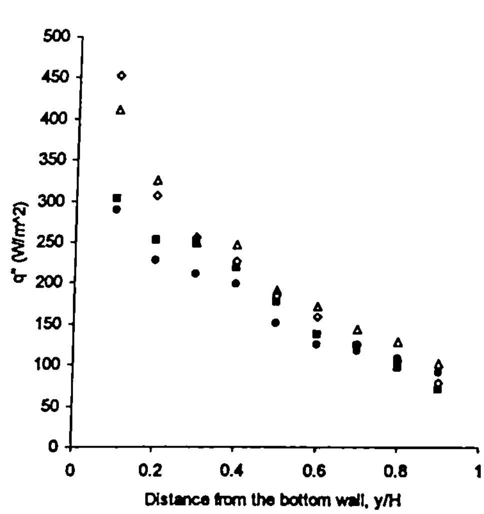

Figure 4.27 Comparison of the local heat flux along the hot vertical wall $q^{"}$ where the top and bottom walls were • $51^\circ C$ and $31^\circ C$ (both insulated), Δ $52^\circ C$(insulated) and $16^\circ C$, ■ $80^\circ C$ and $32^\circ C$(insulated), ◇ $79^\circ C$ and $13^\circ C$.

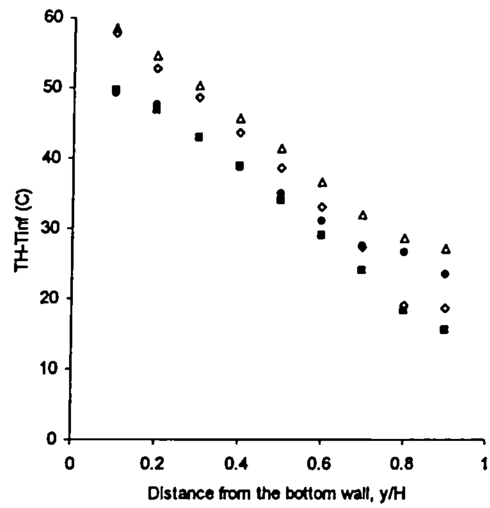

Figure 4.28 Comparison of the temperature difference along the hot vertical wall $T_H - T_\infty$ where the top and bottom walls were ● $51^\circ C$ and $31^\circ C$ (both insulated), Δ $52^\circ C$ (insulated) and $16^\circ C$, ■ $80^\circ C$ and $32^\circ C$ (insulated), ◇ $79^\circ C$ and $13^\circ C$.

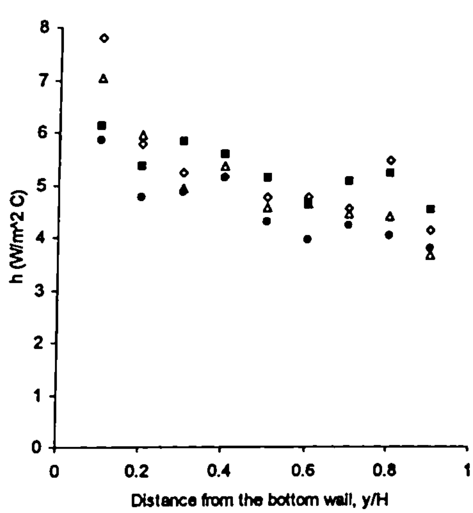

Figure 4.29 Comparison of the heat transfer coefficient for the hot vertical wall h where the top and bottom walls were ● $51^\circ C$ and $31^\circ C$ (both insulated), Δ $52^\circ C$ (insulated) and $16^\circ C$, ■ $80^\circ C$ and $32^\circ C$ (insulated), ◇ $79^\circ C$ and $13^\circ C$.

coefficient increased by 20% to 30% when the bottom wall temperature was decreased for both upper wall temperatures. This suggests that the increase in the local heat flux in this region is not only caused by the cooling of the ambient temperature. There is no clear trend in the heat transfer coefficient at other locations except at y/H=0.8, where a large increase was observed when the top wall was heated, as noted previously.

The changes in the local Nusselt number and the local Rayleigh number along the hot vertical wall are shown in Figure 4.30. The local Nusselt number in the region y/H=0.1 to 0.2 increased when the bottom wall temperature was decreased. The local Rayleigh number was generally larger when the bottom wall was cooled for both upper wall temperatures due to the decrease in the ambient temperature. The correlation between the local Nusselt number and the Rayleigh number for the four cases is shown in Figure 4.31. The slopes of the curve fits to the data were again 0.315 ± 0.005 so the correlation is given by $Nu = C \cdot Ra^{0.315}$. The constant C decreased slightly when the bottom wall temperature decreased for a given top wall temperature. The values of the exponent n and the constant C for the correlation $Nu = C \cdot Ra^{n}$ for the four cases are summarized in Table 4.4.

4.5 Relationship between the stratification rate and heat transfer

The relationship between the stratification rate S, defined as the non-dimensionalized temperature gradient of the ambient air in the vertical direction in the core region of the cavity, and the heat transfer from the hot vertical wall was investigated

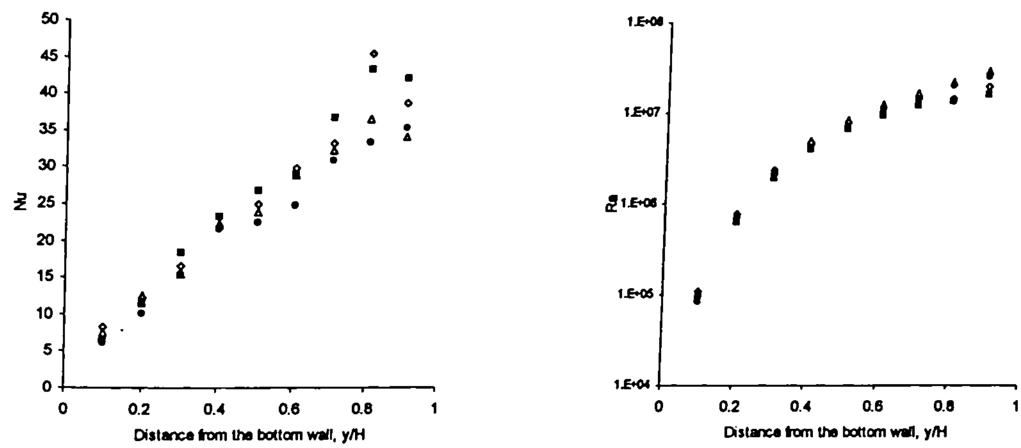

(a) (b)

Figure 4.30 Comparisons of (a) the Nusselt number for the hot vertical wall, and (b) the Rayleigh number along the hot vertical wall determined when the top and bottom walls were ● $51^{\circ}C$ and $31^{\circ}C$ (both insulated), Δ $52^{\circ}C$ (insulated) and $16^{\circ}C$, ■ $80^{\circ}C$ and $32^{\circ}C$ (insulated), ◇ $79^{\circ}C$ and $13^{\circ}C$.

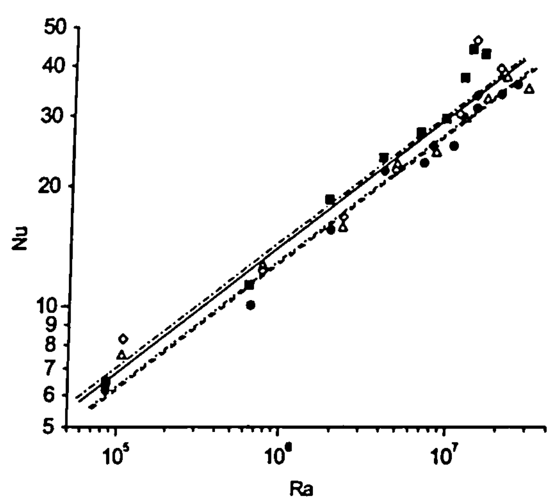

Figure 4.31 Comparison of the change in the local Nusselt number with Rayleigh number where the top and bottom walls were ●–··– $51^{\circ}C$ and $31^{\circ}C$ (both insulated), Δ----$52^{\circ}C$ (insulated) and $16^{\circ}C$, ■–·–· $80^{\circ}C$ and $32^{\circ}C$ (insulated), ◇—— $79^{\circ}C$ and $13^{\circ}C$.

Temperatures of the top wall ($^{\circ}C$), T_{Top}	Temperatures of the bottom wall ($^{\circ}C$), T_{Bottom}	Values of the exponent n	Values of the constant C
Insulated (51)	Insulated (31)	0.32	0.162
Insulated (52)	16	0.32	0.150
80	Insulated (32)	0.32	0.186
79	13	0.31	0.185

Table 4.4 Values of the exponent n and constant C for the form of the Nusselt Rayleigh number correlation $Nu = C \cdot Ra^n$ in the cases when the thermal boundary condition of the bottom wall was changed from being insulated to cooled.

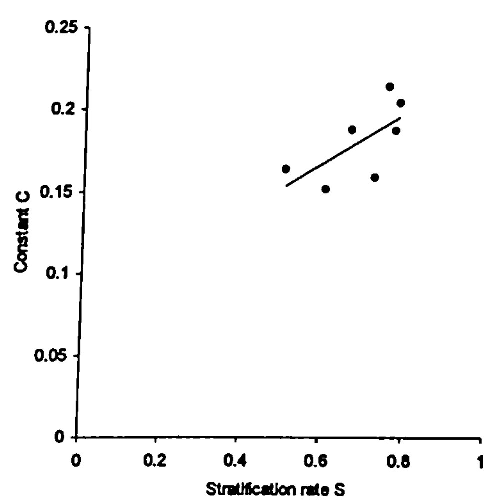

Figure 4.32 Change in the constant C for the correlation $Nu = C \cdot Ra^{0.315}$ with the stratification rate S in the core region of the cavity.

further. The change in the constant C for the correlation $Nu = C \cdot Ra^{0.315}$ with the stratification rate for all the cases is shown in Figure 4.32. In general, the constant C increased as the stratification rate increased but there was considerable scatter in the data that may be due to the differences of the mean temperature in the vertical direction of the cavity when the stratification rate was changed in the different cases. Therefore, the relationship between the constant C and the non-dimensionalized mean temperature in the vertical direction of the cavity $\overline{T}_V$ was investigated (Figure 4.33). The non-dimensionalized mean temperature in the vertical direction was defined as

$$\overline{T}_V = \frac{(T_{Top} + T_{Bottom})/2}{(T_H - T_C)}. \tag{4.5}$$

Furthermore, the relationship between the constant C and the stratification rate S and the non-dimensionalized mean temperature in the vertical direction of the cavity $\overline{T}_V$ was investigated. A regression analysis was performed to determine the functional relation between C and S and $\overline{T}_V$. The equation of this regression line is given by

$$C = 0.231 \cdot S^{0.176} \cdot \overline{T}_V^{\,0.515} \tag{4.6}$$

with R^2 of 0.88 indicating that $\overline{T}_V$ is the more dominant factor. A plot of the constant C with the stratification rate and non-dimentionalized mean temperature in the vertical direction for the present cases is shown in Figure 4.34. Using this equation, the constant C for the case measured by Tian and Karayiannis (2000) was predicted to be 0.18, which is close to the value of 0.2 obtained from their experimental data.

The stratification rate in the correlation in Equation (4.6) can only be determined by measuring the temperature distribution in the cavity and this is not necessarily useful

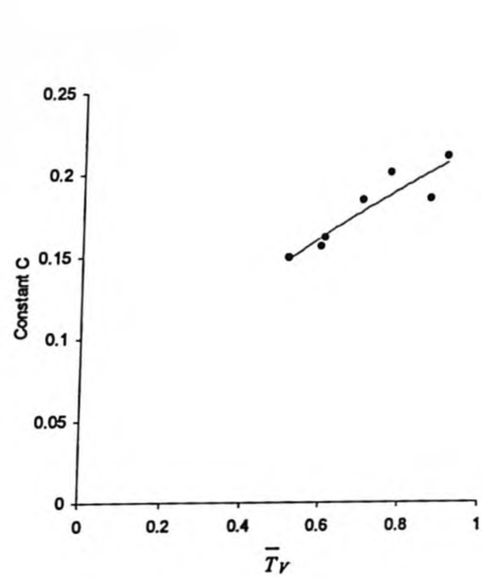

Figure 4.33 Change in the constant C for the correlation $Nu = C \cdot Ra^{0.315}$ with the non-dimensionalized mean temperature in the vertical direction $\overline{T}_V$.

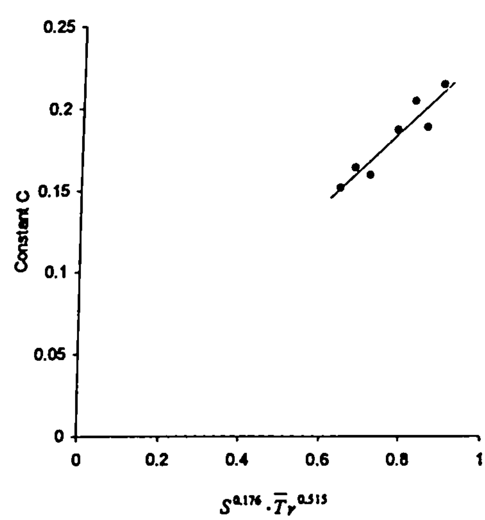

Figure 4.34 Change in the constant C for the correlation $Nu = C \cdot Ra^{0.315}$ with the stratification rate S and non-dimensionalized mean temperature in the vertical direction $\overline{T}_V$.

as a predictive tool since only the boundary conditions are typically known in many applications. The relationship between the constant C and the non-dimensionalized temperature difference between the top and bottom walls S_V, defined as

$$S_V = \frac{T_{Top} - T_{Bottom}}{T_H - T_C}, \tag{4.7}$$

and $\overline{T}_V$ is shown in Figure 4.35. The regression line in this case is given by

$$C = 0.217 \cdot S_V^{\ 0.062} \cdot \overline{T}_V^{\ 0.481} \tag{4.8}$$

with a R^2, regression coefficient, of 0.89.

The main difference between Equations (4.6) and (4.8) is in the powers of S and S_V. The relationship between the stratification rate S and the non-dimensionalized temperature difference between the top and bottom walls S_V is plotted and shown in Figure 4.36. The regression line is given by

$$S = 0.74 \cdot S_V^{\ 0.3} \tag{4.9}$$

with R^2 of 0.93. This indicates that the stratification rate can be estimated from the thermal boundary conditions of the walls.

The change in the average Nusselt number for the hot vertical wall $\overline{Nu}_H$ with the vertical Grashof number Gr_V is shown in Figure 4.37. Here the average Nusselt number is given by

$$\overline{Nu}_H = \frac{\overline{h}H}{k}, \tag{4.10}$$

where $\overline{h}$ is the average heat transfer coefficient for the hot vertical wall, H is the height

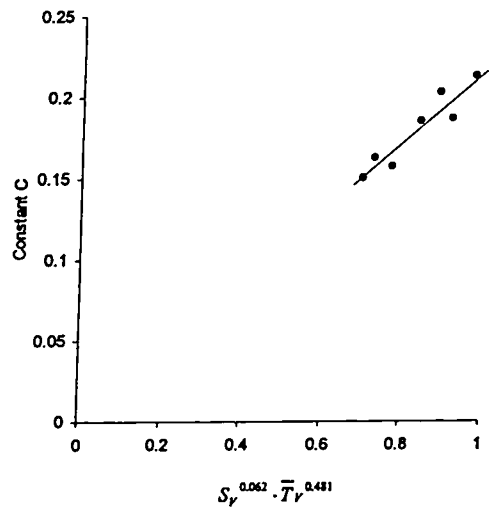

Figure 4.35 Change in the constant C for the correlation $Nu = C \cdot Ra^{0.315}$ with the non-dimensionalized temperature difference between the top and bottom walls S_V and non-dimensionalized mean temperature in the vertical direction $\overline{T}_V$.

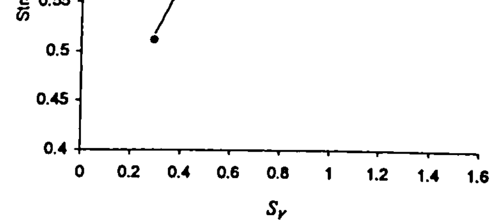

Figure 4.36 Change in the stratification rate S with the non-dimensionalized temperature difference between the top and bottom walls S_V.

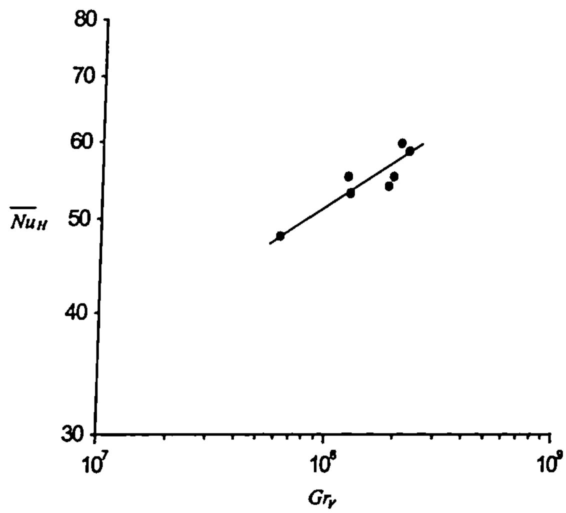

Figure 4.37 Change in the average Nusselt number for the hot vertical wall $\overline{Nu_H}$ with the vertical Grashof number Gr_V.

of the cavity, and k is the thermal conductivity of the air based on the temperature $\left(T_H + \left(T_{Top} + T_{Bottom}\right)/2\right)/2$. The average Nusselt number increases with the vertical Grashof number, as proposed by Shiralkar and Tien (1982). The correlation between $\overline{Nu_H}$ and Gr_V is given by

$$\overline{Nu_H} = 3.58 \cdot Gr_V^{\ 0.145}. \tag{4.11}$$

This, to the author's best knowledge, is the first description of the functional relation between the average Nusselt number for the hot vertical wall $\overline{Nu_H}$ and the vertical Grashof number Gr_V.

Chapter 5 Conclusions

An experimental investigation was performed to examine the effect that stratification has on the natural convection in an air-filled square cavity with heated and cooled vertical walls. The stratification was imposed by changing the temperatures of the top and bottom walls of the enclosure. The natural convection in the enclosure with adiabatic top and bottom walls was examined first, and the temperature profile measurements of the thermal boundary layer on the hot vertical wall were found to be in reasonable agreement with previous measurements reported by Tian and Karayiannis (2000). It was also found that the correlation between the Nusselt number and Rayleigh number had the same form of $Nu = C \cdot Ra^{0.315}$, but the constant C in the correlation was different. It was thought that this may be due to the differences in the stratification and the mean temperature in the vertical direction of the cavity in the two facilities.

The effect of stratification was investigated by changing the temperatures of the top and bottom walls independently. It was found that varying the temperature difference between the top and bottom walls changed the stratification and hence the natural convection heat transfer characteristics in the square cavity. When the temperature of the top wall was increased from $52^{\circ}C$ to $109^{\circ}C$, the temperature distribution in the ambient close to the top wall was not uniform, indicating there was a recirculating flow region near the top wall. This secondary circulation approached the hot vertical wall as the top wall temperature was increased. The non-uniformity in the temperature profiles close to the top wall for the cases of the heated top wall was found to be relatively independent of the bottom wall temperature, indicating the change in this region is a local phenomenon.

In all cases it was found that the Nusselt-Rayleigh number correlation could be expressed in the form of $Nu = CRa^{0.315}$. The constant C increased when the top wall temperature was increased, while it decreased slightly when the bottom wall temperature was decreased. The constant C was found to be a function of the stratification rate S, defined as the non-dimensionalized temperature gradient of the ambient air in the vertical direction in the core region of the cavity, and the non-dimensionalized mean temperature in the vertical direction of the cavity. An empirical relationship for C was developed as

$$C = 0.231 \cdot S^{0.176} \cdot \overline{T}_V^{\,0.515}.$$

The average Nusselt number for the hot vertical wall $\overline{Nu}_H$ increased with an increase of the vertical Grashof number Gr_V. The correlation between $\overline{Nu}_H$ and Gr_V was determined as

$$\overline{Nu}_H = 3.58 \cdot Gr_V^{\,0.145}.$$

In the future, it is recommended that the measurements be extended to examine the temperature profiles throughout the cavity, and examine the thermal boundary layers along the cold vertical wall, and the top and bottom walls. It would be also useful to measure the flow field to fully characterize the natural convection in the cavity. When the aspect ratio of the enclosure is less than one, the viscous forces on the horizontal walls are likely to change the flow pattern in the enclosure significantly. Hence, the effect of the aspect ratio of the cavity on the natural convection should also be investigated. It should be noted that all of these studies could be performed in the current test facility.

Bibliography

Anderson, R., and Bejan, A., 1981, "Heat transfer through single and double vertical walls in natural convection: theory and experiment", International Journal of Heat and Mass Transfer, Vol. 24, No. 10, pp. 1611-1620.

Arnold, J. N., Catton, I., and Edwards, D. K., 1976, "Experimental investigation of natural convection in inclined rectangular regions of differing aspect ratios", Journal of Heat Transfer, Vol. 98, pp.67-71.

Aydin, O., Unal, A., and Ayhan, T., 1999, "Natural convection in rectangular enclosures heated from one side and cooled from the ceiling", International Journal of Heat and Mass Transfer, Vol. 42, pp. 2345-2355.

Bajorek, S. M., and Lloyd, J. R., 1982, "Experimental investigation of natural convection in partitioned enclosures", Journal of Heat Transfer, Vol. 104, pp. 527-532.

Bejan, A., Al-Homoud, A. A., and Imberger, J., 1981, "Experimental study of high-Rayleigh-number convection in a horizontal cavity with different end temperatures", Journal of Fluid Mechanics, Vol. 109, pp. 283-299.

Bejan, A., 1984, "Convection Heat Transfer", JOHN WILEY & SONS, INC., New York.

Bohn, M. S., and Anderson, R., 1986, "Temperature and heat flux distribution in a natural convection enclosure flow", Journal of Heat Transfer, Vol. 108, pp. 471-475.

Briggs, D. G., and Jones, D. N., 1985, "Two-dimensional periodic natural convection in a rectangular enclosure of aspect ratio one", Journal of Heat Transfer, Vol. 107, pp. 850-854.

Brooks, I.H., and Ostrach, S., 1970, "An experimental investigation of natural convection in a horizontal cylider", Journal of Fluid Mechanics, Vol. 44, part 3, pp.545-561.

Chinnakotla, R.B., Angirasa, D., and Mahajan, R.L., 1996, "Parametric study of buoyancy-induced flow and heat transfer from L-shaped corners with asymmetrically heated surfaces", International Journal of Heat and Mass Transfer, 39, pp.851-865

Chu, H. H. –S., Churchill, S. W., and Patterson, C. V. S., 1976, "The effect of heater size, location, aspect ratio, and boundary conditions on two-dimensional, laminar, natural convection in rectangular channels", Journal of Heat Transfer, Vol. 98, pp. 194-201.

Coleman, H.W., and Steele., W.G.JR., 1999, " Experimentation and Uncertainty Analysis for Engineers", JOHN WILEY & SONS, INC., New York.

Cormack, D. E., Leal, L. G., and Imberger, J., 1974a, "Natural convection in a shallow cavity with differentially heated end walls. Part 1. Asymptotic theory", Journal of Fluid Mechanics, Vol. 65, part 2, pp. 209-229.

Cormack, D. E., Leal, L. G., and Seinfeld, J. H., 1974b, "Natural convection in a shallow cavity with differentially heated end walls. Part 2. Numerical solutions", Journal of Fluid Mechanics, Vol. 65, part 2, pp. 231-246.

Dropkin, D., and Somerscales, E., 1965, "Heat transfer by natural convection in liquids confined by two parallel plates which are inclined at various angles with respect to the horizontal", Journal of Heat Transfer, Vol. 87, pp. 77-84.

Drummond, J. E., and Korpela, S. A., 1987, "Natural convection in a shallow cavity", Journal of Fluid Mechanics, Vol. 182, pp. 543-564.

Eckert, E. R. G., and Carlson, W. O., 1961, "Natural convection in an air layer enclosed between two vertical plates with different temperatures", International Journal of Heat and Mass Transfer, Vol. 2, pp. 106-120.

Elder, J. W., 1965, "Laminar free convection in a vertical slot", Journal of Fluid Mechanics, Vol. 23, part 1, pp. 77-98.

Elsherbiny, S. M., Raithby, G. D., and Hollands, K. G. T., 1982, "Heat Transfer by natural convection across vertical and inclined air layers", Journal of Heat Transfer, Vol. 104, pp. 96-102.

Elsherbiny, S. M., 1996, "Free convection in inclined air layers heated from above", International Journal of Heat and Mass Transfer, Vol. 39, pp. 3925-3930.

Emery, A., and Chu, N. C., 1965, "Heat transfer across vertical layers", Journal of Heat Transfer, Vol. 87, pp. 110-114.

Filis, P., and Poulikakos, D., 1986, "An experimental study of the effect of wall temperature nonuniformity on natural convection in an enclosure heated from the side", International Journal of Heat and Fluid Flow, Vol. 7, pp. 258-265.

Flack, R. D., Konopnicki, T. T., and Rooke, J. H., 1979, "The measurement of natural convective heat transfer in triangular enclosures", Journal of Heat Transfer, Vol. 101, pp. 648-654.

Flack, R. D., 1980, "The experimental measurement of natural convection heat transfer in triangular enclosures heated or cooled from below", Journal of Heat Transfer, Vol. 102, pp. 770-772.

Gill, A. E., 1966, "The boundary-layer regime for convection in a rectangular cavity", Journal of Fluid Mechanics, Vol. 26, part 3, pp. 515-536.

Hamady, F. J., Lloyd, J. R., Yang, H. Q., and Yang, K. T., 1989, "Study of local natural convection heat transfer in an inclined enclosure", International Journal of Heat and Mass Transfer, Vol. 32, No. 9, pp.1697-1708.

Hart, J. E., 1983, "Low prandtl number convection between differentially heated end walls", International Journal of Heat and Mass Transfer, Vol. 26, No. 7, pp. 1069-1074.

Holman, J. P., 1986, "Heat Transfer", Sixth Edition, McGraw-Hill Book Company.

Imberger, J., 1974, "Natural convection in a shallow cavity with differentially heated end walls. Part 3. Experimental results", Journal of Fluid Mechanics, Vol. 65, part 2, pp. 247-260.

Khalifa, A. N., 2001, "Natural convective heat transfer coefficient-a review II. Surfaces in two- and three-dimensional enclosures", Energy Conversion and Management Vol. 42, pp. 205-517.

Kimura, S., and Bejan, A., 1980, " Experimental study of natural convection in a horizontal cylinder with different end temperatures", International Journal of Heat and Mass Transfer, Vol. 23, pp. 1117-1126.

Leong, W. H., Hollands, K. G. T. and Brunger, A. P., 1999, "Experimental Nusselt numbers for a cubical-cavity benchmark problem in natural convection", International Journal of Heat and Mass Transfer, No. 42, pp.1979-1989.

Lin, N. N., and Bejan, A., 1983, "Natural convection in a partially divided enclosure", International Journal of Heat and Mass Transfer, Vol. 26, No. 12, pp. 1867-1878.

MacGregor, R. K., and Emery, A. F., 1969, "Free convection through vertical plane layers-moderate and high prandtl number fluids", Journal of Heat Transfer, Vol. 91, No. 3, pp. 391-403.

Meyer, B. A., Mitchell, J. W., and El-Wakil, M. M., 1979, "Natural convection heat transfer in moderate aspect ratio enclosures", Journal of Heat Transfer, Vol. 101, pp. 655-659.

Newell, M. E., and Schmidt, F. W., 1970, "Heat transfer by laminar natural convection within rectangular enclosures", Journal of Heat Transfer, Vol. 92, No. 1, pp.159-168.

Ostrach, S., and Raghavan, C., 1979, "Effect of stabilizing thermal gradients on natural convection in rectangular enclosures", Journal of Heat Transfer, Vol. 101, pp.238-243.

Ostrach, S., 1988, "Natural convection in enclosures", Journal of Heat Transfer, Vol. 110, pp.1175-1190.

Ozoe, H., Yamamoto, K., Sayama, H., and Churchill, S. W., 1974, "Natural circulation in an inclined rectangular channel heated on one side and cooled on the opposing side", International Journal of Heat and Mass Transfer, Vol. 17, pp. 1209-1217.

Ozoe. H., Ohmuro, M., Mouri, A., Mishima, S., Sayama, H., and Churchill, S. W., 1983, "Laser-Doppler measurements of the velocity along a heated vertical wall of a rectangular enclosure", Journal of Heat Transfer, Vol. 105, pp. 782-788.

Poulikakos, D., and Bejan, A., 1983, "Natural convection experiments in a triangular enclosure", Journal of Heat Transfer, Vol. 105, pp. 652-655.

Randall, K. R., Mitchell, J. W., and Ei-Wakil, M. M., 1979, "Natural convection heat transfer characteristics of flat plate enclosures", Journal of Heat Transfer, Vol. 101, pp. 120-125.

Seki, N., Fukusako, S., and Inaba, H., 1978, "Visual observation of natural convective flow in a narrow vertical cavity", Journal of Fluid Mechanics, Vol. 84, part 4, pp. 695-704.

Sernas, V., and Lee, E. I., 1981, "Heat transfer in air enclosures of aspect ratio less than one", Journal of Heat Transfer, Vol. 103, pp. 617-622.

Shiralkar, G. S., and Tien, C. L., 1982, "A numerical study of the effect of a vertical temperature difference imposed in a horizontal enclosure", Numerical Heat Transfer, Vol. 5, pp. 185-197.

Tian, Y. S., and Karayiannis, T. G., 2000, "Low turbulence natural convection in an air filled square cavity. Part I: the thermal and fluid flow fields", International Journal of Heat and Mass Transfer, Vol. 43, pp. 849-866.

Turner, B. L., and Flack, R. D., 1980, "The experimental measurement of natural convective heat transfer in rectangular enclosures with concentrated energy sources", Journal of Heat Transfer, Vol. 102, pp. 236-241.

Viskanta, R., Kim, D. M., and Gau, C., 1986, "Three-dimensional natural convection heat transfer of a liquid metal in a cavity", International Journal of Heat and Mass Transfer, Vol. 29, No. 3, pp. 475-485.

Yewell, R., Poulikakos, D., and Bejan, A., 1982, "Transient natural convection experiments in shallow enclosures", Journal of Heat Transfer, Vol. 104, pp. 533-538.

Yin, S. H., Wung, T. Y., and Chen, K., 1978, "Natural convection in an air layer enclosed within rectangular cavities", International Journal of Heat and Mass Transfer, Vol. 21, pp. 307-315.

Appendix

	% of the height of the hot vertical wall								
	10%	20%	30%	40%	50%	60%	70%	80%	90%
$q^{*}(\frac{W}{m^2})$	288	226.8	209.3	198.3	149.8	122.9	116.2	106.9	89.3
$h(\frac{W}{m^2 C})$	5.9	4.8	4.9	5.1	4.3	4.0	4.2	4.0	3.8
Nu	6.2	10.1	15.5	21.6	22.6	24.9	30.9	33.5	35.46
Ra	8.6×10^4	6.6×10^5	2.0×10^6	4.1×10^6	7.1×10^6	1.1×10^7	1.5×10^7	2.0×10^7	2.5×10^7

Table A.1 Values of local heat flux q^{*}, local heat transfer coefficient h, local Nusselt number Nu, and local Rayleigh number Ra along the hot vertical wall for the case where top and bottom walls were insulated.

	% of the height of the hot vertical wall								
	10%	20%	30%	40%	50%	60%	70%	80%	90%
$q^{*}(\frac{W}{m^2})$	390.9	331.5	280.1	220	194.3	163.6	135.1	110	87.1
$h(\frac{W}{m^2 C})$	6.6	6.1	5.6	4.8	4.8	4.7	4.6	4.7	4.3
Nu	7.0	12.8	17.8	20.3	25.2	29.3	33.8	38. 7	39.9
Ra	1.1×10^5	7.7×10^5	2.3×10^6	4.8×10^6	8.1×10^6	1.2×10^7	1.5×10^7	1.7×10^7	2.1×10^7

Table A.2 Values of local heat flux q^{*}, local heat transfer coefficient h, local Nusselt number Nu, and local Rayleigh number Ra along the hot vertical wall for the case where top and bottom walls were at $71^{\circ}C$ and $12^{\circ}C$, respectively.

	% of the height of the hot vertical wall								
	10%	20%	30%	40%	50%	60%	70%	80%	90%
$q^{\bullet}(\frac{W}{m^2})$	451.7	305.4	254.9	225.8	184.1	157.8	124.2	104.1	77.6
$h(\frac{W}{m^2C})$	7.8	5.8	5.2	5.2	4.8	4.8	4.5	5.5	4.1
Nu	8.3	12.2	16.6	21.7	24.9	29.9	33.3	45.5	38.8
Ra	1.1×10^5	7.7×10^5	2.3×10^6	4.8×10^6	8.0×10^6	1.2×10^7	1.5×10^7	1.4×10^7	2.0×10^7

Table A.3 Values of local heat flux $q^{\bullet}$, local heat transfer coefficient h, local Nusselt number Nu, and local Rayleigh number Ra along the hot vertical wall for the case where top and bottom walls were at $79^{\circ}C$ and $13^{\circ}C$, respectively.

	% of the height of the hot vertical wall								
	10%	20%	30%	40%	50%	60%	70%	80%	90%
$q^{\bullet}(\frac{W}{m^2})$	392.7	325.5	309.5	247.3	182	169	126.7	99.2	79.3
$h(\frac{W}{m^2C})$	6.9	6.3	6.6	5.9	5.0	5.3	4.9	5.8	4.3
Nu	7.3	13.3	20.8	24.8	25.9	33.4	36.0	47.9	40.5
Ra	1.1×10^5	7.4×10^5	2.2×10^6	4.5×10^6	7.4×10^6	1.1×10^7	1.3×10^7	1.3×10^7	1.9×10^7

Table A.4 Values of local heat flux $q^{\bullet}$, local heat transfer coefficient h, local Nusselt number Nu, and local Rayleigh number Ra along the hot vertical wall for the case where top and bottom walls were at $89^{\circ}C$ and $13^{\circ}C$, respectively.

	% of the height of the hot vertical wall								
	10%	20%	30%	40%	50%	60%	70%	80%	90%
$q^{\bullet}(\frac{W}{m^2})$	382.5	352	255.7	218	163.3	144.6	116.3	89.8	62.6
$h(\frac{W}{m^2C})$	7.0	7.0	5.8	5.7	4.9	5.3	5.3	5.8	3.9
Nu	7.5	14.8	18.4	23.7	25.6	32.8	38.2	47.9	36.3
Ra	9.9×10^4	6.9×10^5	2.0×10^6	3.9×10^6	6.4×10^6	9.0×10^6	1.1×10^7	1.1×10^7	1.6×10^7

Table A.5 Values of local heat flux $q^{\bullet}$, local heat transfer coefficient h, local Nusselt number Nu, and local Rayleigh number Ra along the hot vertical wall for the case where top and bottom walls were at $109^{\circ}C$ and $14^{\circ}C$, respectively.

	% of the height of the hot vertical wall								
	10%	20%	30%	40%	50%	60%	70%	80%	90%
$q^{\bullet}(\frac{W}{m^2})$	303.1	251.3	250.8	216.9	175.3	135.4	122	96	69.9
$h(\frac{W}{m^2C})$	6.1	5.4	5.8	5.6	5.1	4.7	5.1	5.2	4.5
Nu	6.5	11.3	18.4	23.3	26.9	29.2	36.9	43.4	42.2
Ra	8.6×10^4	6.4×10^5	1.9×10^6	4.0×10^6	6.7×10^6	9.6×10^6	1.2×10^7	1.4×10^7	1.6×10^7

Table A.6 Values of local heat flux $q^{\bullet}$, local heat transfer coefficient h, local Nusselt number Nu, and local Rayleigh number Ra along the hot vertical wall for the case where top and bottom walls were at $80^{\circ}C$ and insulated, respectively.

	% of the height of the hot vertical wall								
	10%	20%	30%	40%	50%	60%	70%	80%	90%
$q^{*}(\frac{W}{m^2})$	411.2	324.5	247.9	244.9	189.4	169.7	142.5	126.3	99.7
$h(\frac{W}{m^2C})$	7.0	5.9	4.9	5.4	4.6	4.6	4.5	4.4	3.7
Nu	7.5	12.5	15.6	22.4	23.9	29.0	32.4	36.6	34.2
Ra	1.1×10^5	7.7×10^5	2.3×10^6	4.9×10^6	8.4×10^6	1.3×10^7	1.7×10^7	2.2×10^7	3.0×10^7

Table A.7 Values of local heat flux q^{*}, local heat transfer coefficient h, local Nusselt number Nu, and local Rayleigh number Ra along the hot vertical wall for the case where top and bottom walls were insulated and at $16^{*}C$, respectively.

	% of the height of the hot vertical wall									
	10%	20%	30%	40%	50%	60%	70%	80%	90%	Average
$\frac{\Delta q^{*}}{q^{*}}$	4.01%	3.60%	3.95%	3.57%	3.63%	3.50%	3.55%	4.07%	1.22%	**3.27%**
$\frac{\Delta h}{h}$	4.91%	4.63%	5.07%	4.94%	5.22%	5.45%	5.89%	6.56%	5.74%	**5.38%**
$\frac{\Delta Nu}{Nu}$	5.02%	4.75%	5.18%	5.05%	5.33%	5.54%	5.97%	6.64%	5.83%	**5.48%**

Table A.8 Values of the normalized uncertainties of local heat flux q^{*}, local heat transfer coefficient h, and local Nusselt number Nu for the case where top and bottom walls were insulated.

	% of the height of the hot vertical wall									Average
	10%	20%	30%	40%	50%	60%	70%	80%	90%	
$\frac{\Delta q''}{q''}$	6.37%	3.00%	7.02%	6.38%	3.41%	1.74%	3.38%	3.98%	3.25%	**4.28%**
$\frac{\Delta h}{h}$	6.81%	3.96%	7.56%	7.08%	4.87%	4.37%	5.86%	7.04%	7.33%	**6.10%**
$\frac{\Delta Nu}{Nu}$	6.90%	4.11%	7.63%	7.16%	4.97%	4.48%	5.95%	7.10%	7.40%	**6.19%**

Table A.9 Values of the normalized uncertainties of local heat flux q'', local heat transfer coefficient h, and local Nusselt number Nu for the case where top and bottom walls were at $71^{\circ}C$ and $12^{\circ}C$, respectively.

	% of the height of the hot vertical wall									Average
	10%	20%	30%	40%	50%	60%	70%	80%	90%	
$\frac{\Delta q''}{q''}$	9.26%	3.09%	4.88%	5.22%	2.58%	5.79%	2.16%	3.44%	1.49%	**4.21%**
$\frac{\Delta h}{h}$	9.58%	4.07%	5.67%	6.11%	4.42%	7.13%	5.44%	7.77%	7.23%	**6.38%**
$\frac{\Delta Nu}{Nu}$	9.65%	4.21%	5.77%	6.20%	4.54%	7.21%	5.54%	7.83%	7.30%	**6.47%**

Table A.10 Values of the normalized uncertainties of local heat flux q'', local heat transfer coefficient h, and local Nusselt number Nu for the case where top and bottom walls were at $79^{\circ}C$ and $13^{\circ}C$, respectively.

	% of the height of the hot vertical wall									Average
	10%	20%	30%	40%	50%	60%	70%	80%	90%	
$\frac{\Delta q''}{q''}$	6.71%	5.94%	6.70%	3.42%	3.25%	4.60%	3.05%	4.80%	2.76%	**4.58%**
$\frac{\Delta h}{h}$	7.16%	6.54%	7.35%	4.80%	5.01%	6.40%	6.26%	9.13%	7.87%	**6.72%**
$\frac{\Delta Nu}{Nu}$	7.24%	6.62%	7.43%	4.91%	5.11%	6.48%	6.34%	9.19%	7.93%	**6.80%**

Table A.11 Values of the normalized uncertainties of local heat flux q'', local heat transfer coefficient h, and local Nusselt number Nu for the case where top and bottom walls were at $89^{\circ}C$ and $13^{\circ}C$, respectively.

	% of the height of the hot vertical wall									Average
	10%	20%	30%	40%	50%	60%	70%	80%	90%	
$\frac{\Delta q''}{q''}$	3.32%	7.24%	6.18%	5.23%	5.08%	6.12%	3.32%	4.59%	2.43%	**4.83%**
$\frac{\Delta h}{h}$	4.20%	7.78%	6.97%	6.39%	6.60%	7.85%	6.93%	9.63%	8.81%	**7.24%**
$\frac{\Delta Nu}{Nu}$	4.37%	7.85%	7.05%	6.47%	6.67%	7.91%	6.99%	9.68%	8.86%	**7.32%**

Table A.12 Values of the normalized uncertainties of local heat flux q^{*}, local heat transfer coefficient h, and local Nusselt number Nu for the case where top and bottom walls were at $109^{\circ}C$ and $14^{\circ}C$, respectively.

	% of the height of the hot vertical wall									Average
	10%	20%	30%	40%	50%	60%	70%	80%	90%	
$\frac{\Delta q''}{q''}$	7.83%	4.57%	4.41%	10.07%	5.87%	7.20%	1.58%	2.41%	1.84%	**5.09%**
$\frac{\Delta h}{h}$	8.36%	5.53%	5.58%	10.75%	7.24%	8.74%	6.10%	7.86%	8.72%	**7.65%**
$\frac{\Delta Nu}{Nu}$	8.43%	5.64%	5.67%	10.80%	7.31%	8.80%	6.18%	7.92%	8.77%	**7.72%**

Table A.13 Values of the normalized uncertainties of local heat flux q^{*}, local heat transfer coefficient h, and local Nusselt number Nu for the case where top and bottom walls were at $80^{\circ}C$ and insulated, respectively.

	% of the height of the hot vertical wall									Average
	10%	20%	30%	40%	50%	60%	70%	80%	90%	
$\frac{\Delta q''}{q''}$	2.78%	3.15%	7.67%	3.79%	6.24%	3.37%	2.09%	4.33%	2.94%	**4.04%**
$\frac{\Delta h}{h}$	3.67%	4.07%	8.17%	4.87%	7.09%	5.04%	4.76%	6.43%	5.73%	**5.54%**
$\frac{\Delta Nu}{Nu}$	3.84%	4.21%	8.23%	4.97%	7.16%	5.14%	4.86%	6.50%	5.81%	**5.64%**

Table A.14 Values of the normalized uncertainties of local heat flux q^{*}, local heat transfer coefficient h, and local Nusselt number Nu for the case where top and bottom walls were insulated and at $16^{\circ}C$, respectively.

Cases	**Discrepancy in the energy balance in the central area of the hot vertical wall** $\left(Q_{in(a)} - Q_{out(a)}\right)/Q_{in(a)}$
top and bottom walls were insulated	**14%**
top and bottom walls were kept at $71^{\circ}C$ and $12^{\circ}C$, respectively	**23%**
top and bottom walls were kept at $79^{\circ}C$ and $13^{\circ}C$, respectively	**25%**
top and bottom walls were kept at $89^{\circ}C$ and $13^{\circ}C$, respectively	**17%**
top and bottom walls were kept at $109^{\circ}C$ and $14^{\circ}C$, respectively	**20%**
top and bottom walls were kept at $80^{\circ}C$ and insulated, respectively	**20%**
top and bottom walls were insulated and kept at $16^{\circ}C$, respectively	**23%**

Table A.15 Results of the discrepancy in the energy balance in the centre area of the hot vertical wall in the seven cases.

Cases	**Discrepancy in the energy balance for the whole system** $\left(Q_{in(CV)} - Q_{out(CV)}\right)/Q_{in(CV)}$
top and bottom walls were insulated	**8%**
top and bottom walls were kept at $71^{\circ}C$ and $12^{\circ}C$, respectively	**9%**
top and bottom walls were kept at $79^{\circ}C$ and $13^{\circ}C$, respectively	**5%**
top and bottom walls were kept at $89^{\circ}C$ and $13^{\circ}C$, respectively	**10%**
top and bottom walls were kept at $109^{\circ}C$ and $14^{\circ}C$, respectively	**14%**
top and bottom walls were kept at $80^{\circ}C$ and insulated, respectively	**22%**
top and bottom walls were insulated and kept at $16^{\circ}C$, respectively	**12%**

Table A.16 Results of the discrepancy in the energy balance for the whole system in the seven cases.